

Peptidylarginine deiminase type IV sustains
inflammatory response and drives maladaptive cardiac
remodelling after myocardial infarction in mice

Inaugural Dissertation

zur

Erlangung des Doktorgrades

Dr. nat. med.

der Medizinischen Fakultät

und

der Mathematisch-Naturwissenschaftlichen Fakultät

der Universität zu Köln

vorgelegt von

Michelle Holthaus

aus Ibbenbüren

Druck-King Copyshop & Druckerei Köln, Köln

2024

Peptidylarginine deiminase type IV sustains
inflammatory response and drives maladaptive cardiac
remodelling after myocardial infarction in mice

Inaugural Dissertation

zur

Erlangung des Doktorgrades

Dr. nat. med.

der Medizinischen Fakultät

und

der Mathematisch-Naturwissenschaftlichen Fakultät

der Universität zu Köln

vorgelegt von

Michelle Holthaus

aus Ibbenbüren

Druck-King Copyshop & Druckerei Köln, Köln

2024

Betreuer*in

Prof. Dr. Adnana Paunel-Görgülü

Referenten:

Prof. Dr. Thomas Langmann

Prof. Dr. Thomas Wunderlich

Datum der mündlichen Prüfung:

28.11.2024

„Du kannst den Ozean nicht überqueren, wenn du nicht den Mut hast, die Küste aus den Augen zu verlieren.“

Christoph Kolumbus - genuesischer Seefahrer (1451-1506)

Danksagung

Diese Arbeit wäre ohne die Hilfe unzähliger Menschen, die mich sowohl beruflich als auch persönlich begleitet haben, nicht möglich gewesen.

Zuallererst möchte ich Herrn Univ. Prof. Dr. Thorsten Wahlers für die Möglichkeit danken, diese Arbeit im Labor der Herzchirurgie am Universitätsklinikum Köln zu schreiben.

Einen besonderen Dank gilt meiner Doktormutter Prof. Dr. rer. nat. Adnana Paunel-Görgülü. Ohne ihre Unterstützung über die gesamten Jahre, sowie ihre wissenschaftliche Anleitung wäre diese Arbeit nur schwer vorstellbar gewesen. Ich danke ihr für ihr Vertrauen und dafür, dass sie mir dieses spannende Promotionsprojekt ermöglicht hat. Ihre anhaltende Ermutigung und ihr fortwährendes Interesse am Fortschritt dieser Arbeit weiß ich sehr zu schätzen.

Ich danke PD Dr. med. Kaveh Eghbalzadeh für die engagierte Betreuung bei den operativen Eingriffen sowie für seine Hilfsbereitschaft, sein offenes Ohr, anregende Gespräche und sein wertvolles Feedback.

Außerdem möchte ich mich bei Prof. Dr. Thomas Langmann sowie Prof. Dr. Thomas Wunderlich für die Übernahme der Tutorenschaft und den dadurch ermöglichten fachlichen Austausch bedanken.

Mein Besonderer Dank gilt den technischen Assistentinnen Natalie Mierau, Sabine Schmitt und Lei Leu für ihre technische, fachliche, aber vor allem auch moralische Unterstützung. Es war eine wunderschöne Zeit, deren Kontakt ich pflegen und stets in Erinnerung behalten werde.

Vielen Dank auch an Xiaolin Xiong und Clara Großmann, nicht nur für die unzähligen Stunden mit mir im Operationssaal und der Mausepflege an den Wochenenden, sondern auch für die (mehr oder weniger produktiven) Kaffeepausen und wunderbaren Gespräche.

Ferner möchte ich Paul Gehle, PD Dr. Melanie Freifrau von Brandenstein und Sabrina Satzinger von Herzen danken. Sie haben mich über schwere Passagen meiner Arbeit getragen und dafür gesorgt, dass ich mein Lachen und meine Freude auf der Arbeit niemals verloren habe. Neben dem fachlichen Austausch, anregenden Gesprächen und stetiger Unterstützung haben sie mich immer wieder motiviert.

Ein weiterer Dank gebührt neben meiner Familie auch meinen Freunden, die mich stets unterstützt haben und leider viel zu oft auf ein Wiedersehen warten mussten. Aus tiefstem Herzen dank ich euch für eure Geduld und euer Verständnis während meiner Dissertation. Ihr habt euch nicht nur bereit erklärt, meine kurzen Kaffeepausen und knapp bemessenen Freizeitpläne zu akzeptieren, sondern ihr habt auch unzählige Absagen hingenommen. Jeder von euch hat mir ein offenes Ohr geboten, mich mit Rat und Tat unterstützt und mich aufgemuntert, wenn die Herausforderungen überwältigend schienen. Ihr seid ein unschätzbare Teil meines Erfolges und ich bin zutiefst dankbar, euch in meinem Leben zu haben.

Ein ganz besonderer Dank gebührt meiner Schwester Christin sowie meinen Eltern Anne und Thomas, die mich unaufhörlich auf meinem Lebensweg unterstützen. Ihr habt mir stets den Rücken gestärkt und mir das Vertrauen geschenkt, dass ich alles im Leben erreichen kann. Eure Liebe und Unterstützung ist selbstlos und unermüdlich, und dieses Gefühl täglich zu spüren ist für mich unbezahlbar. Ohne eure Hilfe hätte ich diese Arbeit nicht beenden können. Dank euch, bin ich zu dem Menschen geworden, der ich heute bin.

Mein größter Dank gilt jedoch meinem Partner Philipp Müller, der immer an meiner Seite war und diese Arbeit zu seiner eigenen gemacht hat. Obwohl diese Thematik bei weitem nicht zu seinem Fachgebiet zählt, stand er mir täglich mit Rat und Tat zur Seite. Seine ständige Ermutigung und Geduld haben mir in den schwierigsten Momenten den nötigen Halt gegeben. Seine Unterstützung, Liebe und sein Vertrauen haben mich stets inspiriert, mein Bestes zu geben.

Table of content

Danksagung	1
Abstract	6
Zusammenfassung	7
1 Introduction	9
1.1 Cardiovascular diseases (CVDs).....	9
1.2 Acute myocardial infarction (MI)	9
1.3 Clinical cardio-protective strategies against MI	11
1.4 The immune response after MI.....	12
1.5 Initial pro-inflammatory response to MI.....	14
1.6 Proliferation and maturation phase following MI	17
1.7 Posttranslational modifications of arginine.....	20
1.8 Structure and biological function of Peptidylarginine Deiminases (PADs).....	20
1.9 Peptidylarginine Deiminase type 4 (PAD4) and its role in cardiac diseases.....	22
2 Aim of the research	25
3 Material and Methods	26
3.1 Material	26
3.1.1 Instruments and expendable materials	26
3.1.2 Chemicals	27
3.1.3 Cell culture reagents	28
3.1.4 Proteins and enzymes.....	29
3.1.5 Inhibitors and drugs.....	29
3.1.6 Sets and kits	29
3.1.7 Antibodies	30
3.1.8 Staining solutions	31
3.1.9 Buffer solutions	31
3.1.10 Primer.....	33
3.2 Methods	35
3.2.1 Cell culture	35
3.2.1.1 Thawing and freezing of cells	35
3.2.1.2 Isolation of bone marrow cells from mice	35
3.2.1.3 Cultivation of adherent and non-adherent cells	36
3.2.1.4 Polarization of bone marrow-derived macrophages.....	37
3.2.1.5 Assessment of efferocytosis.....	37
3.2.2 Human sample collection	38
3.2.3 Mouse handling and experiments.....	38
3.2.3.1 Animal care	38

3.2.3.2	Mice strains.....	38
3.2.3.3	Pharmacological inhibition of PADs <i>in vivo</i>	39
3.2.3.4	Induction of MI in mice	39
3.2.3.5	Scoring and analgesia.....	40
3.2.3.6	Verification of infarcts by transthoracic echocardiography	40
3.2.3.7	Cardiac plasma collection	41
3.2.3.8	Enzymatic digestion of infarcted mouse hearts	41
3.2.3.9	Isolation of cardiac monocytes/macrophages and cardiac fibroblast	42
3.2.4	Molecular biology	43
3.2.4.1	RNA isolation and quantification.....	43
3.2.4.2	DNA removal from RNA samples	43
3.2.4.3	Bulk RNA sequencing	44
3.2.4.4	Affymetrix microarray analysis	44
3.2.4.5	cDNA synthesis.....	45
3.2.4.6	Real-time PCR	45
3.2.5	Bioinformatical analysis.....	46
3.2.6	Protein biochemistry.....	46
3.2.6.1	Protein isolation from heart tissue	46
3.2.6.2	Quantification of protein concentration	46
3.2.6.3	SDS-PAGE	47
3.2.6.4	Western blot.....	47
3.2.6.5	Cardiac troponin t type 2 quantification	48
3.2.6.6	Total collagen quantification.....	48
3.2.7	Cellular biology.....	49
3.2.7.1	Preparation heart tissue for histological analysis	49
3.2.7.2	Immunohistochemistry	49
3.2.7.3	Immunofluorescence.....	50
3.2.7.4	Assessment of cell death	51
3.2.7	Flow cytometry.....	51
3.2.8	Statistics.....	52
4	Results	53
4.1	Increased PAD4 activity after MI in mice and humans.....	53
4.2	Comparative consequences of genetic or pharmacological PAD4 inhibition on the early pro-inflammatory immune response post-MI (days 1 - 3)	55
4.2.1	Decreased PAD4-mediated citrullination and NETs formation with BB-CI-Amidine.....	55
4.2.2	Induction of massive cardiac damage by pharmacological PAD inhibition in the acute phase	58
4.2.3	Enhanced inflammatory gene expression in WT + BB-CI mice	60

Table of content

4.2.4	Suppression of myeloid cell recruitment by PAD inhibition.....	67
4.2.5	Increased risk of cardiac rupture following pharmacological PAD inhibition post-MI.....	69
4.3	Influence of genetic PAD4 inhibition on the anti-inflammatory phase post-MI (day 7)	71
4.3.1	Attenuation of pro-inflammatory gene expression by PAD4 deficiency	71
4.3.2	Reduced count of cardiac macrophages in PAD4-deficient mice	73
4.3.2	Less inflammatory phenotype observed in PAD4 ^{-/-} macrophages	74
4.3.4	Reduction of cardiac fibrosis after PAD4 ablation in mice	81
4.4	PAD4 deficiency and pharmacological pan-PAD inhibition starting at day 7 post-MI limits maladaptive cardiac remodelling	83
5	Discussion.....	85
6	Conclusion and remarks.....	95
	List of figures.....	97
	List of tables	98
	List of abbreviations	99
	Bibliography	103
	Erklärung	118
	Curriculum Vitae.....	Fehler! Textmarke nicht definiert.

Abstract

Til today cardiovascular diseases (CVDs), including myocardial infarction (MI), are still associated with high morbidity and mortality rate. Although catheter intervention in the acute phase after MI has significantly contributed to reducing mortality, five years later, one in four patients is no longer alive. Sustained inflammation and maladaptive fibrosis represent predictive risk factors for the development of heart failure (HF). Peptidylarginine deiminase type IV (PAD4), a member of the PAD enzyme family catalyses the conversion of arginine residues to citrulline in target proteins. It is critically involved in the regulation of gene expression through histone modification. The pivotal role of PAD4 in cardiac remodelling is acknowledged, yet the underlying mechanisms remain unclear.

In this study, a mouse model of MI with permanent ligation of the left anterior descending artery (LAD) was established. Male WT, PAD4^{-/-} and WT mice treated with the pan-PAD inhibitor BB-CI-Amidine were subjected to MI. The *Padi4* expression was elevated in mice at days 1, 3, 7, and 28 post-MI as well as in humans, who passed from MI. *Padi4* ablation resulted in a reduced immune response, as evidenced by reduced levels of cell necroptosis, diminished expression of inflammation-related genes and reduced infiltration of myeloid cells, in infarcted hearts. At day 7 post-MI, PAD4^{-/-} monocytes/macrophages (Mo/M ϕ) displayed a reparative phenotype characterized by reduced expression of inflammatory genes, like *Ccr2*, *Nos2*, *Tnfa*, *Il6* and *Il1a* and upregulated surface expression of the mannose receptor CD206. Additionally, reduced expression of fibrotic genes and proteins, such as TGF- β , pSMAD2, and Collagen type I were found in hearts of PAD4^{-/-} mice. This was accompanied by diminished fibrotic pathways in isolated PAD4^{-/-} cardiac fibroblasts (CFs), resulting in a decreased abundance of myofibroblasts, reduced scar size, and less fibrosis.

Pharmacological PAD inhibition during the initial inflammatory phase (days 1 and 3) post-MI resulted in massive cardiac damage, increased inflammatory gene expression and reduced total collagen content in infarcted hearts. This led to a higher risk of cardiac rupture and significantly reduced the 7-day survival rate to approximately 20%. On the other hand, pharmacological inhibition starting after resolution of inflammation resulted in a substantial reduction in collagen abundance and fibrotic area, thus improving long-term survival. The same benefits were observed in PAD4^{-/-} mice.

Taken together, these results demonstrate that genetic and pharmacological targeting of PADs, including PAD4, may prevent adverse remodelling by altering the phenotype of macrophages, influencing pro-fibrotic pathways in CFs and thereby diminishing excessive deposition of extracellular matrix (ECM), ventricular stiffness and improving long-term survival.

Zusammenfassung

Herz-Kreislauf-Erkrankungen, einschließlich der Myokardinfarkt (MI), sind bis heute mit einer hohen Morbidität und Mortalität assoziiert. Obwohl die Katheterintervention in der akuten Phase nach einem MI die Sterblichkeit signifikant reduziert hat, ist fünf Jahre später immer noch jeder vierte Patient nicht mehr am Leben. Eine anhaltende Entzündung und eine maladaptive Kollagenproduktion (Fibrose) stellen prädiktive Risikofaktoren für die Entwicklung einer Herzinsuffizienz (HI) dar. Das Enzym Peptidylarginin-Deiminase Typ IV (PAD4), ein Mitglied der PAD-Enzymfamilie, katalysiert die Umwandlung von Argininresten in Citrullin in Zielproteinen. Zudem ist es entscheidend an der Regulation der Genexpression durch Histonmodifikation beteiligt. Die zentrale Rolle von PAD4 im kardialen Remodelling ist anerkannt, jedoch bleiben die zugrundeliegenden Mechanismen unklar.

In dieser Studie wurde ein Mausmodell etabliert, bei dem durch eine permanente Ligatur der linken vorderen absteigenden Koronararterie ein MI imitiert wurde. Männliche, 9-12 Wochen alte WT, PAD4^{-/-} und WT-Mäuse, die mit dem Pan-PAD-Inhibitor BB-CI-Amidin behandelt wurden, wurden einem MI unterzogen. Die *Padi4*-Expression bei WT Mäusen war an den Tagen 1, 3, 7 und 28 nach MI sowie bei Menschen, die nachweislich an MI gestorben sind, erhöht. Zudem führte das Fehlen von *Padi4* in Mäusen zu einer reduzierten Immunantwort, was sich durch eine verringerte Zellnekroptose, verminderte Expression von entzündungsassoziierten Genen und reduzierte Infiltration von myeloiden Zellen in infarzierten Herzen zeigte. Am 7. Tag nach MI zeigten PAD4^{-/-} Monozyten/Makrophagen (Mo/Mφ) einen reparativen Phänotyp, gekennzeichnet durch eine verringerte Expression von inflammatorischen Genen wie z.Bsp. *Ccr2*, *Nos2*, *Tnfa*, *Il6*, und *Il1α* und eine erhöhte Oberflächenexpression von CD206. Zusätzlich konnte im Herzen dieser Mäuse eine reduzierte Expression von fibrotischen Genen und Proteinen wie TGF-β, pSMAD2 und Kollagen Typ I festgestellt werden. Isolierte PAD4^{-/-} kardiale Fibroblasten (KFs) zeigten verminderte profibrotische Signalwege, was zu einer verringerten Anzahl von kollagenproduzierende Myofibroblasten, einer reduzierten Narbengröße und weniger Fibrose führte.

Die pharmakologische PAD-Inhibition während der initialen Entzündungsphase (Tag 1 und 3) nach MI führte zu massiven Herzschäden, einer erhöhter Expression von inflammatorischen Genen und reduzierte den Gesamtkollagengehalt in infarzierten Herzen dieser Mäuse signifikant. Dies hatte ein erhöhtes Risiko für eine Herzruptur zur Folge und reduzierte die 7-Tage-Überlebensrate signifikant auf ca. 20%. Andererseits führte eine pharmakologische Hemmung nach der initialen Entzündungsphase zu einer signifikanten Reduktion des Kollagengehaltes und der Fibrose, wodurch das Langzeitüberleben dieser Tiere verbessert wurde. Vergleichbare Vorteile wurden bei PAD4^{-/-} Mäusen beobachtet.

Zusammengefasst zeigen diese Ergebnisse, dass die genetische und pharmakologische Hemmung von PADs, einschließlich PAD4, das adverse kardiale Remodelling verhindern kann. Dies wird erreicht, indem der Phänotyp von Makrophagen in Richtung eines reparativen Phänotyps gefördert und pro-fibrotische Signalwege in KFs unterdrückt werden. Dadurch kommt es zu einer verminderten Kollagenablagerung im Herzen und einer verbesserten Langzeitüberlebensrate.

1. Introduction

1.1. Cardiovascular diseases (CVDs)

Cardiovascular diseases (CVDs) characterize a multifaceted array of pathophysiological conditions that profoundly influence the vitality of the heart and blood vessels (Nichols et al. 2014). Accounting for 31% of all recorded deaths, CVDs are still associated with a high mortality rate, ultimately affecting 17.9 million people per year worldwide (Virani et al. 2020). In Europe CVDs remain the leading cause of death with nearly 4 million people dying from CVDs each year, accounting for approximately 44% of all fatalities (Townsend et al. 2022). In Germany half of all documented causes of death in 2021 were attributed to CVDs. Among these cases, chronic ischemic heart disease was the leading cause, followed by COVID-19 associated circumstances. Acute myocardial infarction (MI) and heart failure (HF) ranked 4th and 6th, respectively (German Federal Statistical Office, causes of death statistics 2021).

Every year, over 200.000 people in Germany receive a diagnosis of MI in the inpatient sector alone, as reported by the German Heart Report 2021. Given this statistic, the likelihood of hospitalization due to heart decompensation is high. The number of MI cases has been consistently rising in recent years, particularly due to the aging population. In addition to age, risk factors for MI include smoking, obesity, unhealthy diet, and lack of physical activity (Yusuf et al. 2004; Knuuti et al. 2020). These factors are commonly found in our society and often stem from an imbalance in work-life balance or elevated stress levels (Sara et al. 2018).

1.2. Acute myocardial infarction (MI)

The heart, located in the mediastinum between the two lung lobes, is anatomically subdivided into right atrium, right ventricle (RV), left atrium, and left ventricle (LV) and ensures sufficient blood flow throughout the body's vascular system through its pumping action (**Fig. 1**). To fulfill its function, the cardiac muscle requires oxygen. Therefore, the heart exhibits its own system of blood vessels known as coronary veins and coronary arteries. The heart receives oxygen-rich blood through two main arteries: the right coronary artery, which supplies the wall of the right atrium and right ventricle, and the left coronary artery, which supplies the wall of the left atrium and left ventricle. The latter divides into two main branches: the left anterior descending artery (LAD), which runs between the right and left ventricles to the apex of the heart, and the left circumflex artery (LCx), which extends along the left atrial border toward the left side of the heart (Rehman et al. 2024).

The complete blockage of a coronary artery, which leads to an interruption of oxygen supply, is referred to as a MI (**Fig. 1**). Rupture of atherosclerotic plaque often causes such blockage in coronary arteries (Quillard et al. 2017). The complete loss of blood flow in the segments of the myocardium supplied by these arteries can lead to chronic HF and death (Prabhu 2005; Tanai und Frantz 2015). HF is a common condition among individuals who survived MI and develops as a consequence of cardiomyocyte death and scar formation (Sutton and Sharpe 2000; Johansson et al. 2017). Following MI, the heart experiences structural and functional alterations, including hypertrophy of the non-infarcted regions and dilatation or thinning of the infarcted areas. These changes lead to a decline in the heart's pumping efficiency, a phenomenon known as adverse remodelling (Frangogiannis 2012). In the end, MI induces a swift and drastic transformation in the structural and cellular composition of the heart, severely impairing cardiac function (Sandoval and Jaffe 2019). Given the inability of human cardiac muscle cells to self-renew and the heart's inherent lack of autonomous regeneration, ongoing remodelling processes are crucial to sustaining any cardiac function (Bergmann et al. 2009; Tenreiro et al. 2021).

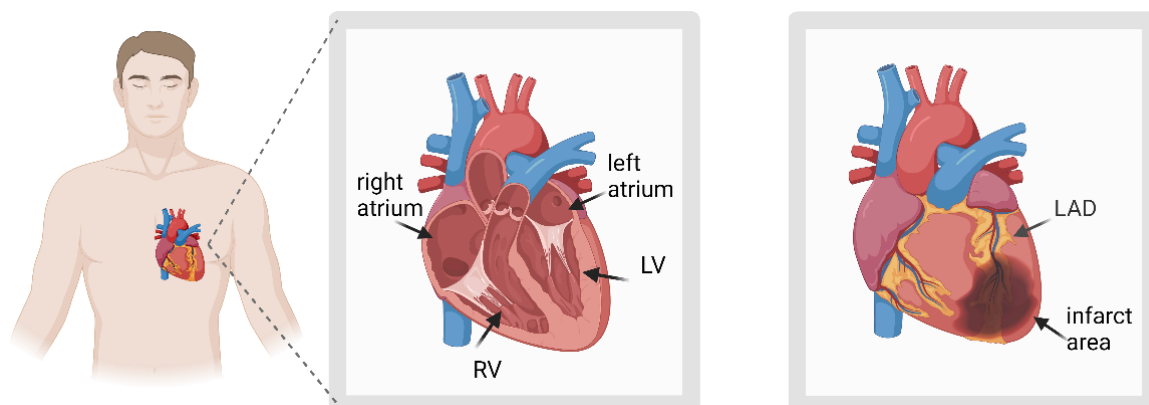


Figure 1: Anatomy of the human heart. The human heart is segmented into the right atrium, right ventricle (RV), left atrium, and left ventricle (LV). On the right side: Representation of acute myocardial infarction (MI) where the left anterior descending artery (LAD), which runs between the right and left ventricles, is blocked and oxygen supply is interrupted. The infarcted area is shown as a dark shadow. Graphic created with BioRender.

1.3. Clinical cardio-protective strategies against MI

MI is one of the most life-threatening conditions, partly due to the fact that there is only a narrow time window for successful reperfusion and maintenance of cardiac function (Fox et al. 2007). Experimental investigations have consistently demonstrated that the duration of myocardial ischemia following acute coronary artery occlusion serves as a pivotal factor influencing the resultant infarct size (Engblom et al. 2009; Schirone et al. 2022). Over the years, various cardioprotective strategies against MI have been developed, focusing on both pharmacological interventions and surgical procedures aimed at restoring optimal blood perfusion. While some medical approaches have shown limited effectiveness or inconsistent results, others have been clinically validated. For instance, emergent pharmacotherapy such as Aspirin, Heparin, and other anticoagulants is utilized to prevent thrombus formation, while thrombolytic agents are employed to dissolve existing clots. Statins are prescribed to reduce cholesterol levels, whereas nitrates are administered to alleviate symptoms of angina. Beta blockers, calcium channel blockers, and ACE inhibitors are used to improve blood flow, reduce cardiac workload, and attenuate hypertension (Davidson et al. 2019). Moreover, there have been significant advancements in the acute treatment of MI, with a primary focus on percutaneous coronary intervention (PCI) to lower immediate mortality. PCI aims to clear blocked arteries and restore blood flow to the heart by inserting stents via surgical intervention (Ferreira et al. 2018; Gale et al. 2014). Paradoxically, while reperfusion of the ischemic myocardium is intended to preserve tissue viability, it triggers reperfusion-related cardiac damage. These issues include increased production of reactive oxygen species (ROS) due to mitochondrial dysfunction, cardiac calcium overload, inflammation, and irreversible damage to heart cells caused by necrosis and apoptosis (Saito et al. 2022; Gray et al. 2018; Eltzschig and Eckle 2011). Consequently, reperfusion injury can contribute to nearly half of the final infarct area. It has been suggested that preventing reperfusion injury could spare an additional 50 to 80% of the myocardium (Fröhlich et al. 2013; Nishihira et al. 2022). Additionally, "silent" heart attacks, devoid of symptoms, can also lead to HF, accounting for a significant portion (22 - 50%) of all infarctions (Cheng et al. 2021b).

Ultimately, the morbidity and mortality stemming from adaptive symptoms post-MI remain unacceptably high and necessitate a deeper understanding. Such understanding is crucial, particularly in unravelling the complex pathways and their interconnected and sequential interactions.

1.4. The immune response after MI

Triggered by the demise of parenchymal cells and cardiomyocytes (CMs) following MI, a sequence of events is initiated, comprising inflammation, repair (proliferation), and maturation (**Fig. 2**). This sequence aims to mitigate further damage, maladaptive cardiac remodelling and prevent rupture of the ventricular wall impacted by MI (Kologrivova et al. 2021; Frangogiannis 2012). Molecules known as damage-associated molecular patterns (DAMPs), released by necrotic, stressed, or injured cells initiate the inflammatory phase (Talman and Ruskoaho 2016).

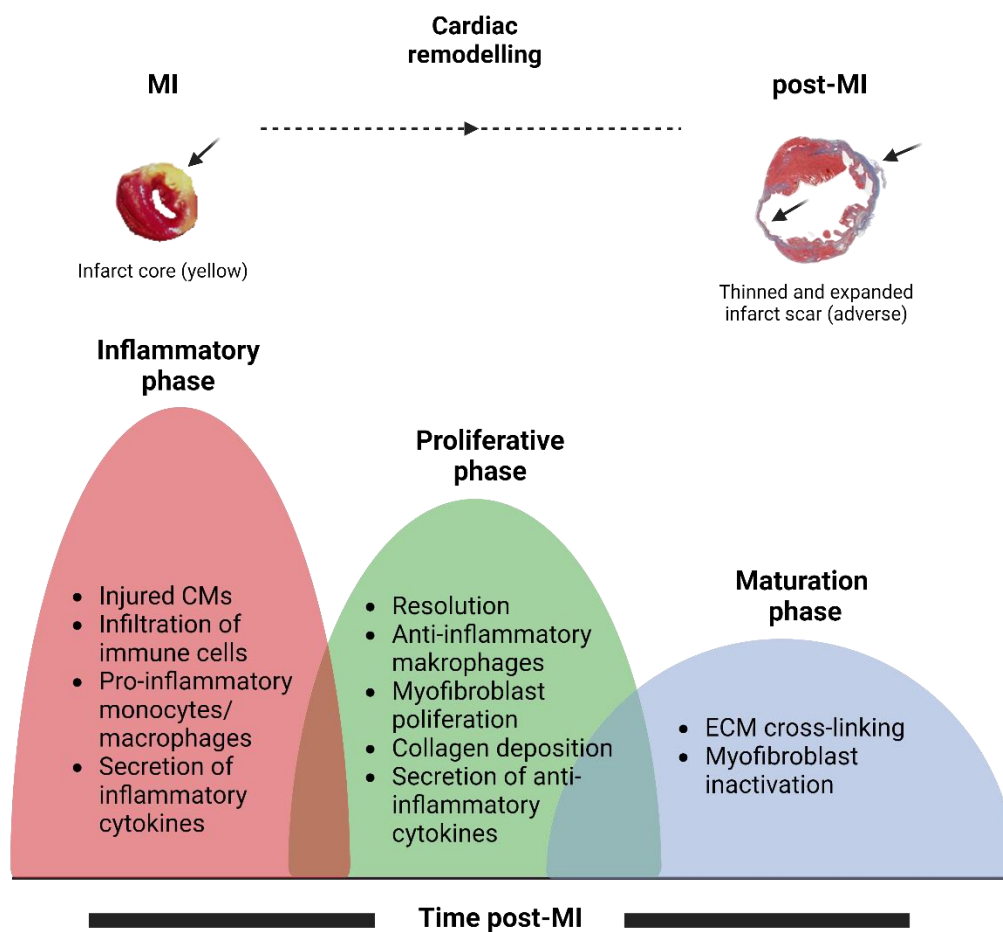


Figure 2: Multifaceted immune response post-MI. Following MI, there are distinct phases of regeneration. Initially, within the first 3 days, there is an intense inflammatory response characterized by significant infiltration of immune cells and tissue degradation. This phase is followed by a period of resolution spanning approximately from 3 to 10 days, marked by myofibroblast proliferation and the initiation of wound repair. During this stage, immune cells shift towards an anti-inflammatory state. Subsequently, the process moves into a maturation phase, leading to scar formation. Collectively, these phases constitute cardiac remodelling. Notably, in cases of larger infarctions with heightened inflammatory activity, there is a tendency for progressive maladaptive scar formation. Graphic created with BioRender.

The extracellular matrix (ECM), primarily composed of collagen fibres, serves as the foundational framework for the stability of the heart (Frangogiannis 2012). Following MI, ECM fragmentation occurs, leading to the spillage of DAMPs as a consequence. Enzymes, called matrix metalloproteinases (MMPs), which are secreted for example by surviving cardiac fibroblasts (CFs), macrophages or endothelial cells, activate this ECM degradation. These CFs build up the connective tissue and synthesize new collagen (Frangogiannis 2012). The secretion of DAMPs aims to facilitate cell migration into the injured area (Nahrendorf et al. 2010). Here DAMPs stimulate the innate immune system by interacting with specific pattern recognition receptors (PRRs) on surviving cardiac cells and infiltrating leukocytes (Newton and Dixit 2012; Ong et al. 2018; Penberthy and Ravichandran 2016). During ischemia, hypoxia compromises endothelial cell integrity, leading to increased vessel permeability and enabling leukocyte infiltration (Kain et al. 2014). PRRs then initiate downstream cellular signalling pathways, ultimately leading to the release of a cascade of inflammatory cytokines, chemokines, and cell adhesion molecules. This interaction prompts the recruitment of leukocytes to the injured tissue area (Kologrivova et al. 2021; Ma et al. 2016). These leukocytes, especially macrophages and neutrophils, phagocytize dead cells and damaged ECM to improve cardiac healing (Horckmans et al. 2017). Moreover, infiltrating leukocytes accelerate the repopulation of the infarcted area with proliferating immune cells and later myofibroblasts. To ensure nutrient and oxygen supply for infiltrating cells, an upregulation of vascular endothelial growth factor (VEGF) is initiated after MI, starting in the viable border zone and gradually extending into the core infarct zone (Zhao et al. 2010). In summary, the infarct area or border zone exhibits dynamic and highly metabolically active characteristics.

1.5. Initial pro-inflammatory response to MI

Insufficient oxygen supply initiates the cell death of CMs, endothelial cells and CFs. This sets off pro-inflammatory responses through the coordinated interplay of several processes (**Fig. 3**). This includes the activation of the complement system, production of ROS and DAMPs, and the release of various pro-inflammatory mediators. These processes promote the recruitment of inflammatory cells into the infarct zone and amplify the pro-inflammatory response following MI (Zhao et al. 2000).

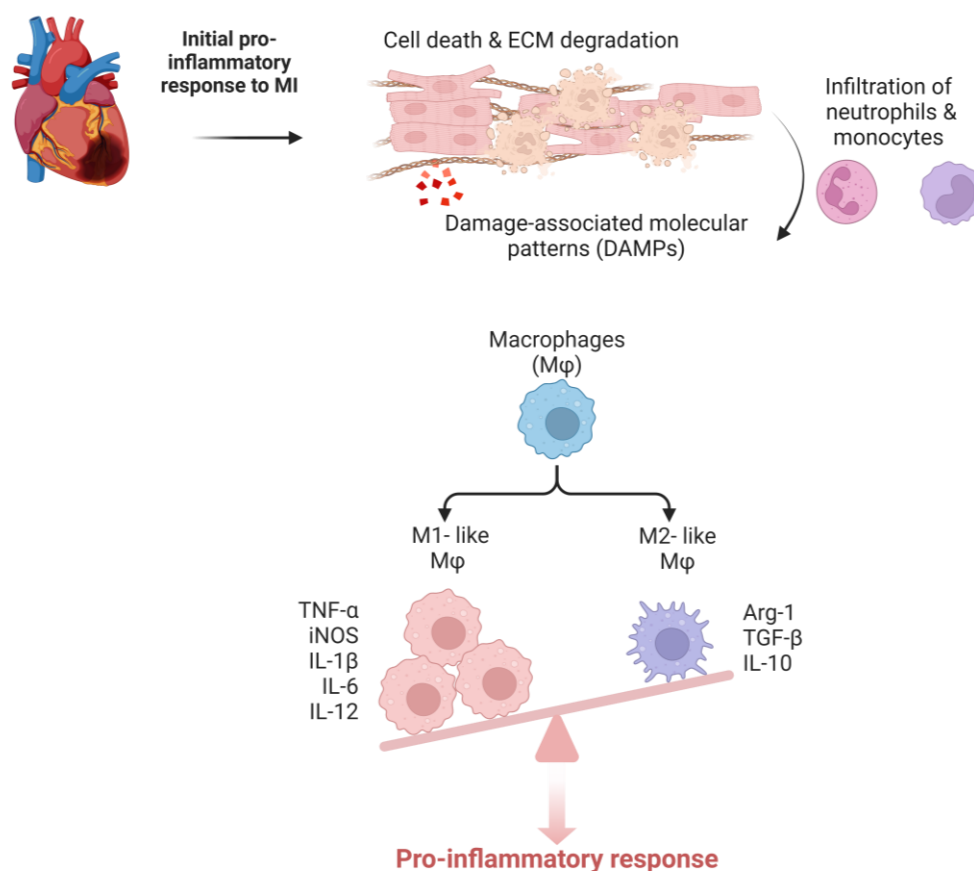


Figure 3: Characteristics of the initial inflammatory immune response post-MI. After MI, the extracellular matrix (ECM) becomes degraded and necrotic cardiomyocytes release damage-associated molecular patterns (DAMPs), which stimulate neutrophil and monocyte infiltration from the bloodstream. Blood monocytes infiltrate the infarct area and are initially polarized to inflammatory M1-like macrophages. In the initial phase post-MI, the ratio of inflammatory (M1-like) to anti-inflammatory (M2-like) macrophages shifts heavily towards M1. M1-like macrophages predominantly express a variety of markers such as TNF- α , iNOS, IL-1 β , IL-6, and IL-12 and contribute to inflammation, whereas the M2-like macrophages express markers like IL-10, TGF- β , Arginase 1 (Arg1). Graphic created with BioRender.

The mononuclear phagocytic ensemble, originating from bone marrow progenitor cells, encompasses monocytes, macrophages, neutrophils and dendritic cells (Kologrivova et al. 2021). These cell populations have important regulatory functions post-MI. During the initial 1-4 days following MI, they dominate the cellular infiltration and actively contribute to infarct healing (Ma et al. 2016; Dutta et al. 2015). Attracted by different chemotactic molecules, neutrophils are the first cells recruited to the damaged site within 6-24h after MI. They transmigrate across the endothelial cell wall of blood vessels by adhesion to P- and E-selectin as well as to the inter-cellular adhesion molecules 1 and 2 (ICAM-1 and -2) to the infarcted tissue (Horckmans et al. 2017). All neutrophils contain granules comprising proteases like myeloperoxidase (MPO), neutrophil elastase (NE), and biologically active substances (Kain and Halade 2020). Neutrophilic activity is mostly mediated by phagocytosis, degranulation, and production of ROS and NETosis, characterized by the release of chromatin fibres into the extracellular space and formation of neutrophil extracellular traps (NETs) (Brinkmann et al. 2004; Brinkmann and Zychlinsky 2012). Activated neutrophils release superoxide-anions and other ROS during the respiratory burst, which can exacerbate oxidative stress in the myocardial tissue and worsen cardiac outcome (Poznyak et al. 2020; Itagaki et al. 2015). Under physiological conditions, apoptotic cells, like neutrophils, typically undergo phagocytosis by macrophages and diminish in numbers within a few days of the healing process (Horckmans et al. 2017; Frantz and Nahrendorf 2014). While some tissue-resident macrophages may already be present at the injury site, the majority are recruited from the bloodstream. Monocytes exit the bloodstream through adhesion to selectins, ICAMs, or integrins expressed by endothelial cells similar to neutrophils (Prame Kumar et al. 2018). The infiltration of macrophages is regulated by gradients of various chemotactic factors, such as macrophage inflammatory protein-1 α (MIP-1 α) and chemokine (C-C motif) ligand 2 (CCL2), also known as monocyte chemoattractant protein-1, MCP-1), which are secreted by various cells including CFs and subsets of leukocytes (Mouton et al. 2018). Upon entering the wound environment, macrophages differentiate into activated tissue macrophages in response to different stimuli. The primary functions of pro-inflammatory infiltrating macrophages, derived from differentiated peripheral monocytes, is antigen presentation, phagocytosis of cell debris, degradation of ECM, and immunomodulation (Yano et al. 2006; Davies et al. 2013; Wynn et al. 2013). This type of cell activation is characterized by a highly pro-inflammatory response, including secretion of interleukin 6 (IL-6), TNF- α , and ROS as well as upregulation of inducible nitric oxide synthase (iNOS). iNOS metabolizes L-arginine to nitric oxide (NO), an important mediator in the inflammatory process (Prame Kumar et al. 2018). In the literature, pro-inflammatory macrophages are commonly referred to as classical activated M1 macrophages, while the less inflammatory phenotype is known as alternatively activated M2 macrophages, which are more prevalent during the reparative phase following MI (Mosser and Edwards 2008;

Duncan et al. 2020; Shapouri-Moghaddam et al. 2018; Martinez and Gordon 2014). Activation signals for the inflammatory macrophages include contact with interferon gamma (IFN- γ), granulocyte-macrophage colony-stimulating factor (GM-CSF), TNF- α , microbial products (e.g. lipopolysaccharide), immune complexes, chemical mediators, and extracellular matrix proteins, leading to the transition from the resting to the activated state, that can also be influenced *in vitro* (Murray et al. 2014; Bashir et al. 2016). Macrophages exposed to inflammatory stimuli release high levels of inflammatory cytokines and modulate the activities of leukocytes, fibroblasts, endothelial cells and contribute to the subsequent healing process (Duncan et al. 2020). IL-6 and TNF- α , for example, are linked to fibrosis by stimulating CFs proliferation and collagen synthesis, contributing to the fibrotic remodelling of the heart (Thomas and Grisanti 2020).

Essential for the following healing phases and long-term survival post-MI is the regulation of factors that affect CF activation. CFs are the central players during the entire proliferative and maturation phase in cardiac healing up to the point of scar tissue formation (Chistiakov et al. 2016; Frangogiannis 2012; Camelliti et al. 2005). The process of CFs activation involves the transition from a homeostatic fibroblast phenotype to a phenotype that is tailored to the surrounding milieu (Mouton et al. 2019). For instance, CFs respond similarly to macrophages and neutrophils to inflammatory molecules released by for example necrotic CMs (Turner 2016). It is well known, that CFs express multiple DAMP receptors like toll-like receptors (TLRs) (Mouton et al. 2019; Turner 2016). During the early phase post-MI, CFs adopt a pro-inflammatory phenotype, hallmarked by the secretion of cytokines and chemokines, and exhibit matrix degrading properties. ROS, cytokines such as IL-1 β and TNF- α and matrix fragments induce inflammatory fibroblast activation and promote this phenotype (Li et al. 2021). Activation of CFs in the infarct border zone and in the non-infarcted myocardium may play an important role in the pathogenesis of post-MI remodelling by modulating aspects of the initial response such as leucocyte infiltration and contribution to ECM, which serves as a structural scaffold for CMs (Travers et al. 2016).

1.6. Proliferation and maturation phase following MI

The reparative process (day 7 - day 28) following MI is characterized by suppression, resolution and containment of the initial pro-inflammatory response, with key players being pro-resolving fibroblasts/myofibroblasts and M2-macrophages (**Fig. 4**) (Chalise et al. 2023).

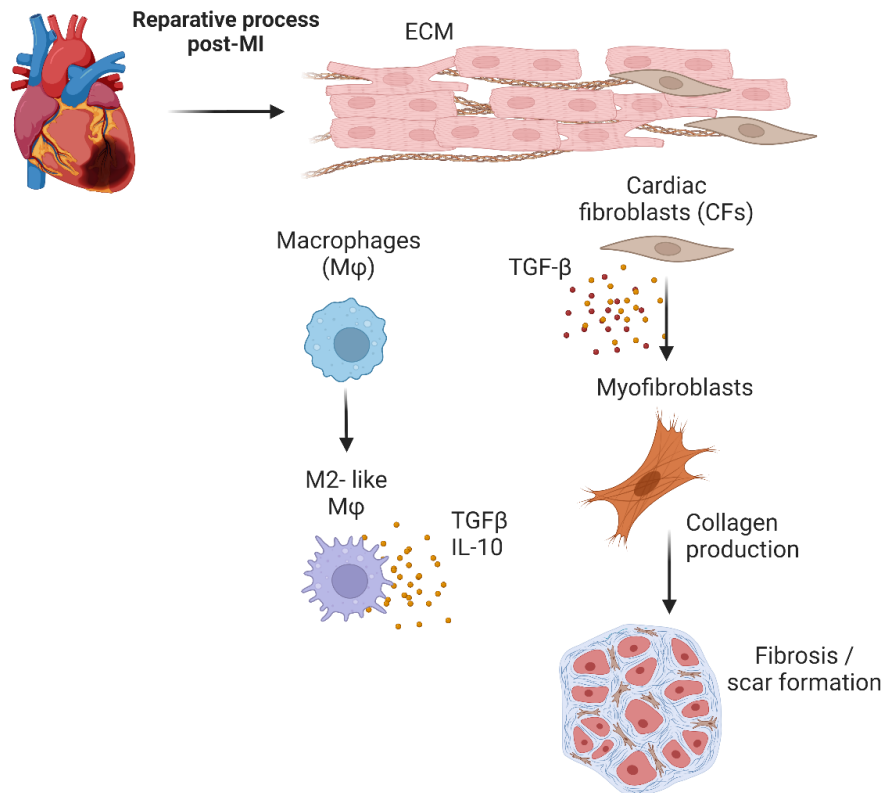


Figure 4: Characteristics of the reparative process post-MI. After the initial pro-inflammatory phase, the transition of tissue macrophages - whether resident or recruited (monocyte derived) - undergo a polarization shift towards an anti-inflammatory phenotype, accompanied by the production of TGF- β and IL-10. In addition to TGF- β , other pro-inflammatory cytokines (e.g. IL-6) trigger the transition of cardiac fibroblasts (CFs) into collagen-producing myofibroblasts. Over several weeks, monocyte recruitment ceases, and the scar matures, a process facilitated by ECM cross-linking, which is mediated by myofibroblasts. Graphic created with BioRender.

Key feature of the early reparative process is the reduced monocyte recruitment due to the downregulation of chemokines and functional alterations of macrophage populations (Duncan et al. 2020). These initial infiltrating populations exhibit a pro-inflammatory phenotype, which, over the following days, shifts to a predominantly reparative M2-like phenotype. Pro-resolving M2-like macrophages are characterized by the production of high levels of anti-inflammatory cytokines such as IL-4, IL-13, IL-10, IL-1 β , and TGF- β , thereby influencing or modulating fibrosis (Mouton et al. 2018; Bashir et al. 2016; Murray et al. 2014). These mediators act to suppress the pro-inflammatory response, as heightened inflammation is associated with fibrosis (Lis-López et al. 2021). This M2-like phenotype of macrophages can be divided into

subtypes known as M2a, M2b, M2c and M2d (only in mice) (Murray et al. 2014; Mosser 2003). The differentiation of pro-resolving macrophages can be induced by various stimuli, including IL-4 and IL-13, TLR ligands, IL1 receptor ligands, or IL-10 and plays pivotal roles in tissue repair, immunosuppression, crosstalk with B cells, induction of Th2-type humoral immune responses and scavenging mechanisms (Funes et al. 2018; Mosser 2003; Foey 2014). Recent studies have revealed that the conventional classification of macrophage subtypes into distinct categories such as classical M1/M2 macrophages cannot be reliably upheld *in vivo*. By performing single-cell RNA sequencing analysis of macrophages following diseases like MI in mice, it has been observed that pro-inflammatory M1-like macrophages also express cytokines typically associated with anti-inflammatory phenotypes (Mouton et al. 2018; Zhuang et al. 2022). Consequently, it is increasingly evident that macrophage phenotypes exist along a continuum, displaying characteristics of both pro-inflammatory and anti-inflammatory states, thereby suggesting the presence of intermediate phenotypes.

Simultaneously, resident fibroblasts start to proliferate and migrate from the remote zone into the border zone of the infarct in response to TGF- β secretion and other cytokines that influence proliferation of fibroblasts like IL-10, VEGF, IL-6 and TNF- α (Chistiakov et al. 2016; Ma et al. 2017). Once arrived, they transdifferentiate into alpha smooth muscle actin (α -SMA)-expressing myofibroblasts with an extensive endoplasmic reticulum, which can produce significant amounts of ECM proteins such as collagens (Humeres and Frangogiannis 2019). Excessive collagen deposition can give rise to substantial scarring and fibrosis, ultimately contributing to recurrent HF by affecting cardiac function due to the stiffness of the non-elastic collagen (Kong et al. 2014; Frangogiannis 2021). Therefore, it is crucial to promote a balanced scar formation. Specifically, collagen types with elastic functionality, such as collagen III (Col III) play a pivotal role in supporting the cardiac pumping function. Conversely, a lower abundance of collagen I (Col I) is advantageous in order to achieve optimal outcomes in heart tissue repair and regeneration (Kong et al. 2014). Collagen type I constitutes 85% of cardiac collagen, showing a lower turnover rate, yet imparting tensile strength and resistance to stretch and deformation of heart tissue. Conversely, collagen type III, though less abundant, is more specialized or particular to the structure and function of the heart and imparts resilience. Therefore, a decreased collagen type I / collagen type III ratio is associated with improved cardiac function (Mukherjee and Sen 1993; Frangogiannis 2021; Humeres and Frangogiannis 2019).

Finally, as healing progresses, a mature scar forms, marking the resolution of the proliferative phase and signalling the beginning of the maturation phase (Humeres and Frangogiannis 2019). Scar formation, also known as the maturation phase, is characterized by the strengthening of the ECM through cross-linking and the gradual removal of myofibroblasts, macrophages, and cardiomyocytes via apoptosis (Turner 2016). There are different types of

cardiac fibrosis that can be observed in patients post-MI. Replacement fibrosis is the predominant pathology post-MI and is reflected in the building of fibrous scar tissue in areas of CM necrosis (Frangogiannis 2015). By enzymes, like lysyl oxidase, the collagen is cross-linked and the number of activated myofibroblasts in the infarct becomes markedly reduced. At this stage, myofibroblasts become quiescent with limited capacity of matrix-synthesis or expression of contractile proteins. The accumulation and maturation of collagens contribute to the formation of fibrotic scars, influencing cardiac contractility, relaxation, and electric coupling. However, scar formation remains essential to prevent conditions such as cardiac rupture and promote optimal cardiac function. In areas of the heart that were not directly impacted by MI but still in the remote zone, CFs may remain in a chronically activated state due to increased pressure on the heart (Moore-Morris et al. 2014). This chronic activation triggers an initiation of processes related to ECM deposition, contributing to cardiac fibrosis and diastolic dysfunction (Mouton et al. 2019). In contrast, a volume overload is linked to ECM loss and enlargement of the heart's chambers (van der Laan et al. 2012). The specific molecular mechanisms underlying the regulation of these different responses in the matrix due to varying pressure and volume remain unclear, but are significantly associated with tissue remodelling and HF.

1.7. Posttranslational modifications of arginine

Arginine, a vital amino acid, can undergo various posttranslational modifications (PTMs) that significantly influence cellular processes in both prokaryotes and eukaryotes (Yang and Bedford 2013; Guccione and Richard 2019; Paik and Kim 1967). These modifications, including citrullination, methylation, phosphorylation, ADP-ribosylation, carbonylation, and advanced glycation end-products (AGEs), intricately regulate DNA binding, gene transcription, protein-protein interactions, immune system activation, and proteolysis (Slade et al. 2014). Consequently, processes like apoptosis, immune response and inflammation are affected. Enzymatic PTMs of arginine, such as citrullination catalysed by protein arginine deiminases (PADs), are tightly regulated in normal cellular functioning but can be significantly altered under different pathological conditions (Bicker et al. 2012; Di Zhu et al. 2022). Citrullination, also known as deimination, encapsulates the conversion of arginine into citrulline, eliminating its positive charge and potentially interfering with methylation of the same residue (Bicker et al. 2012; Jones et al. 2009). Conversely, arginine methylation does not affect the positive charge of arginine but increases its bulkiness and hydrophobicity, presumably affecting the protein-protein interaction (Bedford and Clarke 2009). However, methyl-arginines exhibit poor susceptibility to PAD-mediated modifications, with significantly slower rates compared to unmodified arginine (Slade et al. 2014). Citrullination itself is a chemical transformation that changes the structure, charge and properties of the modified proteins. It can affect their function and their ability to interact with other molecules but is also essential for a variety of physiological and pathological processes, enabling proteins to participate in various cellular functions and disease-related processes (Stadler et al. 2013; Al-U'datt et al. 2021).

1.8. Structure and biological function of Peptidylarginine Deiminases (PADs)

PAD enzymes play a crucial role in PTM by converting the amino acid arginine to a citrulline residue (Kaore et al. 2013; Jones et al. 2009). Citrulline is also a by-product of the urea cycle, a metabolic pathway that converts toxic ammonia into urea, which is subsequently excreted through the bladder. In this cycle, carbamoylphosphate combines with ornithine to form citrulline. This reaction is catalysed by the enzyme ornithine transcarbamylase (Endo et al. 2004). PADs catalyse the deamination of arginine residues in a polypeptide chain (**Fig. 5**). In turn arginine deiminases (ADIs) catalyse the deamination of free arginine (Curis et al. 2005).

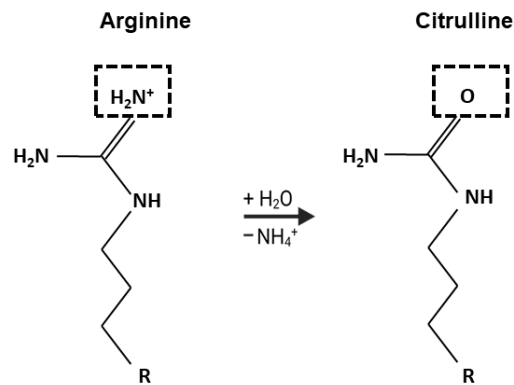


Figure 5: PAD-dependent citrullination. PADs catalyse the conversion of arginine into citrulline. Arginine deimination changes the charge of a protonated arginine residue to the neutral uncharged citrulline. The ketimine group (>C=NH) is replaced by a ketone group (>C=O). Graphic created with BioRender.

The first descriptions of a PAD enzyme responsible for this PTM were published in the late 1970s by Rogers et al. (ROGERS et al. 1977). PADs represent a category of enzymes, which divide up into PAD1-4 and PAD6 (Vossenaar et al. 2003). The genes of the PAD members are localized in a gene cluster on the human chromosome 1 (Vossenaar et al. 2003). In contrast to the well-preserved C-terminal region, each PAD isozyme exhibits substantial dissimilarity in its N-terminus. In mammals, the isozymes share a 50-70% sequence similarity (Knuckley et al. 2010; Vossenaar et al. 2003). However, the PAD activity is strictly regulated by calcium (Ca²⁺) (Nakashima et al. 2002). Considering the importance of high Ca²⁺ concentrations for PAD activation, it is still unclear how protein citrullination occurs under physiological conditions when calcium levels are kept low. Knuckley et al. showed that for PAD activation a Ca²⁺ concentration ranging between micro and millimolar is required, this process is usually found in the extracellular space (Knuckley et al. 2010). PAD1 is predominantly expressed in the epidermis and uterus. Citrullination of keratin and filaggrin, key components of keratinocytes and abundant in the skin/epidermis, has been observed (Vossenaar et al. 2003). PAD2 is highly expressed in the central nervous system; this includes the eye, brain, skeletal muscle as well as the spleen. In addition, PAD2 was found to be expressed in immune and blood cells like macrophages and granulocytes and to a lower degree in monocytes. The mRNA levels of *Padi2* remain constant during macrophage differentiation but the fully PAD2 protein is only detected in macrophages (Vossenaar et al. 2004). PAD3 influences structural proteins like filaggrin in the hair follicle and trichohyalin in the inner root sheath. Together with PAD1, PAD3 plays a role in terminal differentiation of the epidermis. PAD4 regulates gene expression through histone modification and is the only isoform with a classic nuclear localization sequence (NLS) (Jones et al. 2009; Vossenaar et al. 2003; Arita et al. 2004). It is normally localized in the nucleus and in cytoplasmic granules of immune and blood cells, tumor cells and stem cells. Therefore, PAD4 participates in various biological processes including

apoptosis, immune response and fibrosis (Mondal and Thompson 2019). In detail, PAD4 expression can be detected in many different types of tissues including spleen, kidney, colon, heart, brain and bone marrow and is found in both, immune cells such as neutrophils, monocytes, macrophages and non-immune cells such as epithelial cells, cardiomyocytes and fibroblasts (Mouton et al. 2019; Kain and Halade 2020; Mouton et al. 2018; Ko et al. 2022). It was long believed that PAD4 is the only PAD that can localize to the nucleus but Zeng et al. demonstrated that PAD2 also translocates into the nucleus in response to Ca^{2+} signalling (Zheng et al. 2019). PAD6 is expressed in eggs, ovaries and early embryos and is not enzymatically active due to mutations in the active site (Jones et al. 2009; Mondal and Thompson 2019).

1.9. Peptidylarginine Deiminase type 4 (PAD4) and its role in cardiac diseases

PAD4, consisting of 663 amino acids, was first identified in human myeloid leukemia HL-60 cells (Hagiwara et al. 2002). It features distinct N- and C-terminal domains, with the N-domain further divided into two immunoglobulin-like subdomains: Subdomain 1 (residues 1–118) and subdomain 2 (residues 119–300). Subdomain 2 contains three Ca^{2+} binding sites (Arita et al. 2006). Two additional Ca^{2+} binding sites are located in the C-terminal domain (**Fig. 6**). Ca^{2+} serves to stabilize the intermediate folding of PAD4 dimers, ensuring their proper conformation (Knuckley et al. 2010). The N-terminal domain includes a nuclear localization sequence (NLS: P₅₆PAKKKST₆₃), enabling interaction with various substrates.

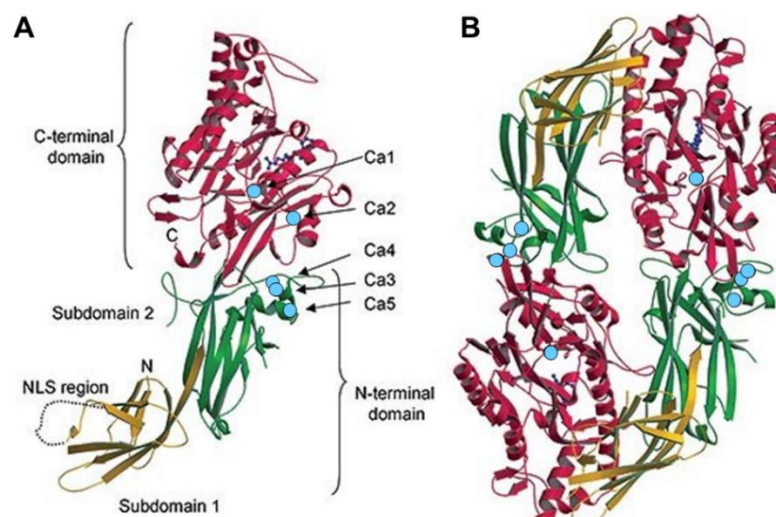


Figure 6: Structure and calcium binding sites of PAD4. (A) Representative three-dimensional representation of a PAD4 monomer with all five Ca^{2+} binding sites. Ca^{2+} ions are blue circles and arginine amide is a blue ball-and-stick model. The subdomains 1 and 2 and the C-terminal domain are indicated in yellow, green and red, respectively. The nuclear localization sequence (NLS) can be found in the N-terminal domain. (B) Representation of the dimeric form of PAD4 (adapted from Arita et al. 2004).

Among PAD4's most extensively studied substrates are histones (H1, H2A, H2B, H3, and H4). Citrullination by PAD4 at specific sites alters histone interactions with DNA and other nuclear proteins (Yang et al. 2021). Upon activation, PAD4 undergoes conformational changes, develops an active enzyme binding site and relocates to the nucleus. Its ability to citrullinate histones significantly influences gene expression (Knuckley et al. 2010). For instance, PAD4 contributes to the suppression of p53 activity, thereby modulating the expression of p53 target genes (Li et al. 2008). Moreover, the citrullination of histone H3 in neutrophils drives the formation of NETs and thereby facilitates host defence mechanisms (Brinkmann et al. 2004). Nevertheless, the function of PAD4 in the heart and in cardiac immune and non-immune cell populations remains poorly understood. Upregulation of PAD4 has been observed in various diseases, including atherosclerosis, cardiac fibrosis, HF and venous thrombosis as well as rheumatic arthritis (RA) (Al-U'datt et al. 2021; Fert-Bober et al. 2015). Numerous studies proposed that PAD4-mediated citrullination may influence the immune response in several ways (Eghbalzadeh et al. 2019; Fert-Bober et al. 2015). For example, as previously mentioned, PAD4 plays a role in NETosis, a process associated with neutrophil-mediated inflammation and tissue damage. Excessive NET formation has been linked with increased inflammation and adverse cardiac remodelling (Wu et al. 2023). Moreover, a correlation between elevated levels of NETs and various detrimental outcomes in patients suffering MI has been suggested. These outcomes included more frequent occurrences of microvascular obstruction, a larger area-at-risk and increased infarct size, reduced myocardial salvage index, and reduced left ventricular ejection fraction (He et al. 2021). On the other hand, NETs may exhibit anti-inflammatory features. Serine proteases within NETs can degrade cytokines and chemokines thus blunting inflammation (Hahn et al. 2019). Previous findings from our working group showed that mice with PAD4 deficiency, resulting in an inability to produce NETs, exhibit improved cardiac recovery, a benefit that appears to be independent of NETs formation (Eghbalzadeh et al. 2019). Collectively, whether NETs exert pro-inflammatory or anti-inflammatory effects post-MI remains a topic of ongoing research. However, apart from NETs, PAD4-mediated citrullination has been observed to alter proteins, resulting in changes to their structure and functionality (Mao et al. 2021; Yang et al. 2021). For example, Shelef et al. demonstrated that the citrullination of fibronectin modifies the behaviour of synovial fibroblasts, impacting their adhesion and invasiveness (Shelef et al. 2012). Studies by Li et al. revealed that the citrullination of vimentin triggers fibroblast activation and tissue inflammation, leading to the expression of fibrotic proteins and subsequently promoting pulmonary fibrosis (Li et al. 2021). Therefore, this modification contributes to inflammation and worsens tissue damage. Studies conducted by Fert-Bober et al. have identified unique citrullination patterns in the cardiac proteome using mass spectrometry. Their research revealed citrullination at numerous arginine sites in various proteins from heart samples of patients with HF compared to those

from healthy donors. Specifically, they detected nearly ten citrullinated proteins including several myofilament (Myosin heavy chain, Myosin binding protein C , Actin) and mitochondrial proteins (Fert-Bober et al. 2015). Furthermore, biochemical results revealed that citrullination of the contractile proteins may affect different aspects of regulatory function, by triggering a structurally change that is important for ATPase cycle (Fert-Bober et al. 2015). Additionally, citrullination of cytokines, chemokines, Glycogen Synthase Kinase-3 (GSK-3) and TGF- β was reported (Sipilä et al. 2016; Mao et al. 2021). Citrullination of active TGF- β hindered its binding to recombinant TGF- β receptor II, impeding its ability to activate TGF- β signalling. While these studies did not directly link citrullination of TGF- β to cardiovascular diseases, its role in cardiac fibrosis is unique. TGF β 1 signalling pathways drive myofibroblast transformation and induce myocardial fibrosis (Frangogiannis 2021, 2012).

Overall, several lines of evidence point towards a multifaceted importance of PAD4 and PAD4-mediated citrullination in pathophysiological events. However, potential detrimental effects of PAD4 in promotion of regenerative healing processes remain insufficiently explored. Therefore, further investigations are needed to better comprehend the functional role of PAD4 in mediating tissue regeneration.

2. Aim of the research

Citrullination of proteins has been observed to be elevated in individuals with HF, correlating with increased cardiac fibrosis and other cardiac complications. PAD enzymes, which regulate citrullination, are acknowledged as key players in modulating the immune response and cardiac remodelling. Among these, PAD4 stands out due to its direct involvement in regulating gene expression, primarily owing to its possession of a NLS and expression in immune cells.

Given the current absence of therapeutic interventions specifically targeting cardiac fibrosis and the limited comprehension of the interplay between inflammation and HF, targeting PADs/PAD4 emerges as a promising avenue. Pilot studies with PAD4-deficient mice showed significantly improved cardiac function after MI compared to WT. Moreover, research on CFs from PAD4^{-/-} mice revealed disrupted TGF- β signalling in these cells, which impacts the transition of CFs to myofibroblasts. Additionally, following TGF- β treatment, PAD4^{-/-} CFs exhibited decreased expression of type 1 collagen, underscoring the critical role of PAD4 in fibrosis regulation. Taking this into account, this study aims to elucidate the impact of PAD4 on the inflammatory response and subsequent cardiac remodelling following MI in mice. Additionally, it is proposed to investigate whether potential effects can be reproduced through pharmacological inhibition using a PAD inhibitor, thereby considering its clinical applicability. For this purpose, a mouse model was employed, in which MI was induced by permanent ligation of the LAD. This procedure leads to a permanent interruption of oxygen supply to the heart thereby supporting HF development. The following hypotheses were formulated and addressed:

1. Ablation of *Padi4* in mice and pharmacological inhibition of PADs reduce the inflammatory response following MI
2. PAD4 deficiency attenuates the extent of fibrosis post-MI
3. The absence or inhibition of PAD4 results in an improved survival rate at later stages post-MI

3. Material and Methods

3.1 Material

3.1.1 Instruments and expendable materials

Table 1: Overview of used instruments.

Instrument	Supplier
autoMACS Separator	Miltenyi Biotec
Binokular OLYMPUS SZ51	Leica
Benchtop anesthesia machine	Dr. Wilfried Müller GmbH
Centrifuge Allegra X-15R	Beckman Coulter
Centrifuge Microfuge 16	Beckman Coulter
ChemiDoc XRS+ Molecular Imager	BIO RAD
Control Unit M/S for Heating plate	BiosebLab
FACS Canto II	BD Biosciences
Flat Heating Plate	BiosebLab
Incubator CO ₂	Panasonic
Light OLYMPUS KL1500	Schott
Infrared lamp	TH. Geyer
Microcentrifuge 24R refrigerated PerfectSpin	Peqlab
Microscope inverted, Eclipse Ti-U 100	Nikon
Mouse Ventilator minivent Type 1	Hugo Sachs Elektronik-Harvard Apparatus
NanoDrop 2000c Spectrophotometer	ThermoFisher Scientific
pH meter	Mettler Toledo
Plate reader multimode VICTOR X3	Perkin Elmer
Precellys 24 Touch homogenizer	Bertin Technologies
Real time PCR System, StepOnePlus	Applied Biosystems
PCR QuantStudio 7 Flex	Applied Biosystems
Shaker 3006	GFL
Tube roller	Phoenix Instrument, CAT
Trans-Blot Turbo Transfer System	BIO RAD
Vortex genie 2	Scientific Industries
Water bath	Memmert

Table 2: Overview of used consumables.

Consumables	Supplier
Blotting filter paper	Invitrogen (ThermoFisher Scientific)
Bepanthen® Augen- und Nasensalbe	Bayer
Cell culture flasks T25, T75	VWR
Cell culture plates 6-,12-,96- well	VWR
Cell scraper	Sarstedt
Cell strainer 40 µm	Becton Dickinson
1.4 mm Zirconium oxide beads	Bertin Technologies
Cryotubes	VWR
Coverslips	VWR
Falcon tubes 15 ml, 50 ml	Sarstedt

Material and Methods

Introcan safety winged PUR	Braun
Kodan Tinktur forte	Schülke
Medicomp sterile 5 cm x 5 cm	Hartmann
MiniCollect Tube 1 ml EDTA plasma	Greiner
MicroAmp Fast 96-Well Reaction Plate	Applied Biosystems
Microwell plate 96F	ThermoFisher Scientific
Micro tubes 0.5 ml, 1.0, 2.0 ml	Sarstedt
2.0 ml tube with O-ring	Bertin Technologies
Needle	Becton Dickinson
Nitrocellulose membrane 0.2 µm	ThermoFisher Scientific
Petri dish 100 x 20 mm style	Sigma-Aldrich
Polystyrene tubes 5 ml, FACS tubes	Falcon
Stripettes, serological pipettes 5, 10, 25 ml	Sarstedt
8.0 PROLENE Polypropylen Suture	ETHICON
6.0 PROLENE Polypropylen Suture	ETHICON

3.1.2 Chemicals

Table 3: Overview of used chemicals.

Chemicals	Supplier
Albumin Fraktion V	Carl Roth
Albumin Fraktion V, endotoxin-tested	Carl Roth
Ampuwa water	Fresenius Kabi
APS	Sigma-Aldrich
Aqua dest.	Robbyrob
Agarose	Carl Roth
Chloroform	Carl Roth
Dimethyl sulfoxide (DMSO)	Carl Roth
Direct Red	Sigma-Aldrich
EDTA	Carl Roth
Ethanol	Carl Roth
FCS premium	PAN Biotech
Griess Reagent	Sigma-Aldrich
HBSS buffer with Ca and Mg	ThermoFisher Scientific
Heparin	Braun
Hydrochloric acid	Sigma-Aldrich
Isofluran	Piramal
RBC Lysis buffer	Merck Group
ROTIPHORESE®Gel 30	Carl Roth
2-Mercaptoethanol	Carl Roth, Invitrogen
Milk powder	Carl Roth
Mounting medium	DAKO
Sodium chloride (NaCl) solution	Carl Roth
Nuclease free water	Invitrogen
Paraformaldehyde	Merck, Acros organics
PBS	Sigma-Aldrich
Picric acid	Sigma-Aldrich
Phosphatase Inhibitor Cocktail	Cell Signaling Technology
Phenol	Sigma-Aldrich
Protease Inhibitor Cocktail	Cell Signaling Technology
PowerUp™ SYBR™ Green Master Mix	Applied Biosystems

Ponceau S	Carl Roth
SDS	Carl Roth
Sulfuric acid	Sigma-Aldrich
Sodium acetat	Sigma-Aldrich
Sodium nitrite	Carl Roth
TEMED	Carl Roth
TBS	Sigma-Aldrich
Tris	Carl Roth
Tris Base	Carl Roth
Tris-HCl	Carl Roth
Triton X-100	Sigma-Aldrich
TRIzol™ Reagenz	Ambion (ThermoFisher Scientific)
Trypane blue stain 0.4%	Invitrogen (ThermoFisher Scientific)
Trypsin-EDTA	Gibco (ThermoFisher Scientific)
Tween 20	Sigma-Aldrich
Xylene	TH. Geyer

3.1.3 Cell culture reagents

Table 4: Overview of used mediums for cell culture.

Cell culture medium	Supplier	Catalog No.
DMEM, high glucose	Gibco (ThermoFisher Scientific)	41965-039
DMEM, low glucose, pyruvate	Gibco (ThermoFisher Scientific)	31885-023
DMEM/F-12, GlutaMAX™ Supplement	Gibco (ThermoFisher Scientific)	31331-028
RPMI 1640, w: stable Glutamine, w: 2.0 g/L NaHCO ₃	PAN Biotech	P04-18500

Table 5: Overview of used cytokines and stimulating/growth factors in cell culture.

Cytokines and stimulating/growth factors	Supplier
Interferon gamma (IFN-γ)	Peprtech
Interleukin 4 (IL-4)	Peprtech
Lipopolysaccharides	Sigma-Aldrich
Macrophage colony stimulating factor (MCS-F)	Peprtech

3.1.4 Proteins and Enzymes

Table 6: Overview of used enzymes.

Proteins / Enzymes	Supplier	Catalog No.
Collagenase Type II	Sigma-Aldrich	C2-BIOC
DNase I recombinant	Sigma-Aldrich	04536282001
Hyaluronidase from bovine testes	Sigma-Aldrich	H3506
Proteinkinase K	Qiagen	154047662

3.1.5 Inhibitors and drugs

Table 7: Overview of inhibitors and drugs.

Inhibitors / drugs	Supplier	Stock solution
BB-CI-Amidine	Cayman Chemical	5 mg/500 µl in DMSO
Buprenorphin – hydrochlorid	Temgesic	0.324 mg/ml
CI-Amidine	Cayman Chemical	1 mg/100 µl in DMSO
Enrofloraxin	Baytril®	25 mg/ml
Penicillin/Streptomycin	Sigma-Aldrich	10.000 U penicillin and 10 mg streptomycin /ml in 0.9% NaCl
Staurosporine	Enzo	250 µg/2.140µl in DMSO

3.1.6 Sets and Kits

Table 8: Overview of sets and kits used in this study.

Kits	Supplier
ArC Amine Reactive Compensation Bead Kit	Invitrogen
BD™ CompBeads	BD Biosciences
CS&T Research Beads	BD Biosciences
CFSE Cell Division Tracker Kit	Biologend
cTnT / TNNT2 ELISA Kit	Elabscience
DNA-free™ Kit, DNase Treatment & Removal	Invitrogen (ThermoFisher Scientific)
Ghost Dye™ Violet 510 Viability Dye	Cell Signaling Technology
High Capacity cDNA Reverse Transcription Kit	Applied Biosystems
Mouse Clariom S Assay	ThermoFisher
One-step TUNEL <i>in situ</i> Apoptosis Kit	Elabscience
Pierce™ BCA Protein Assay Kit	ThermoFisher Scientific
Pierce™ ECL Western Blotting-Substrat	ThermoFisher Scientific
Precision Plus Protein™ Unstained Standards	BIO RAD
RNeasy Mini Kit	Qiagen
RNeasy FFPE Kit	Qiagen
Total Collagen Assay Kit (Perchlorate-Free)	Abcam
Trichrome Stain (Masson) Kit	Sigma-Aldrich
UptiLight™ HRP WB Chemiluminescent substrate	Interchim

3.1.7 Antibodies

Table 9: Overview of monoclonal antibodies used for flow cytometry.

Antibody	Host	Reactivity	Conjugate	Dilution	Company	Catalog No.
TruStain FcX™ (CD16/32)	rat	Mouse	/	1:500	Biolegend	101319
CD45	rat	mouse	PerCP-Cy5.5	1:80	Biolegend	103131
CD11b	rat	mouse	APC-Cy7	1:80	Biolegend	101225
Ly6G	rat	mouse	FITC	1:200	Biolegend	127605
F4/80	rat	mouse	PE-Cy7	1:100	Biolegend	123113
CCR2	rat	mouse	PE	1:50	Biolegend	150609
CD206	rat	mouse	FITC	1:20	Biolegend	141703

Table 10: Overview of products and antibodies used for autoMACS separation.

Product	Company	Catalog No.
MACS Columns MS	Miltenyi Biotec	130-042-201
Anti-Ly6G-Biotin, mouse	Miltenyi Biotec	130-123-854
Anti-CD11b-Biotin, mouse	Miltenyi Biotec	130-113-804
Anti-Biotin MicroBeads UltraPure	Miltenyi Biotec	130-105-637

Table 11: Overview of antibodies used for western blot.

Antibody	Host	Reactivity	Company	Catalog No.
Anti-TGF-β1	rabbit	mouse	Abcam	ab179695
Anti-Smad2	rabbit	mouse	Cell Signaling	5339
Anti-p-Smad2	rabbit	mouse	Cell Signaling	3108
Anti-β-Actin	rabbit	mouse	Cell Signaling	4967
Anti-GAPDH	rabbit	mouse	Cell Signaling	5174
Anti-collagen I	rabbit	mouse	Invitrogen	PA5-29569
Anti-collagen III	rabbit	mouse	Invitrogen	PA5-27828
Anti-Histone H3 (citrulline R2+R8+R17)	rabbit	mouse	Abcam	ab5103
Anti-pMLKL (Ser358)	rabbit	mouse	Cell Signaling	91689
HRP-conjugated polyclonal IgG	goat	rabbit	DAKO	P0448

Table 12: Overview of antibodies used for immunofluorescence.

Antibody	Host	Reactivity	Company	Catalog No.
Anti-α-SMA	rabbit	mouse	Abcam	ab5694
Anti-Histone H3 (citrulline R2+R8+R17)	rabbit	mouse	Abcam	ab5103
Anti-599 MPO antibody	goat	mouse	R&D Systems	AF3667
Anti-rabbit Alexa 593 Fluor 488	goat	mouse	Cell Signaling	4412
Anti-goat Alexa Fluor 488	donkey	mouse	Abcam	ab150129
Anti-rabbit Alexa 555	donkey	mouse	Abcam	ab150074

3.1.8 Staining solutions

Table 13: Overview of staining solutions used in this study.

Staining solutions	Company	Composition
DAPI	Sigma-Aldrich	1 mg/mL
Ghost Dye™ Violet 510	Cell Signaling Technology	ready to use
Sirius red solution	Sigma-Aldrich	0.5 g Direct Red in 500 ml Picric acid
Ponceau S solution	Carl Roth	0.1% Ponceau + 3% acetic acid
Trypane blue stain	ThermoFisher Scientific	0.4% in PBS

3.1.9 Buffer solutions

Table 14: Overview of buffers (self-made) used in this study.

For western blot:

Name	Composition
Blotting buffer	25 mM Tris, 192 mM glycine+ 20% methanol in H ₂ O
Laemmli sample buffer	250 mM Tris-HCl + 40% Glycerol + 8% SDS+ 0.01% Bromphenolblau in H ₂ O
RIPA buffer	50 mM Tris + 150 mM sodium chloride (NaCl) + 1% NP - 40 + 0.5% Na-deoxycholat + 0.1% SDS
Running buffer	25 mM Tris (pH 8.3 - 8.8) + 92 mM Glycin + 0.1% SDS + H ₂ O
Separating gel buffer	1.5 M Tris + 0.4% SDS in H ₂ O
Stacking gel buffer	0.5 M Tris + 0.4% SDS in H ₂ O
Stripping buffer	62.5 mM Tris (pH 6.8) + 2% SDS in H ₂ O
TBS buffer	7.7 mM Tris (pH 7.5) + 150 mM sodium chloride (NaCl) in H ₂ O
TBS/T buffer	7.7 mM Tris (pH 7.5) + 150 mM sodium chloride (NaCl) + 0.1% Tween 20 in H ₂ O

For Enzymatic digestion of hearts and flow cytometry:

Name	Composition
FACS buffer	PBS + 2% FCS and 1 mM EDTA, pH 8.0
HBB buffer	HBSS + 2% FCS + 0.2% BSA
MACS buffer	PBS + 0.5% BSA and 2 mM EDTA, pH 8.0
Viability staining buffer	PBS + 0.5% BSA

For immunofluorescence:

Name	Composition
Citrate buffer	10 nM sodium citrate + 0.05% Tween 20; pH 6.0 + H ₂ O
Permeabilization buffer	TBS + 0.5% TritonX-100
Washing buffer (for staining)	TBS + 0.05% TritonX-100

For genotyping:

Name	Composition
Digestion buffer	1% SDS + 100 mM NaCl + 50 mM Tris-HCl (pH 8.0) + 10mM EDTA (pH 8.0) + H ₂ O
TAE buffer	40 mM Tris base + 2 mM EDTA + 20 mM acetic acid + H ₂ O, pH 8.5

3.1.10 Primer

Table 15: Primer sequences. Fwd, forward primer. Rev, reverse primer.

Species	Gene	Sequence
Homo sapiens	<i>Padi4</i>	Fwd: 5'- AGCAACATCTGGGGACAAAC -3' Rev: 5'- CCCAGGTTTCAGTTTGCATT -3'
	<i>18s</i>	Fwd: 5'- CGGCTACCACATCCAAGGAA -3' Rev: 5'- GCTGGAATTACCGCGGCT -3'
Mus musculus	<i>18s</i>	Fwd: 5'- CGGCTACCACATCCAAGGAA -3' Rev: 5'- GCTGGAATTACCGCGGCT -3'
	<i>Acta2</i>	Fwd: 5'- GGCTCTGGGCTCTGTAAGG -3' Rev: 5'- CTCTTGCTCTGGGCTTCATC -3'
	<i>Ccl2</i>	Fwd: 5'- AGCACCAGCCAACTCTCACT -3' Rev: 5'- CGTTAACTGCATCTGGCTGA -3'
	<i>Ccr2</i>	Fwd: 5'- ATTCTCCACACCCTGTTTCG-3' Rev: 5'- CTGCATGGCCTGGTCTAAGT-3'
	<i>Ccl6</i>	Fwd: 5'- GGCTGGCCTCATACAAGAAA -3' Rev: 5'- TCCCCTCCTGCTGATAAAGA -3'
	<i>Ccl9</i>	Fwd: 5'- TGTTTCACATGGGCTTTCAA -3' Rev: 5'- TTGTAGGTCCGTGGTTGTGA -3'
	<i>Col1a1</i>	Fwd: 5'- GTAATCCTGGTGGTGTGATG -3' Rev: 5'- GAAGCCTCTTTCTCCTCTCTGA -3'
	<i>Col3a1</i>	Fwd: 5'- GCCCACAGCCTTCTACAC -3' Rev: 5'- CCAGGGTCACCATTTCTC -3'
	<i>Col6a3</i>	Fwd: 5'- TGTGAATGGCACACAAGGTT -3' Rev: 5'- CTTCCAGGACTCCCCTTTTC -3'
	<i>Fzd1</i>	Fwd: 5'- CAAGGTTTACGGGCTCATGT -3' Rev: 5'- GTAACAGCCGGACAGGAAAA -3'
	<i>Gapdh</i>	Fwd: 5'- CGACTTCAACAGCAACTCCCCTCTTCC -3' Rev: 5'- TGGGTGGTCCAGGG-TTTCTTACTCCTT -3'
	<i>Il1a</i>	Fwd: 5'- GCAACGGGAAGATTCTGAAG-3' Rev: 5'- TGACAAACTTCTGCCTGACG-3'
	<i>Il6</i>	Fwd: 5'- CCACTTCACAAGTCGGAGGCTTA -3' Rev: 5'- GCAAGTGCATCATCGTTGTTTCATAC -3'
	<i>Il12</i>	Fwd: 5'- GGTCACTGGACCAAGGGACTATG -3' Rev: 5'- ATTCTGCTGCCGTGCTTCCAAC -3'
	<i>Mmp2</i>	Fwd: 5'- TTCCCCCGCAAGCCCAAGTG -3' Rev: 5'- GAGAAAAGCGCAGCGGAGTGACG -3'
	<i>Mmp9</i>	Fwd: 5'- TCACCTTCACCCGCGTGTA -3' Rev: 5'- GTCCTCCGCGACACCAA -3'
	<i>Mpo</i>	Fwd: 5'- GCCAAACTGAATCGCCAGA -3' Rev: 5'- ATGTTAAGAGCAGGCAAATCCA -3'
	<i>Nos2</i>	Fwd: 5'- CTGCTGGTGGTGACAAGCACATTT -3' Rev: 5'- ATGTCATGAGCAAAGGCGCAGAAC -3'
	<i>Padi1</i>	Fwd: 5'- GCCCTGATGAGCTTTTTGAG -3' Rev: 5'- GAGAGAGAGCAGCCCTGAGA -3'
	<i>Padi2</i>	Fwd: 5'- GAGGAGCGTTCTTCACTTTCT -3' Rev: 5'- GGCAGGAGCATCTTCATATAACC -3'
	<i>Padi3</i>	Fwd: 5'- ATAAGAGGCAGTGGGTGTGG -3' Rev: 5'- GCTGGAGGTGTGGAGGATAA -3'
	<i>Padi4</i>	Fwd: 5'- GGCTACACAACCTTCGGCAT -3' Rev: 5'- GCTGCTTTCACCTGTAGGGT -3'

<i>Padi6</i>	Fwd: 5'- ATTCCCATCTCCCAGCTTCT -3' Rev: 5'- ACCACCTGCACTTTGCTCTT -3'
<i>Pdgfra</i>	Fwd: 5'- TTGGTGCTGTTGGTGATTGT -3' Rev: 5'- TCCCATCTGGAGTCGTAAGG -3'
<i>Smad7</i>	Fwd: 5'- CAGCTCAATTCGGACAACAA -3' Rev: 5'- AACCAGGGAACACTTTGTGC -3'
<i>Tgfb1</i>	Fwd: 5'- GGCGAAGGCATTACAGTGTT -3' Rev: 5'- TGCACATACAAATGGCCTGT -3'
<i>Tgfβ</i>	Fwd: 5'- TGACGTCCTGGAGTTGTACGG -3' Rev: 5'- GGTTTCATGTCATGGATGGTGC -3'
<i>Tnfa</i>	Fwd: 5'- CCGATGGGTTGTACCTTGTC -3' Rev: 5'- GGGCTGGGTAGAGAATGGAT -3'

3.2 Methods

3.2.1 Cell culture

3.2.1.1 Thawing and freezing of cells

Cryogenically preserved cells were thawed by immersion in a 37°C water bath until approximately 80% of the cell suspension was defrosted. Then, cells were resuspended in 1 ml of pre-warmed cell culture medium supplemented with a minimum of 5% FCS. Subsequently, the cells were rapidly transferred into a 15 ml tube containing 9 ml of appropriate culture medium to dilute the cryopreservation agent dimethyl sulfoxide (DMSO). Following this, centrifugation was performed at 400 × g for 5 min at 4°C. Afterwards, supernatants were removed and cells were resuspended in an adequate volume of cell culture medium, transferred to cell culture dishes, and then incubated at 37°C with 5% CO₂ for subsequent experiments.

For freezing, adherent cells were detached from the culture surface using 0.05% trypsin / 0.02% EDTA in PBS for 5 min at 37°C and 5% CO₂. After microscopical verification, cell culture medium containing at least 5% FCS was added to stop the trypsin-EDTA reaction. Cells were collected in a 15 ml tube and centrifuged at 400 × g for 5 min at 4°C. Then the supernatant was aspirated, and the cell pellet was resuspended in 1 ml of freezing medium consisting of FCS and 10% DMSO. The cell suspension was then aliquoted into cryotubes and gradually frozen overnight at -80°C using a freezing container filled with 100% isopropanol to achieve a controlled cooling rate of 1°C per minute. For long-term storage, cells were placed in liquid nitrogen.

3.2.1.2 Isolation of bone marrow cells from mice

For isolation of bone marrow (BM) cells, 8-12-week old WT or PAD4^{-/-} mice were euthanized by cervical dislocation. The skin of the hind legs was peeled off and legs were dissected to remove the femur and tibia. All muscle tissue was removed from femur and tibia. To separate the femur and tibia, the bones were cut below the knee joint and between the foot end of the tibia and the pelvic end of the femur. The femurs and tibias were collected in PBS on ice, washed with 70% ethanol for 10 min and placed under the clean bench to ensure sterility. Then, bones were washed with sterile PBS before collection of BM. Both epiphyses of each bone were removed with sterile scissors and forceps. To isolate the whole BM, each bone was flushed with PBS by inserting a 2 ml syringe with a 25-needle into the bone shaft. The BM obtained was collected in a culture dish containing cold PBS. The cell suspension was transferred to a 50 ml tube, and cells were centrifuged at 400 × g for 5 min at RT. Afterwards,

to remove the erythrocytes, the cell pellet was suspended in 6 ml of sterile 0.2% sodium chloride and incubated for 45 sec. The lysis reaction was stopped by adding 14 ml of sterile 1.2% sodium chloride. The cell suspension was then transferred to a new tube using a 70 µm filter to remove cell aggregates. After centrifugation at 400 × g for 5 min at 4°C, cells were resuspended according to intended use.

3.2.1.3 Cultivation of adherent and non-adherent cells

Bone marrow-derived macrophages

Macrophages were differentiated from thawed or freshly isolated BM cells. For this purpose, cells were cultured in RPMI-1640 medium supplemented with 20% FCS and 100 U/ml penicillin, 10 µg/ml streptomycin, and 20 ng/ml recombinant murine macrophage colony-stimulating factor (M-CSF) at 37°C and 5% CO₂ for 7 days. On days 3 and 6, the differentiation medium was renewed by removing 1 ml of medium from the cultured cells and adding 1 ml of differentiation medium supplemented with 40 ng/ml M-CSF. Differentiated macrophages (M0) were obtained on day 7.

Cardiac fibroblasts

Cardiac fibroblasts (CFs) were isolated by magnetic-activated cell sorting as described in section 3.2.3.9. To cultivate CFs, 25 cm² flasks were precoated with 1 ml of sterile 0.1% gelatine in distilled water and incubated at 37°C with 5% CO₂ for 1 h. Subsequently, after gelatine was removed, the isolated cell suspensions from two pooled hearts were seeded in DMEM/F12 medium supplemented with 10% FCS, 100 U/ml penicillin, and 10 µg/ml streptomycin. Non-adherent cells were removed after 4 h of cultivation, and the remaining cells were cultured until reaching 90% confluence, representing passage 1.

Jurkat cells

Jurkat cells were cultured in RPMI-1640 medium supplemented with 20% FCS and 100 U/ml penicillin, 10 µg/ml streptomycin at 37°C and 5% CO₂. The culture was sustained by regular medium replacement or addition of fresh medium. To maintain optimal viability, the cell concentration was kept between 1 × 10⁵ and a maximum of 1 × 10⁶ viable cells/ml.

To passage the cells, non-adherent Jurkat cells were collected in a falcon tube and centrifuged at 200 × g for 5 min, counted and seeded to a density of 1 × 10⁵ viable cells/ml in a 75 cm² culture flask.

3.2.1.4 Polarization of bone marrow-derived macrophages

For polarization of M0 macrophages into pro-inflammatory M1-like cells, the RPMI-1640 medium supplemented with 20% FCS and 100 U/ml penicillin, 10 µg/ml streptomycin was removed, cells were washed once with PBS, and 2 ml of RPMI-1640 medium supplemented with 10% FCS and 100 U/ml penicillin, 10 µg/ml streptomycin was added. Then, 20 ng/ml recombinant mouse IFN-γ and 100 ng/ml LPS were added and cells were incubated for 24 h at 37°C and 5% CO₂. To inhibit PAD activity, M0 macrophages were pre-incubated with the pan-PAD inhibitor Cl-Amidine (200 µM) for 1h at 37°C with 5% CO₂. Subsequently, the cells were polarized into pro-inflammatory M1-like cells, as described above, in the presence of Cl-Amidine.

3.2.1.5 Assessment of efferocytosis

To assess the efferocytosis capacity of WT and PAD4^{-/-} macrophages, BMDM were plated in a density of 2×10^5 cells/well in a 48-well plate in RPMI-1640 medium supplemented with 10% FCS and 100 U/ml penicillin, 10 µg/ml streptomycin and polarized to an M1-like phenotype as previously described. Afterwards, 1×10^6 Jurkat cells were labelled with CFSE Cell Division Tracker Kit according to the manufacturer's instructions for 20 min in the dark in a 6-well plate. Labelled Jurkat cells were exposed to 1 µM staurosporine for 3 h to induce apoptosis. After centrifugation by $400 \times g$ for 5 min at 4°C, apoptotic cells were added to macrophage cultures in a 1:4 ratio for 30 min at 37°C and 5% CO₂. Afterwards, the supernatant was carefully removed, and macrophages were washed three times with PBS to remove non-engulfed Jurkat cells. Subsequently, macrophages were detached using 0.05% trypsin-EDTA, centrifuged by $400 \times g$ for 5 min at 4°C, and suspended in FACS buffer. After incubation with Fc blocking antibody (1 µg/ 1×10^6 cells) for 5 min, cells were incubated with PE-Cy7-conjugated antibody targeting F4/80 for 25 min on ice and further analysed for carboxyfluorescein diacetate, succinimidyl ester (CFSE) uptake by FACS analysis. The excitation and emission wavelengths of CFSE labelled cells are 492 nm and 517 nm, respectively. Double-positive cells indicated engulfment of apoptotic Jurkat cells.

3.2.2 Human sample collection

In collaboration with Univ.-Prof. Dr. Rothschild and PD Dr. Kamphausen of the Institut of Forensic Medicine in Cologne, *post-mortem* human heart tissue samples were collected from the infarcted LV of individuals, along with samples from the corresponding RV and control patients without cardiac diseases. The duration of *post-mortem* days did not surpass four days. The ethics committee of the University of Cologne approved this study (No. 23-1146). Isolated *post-mortem* human heart tissue, used for this study, was collected, fixed in 4% paraformaldehyde overnight, dehydrated and embedded in paraffin in the Institut of Forensic Medicine.

3.2.3 Mouse handling and experiments

3.2.3.1 Animal care

All animal procedures were reviewed and approved by the local animal care committee (Bezirksregierung Köln; Landesamtes für Natur, Umwelt und Verbraucherschutz (LANUV), Germany, No. 81-02.04.2019.A318). All experiments and protocols were performed in accordance with European, national, and institutional guidelines. Mice were housed at 22 – 24°C in a 12/12h light/dark cycle under specific pathogen free conditions and free access to water and standard rodent chow. For breeding, male and female mice were placed together at an age of 8 weeks minimum. Litters were marked with ear punches and weaned at the age of 3 weeks.

3.2.3.2 Mice strains

The PAD4-deficient mouse strain has been successfully established in the working group (Egbalzadeh et al.). PAD4^{-/-} mice are vital, fertile and have no visible phenotype. In brief, PAD4-deficient mice were generated by mating Padi4^{fllox/fllox} (#026708, Jackson Laboratory) with CMV-Cre mice (#006054, Jackson Laboratory) for deletion of *loxP*-flanked exons 9-10 in the *Padi4* gene. These exons encompass part of the PAD4 active site, as well as four additional residues that are essential for Ca²⁺ binding. PAD4^{-/-} mice are on a C57BL/6J genetic background. C57BL/6J WT mice were obtained from the Jackson laboratory and bred in the working group. Genotyping was routinely performed by laboratory staff using PCR and agarose gel electrophoresis. DNA used for genotyping was isolated from ear punches from animal markings.

3.2.3.3 Pharmacological inhibition of PADs *in vivo*

BB-CI-Amidine is a modified form of a common PAD inhibitor CI-Amidine (chloramidine). It irreversibly inhibits the activity of all PAD isoforms, but has a 20-fold higher sensitivity for the PAD4 isoform. The inhibitor (stock solution in DMSO) was administered s.c. at a concentration of 1 mg/ml in 0.9% NaCl solution (total volume: 50 µl/10 g body weight) starting 30 min before surgery or at day 7 post-MI and then once daily until the final day of experiment.

3.2.3.4 Induction of MI in mice

Mice were placed in a chamber and exposed to 3% isoflurane with an oxygen flow rate of 1 l/min for initial anesthesia induction. Following a brief interval of 2 min, the animals were removed from the chamber and positioned supine on a warming plate to prevent hypothermia. To maintain anesthesia, mice were promptly intubated with a continuous oxygen flow rate of 1 l/min and 2% isoflurane, and then subjected to mechanical ventilation at a rate of 120 breaths/min. A slight hyperextension of the head was required during intubation to adequately separate the trachea from the esophagus.

After local removal of body hair, an intercostal incision was made between the 4th and 5th left rib to access the thoracic cavity, exposing the left ventricle. Once the left anterior descending artery (LAD) was identified, it was ligated with an 8-0 polypropylene suture. It was crucial to incorporate some surrounding tissue within the knot to achieve successful ischemia (**Fig. 7**). Ischemia was visually confirmed by observing blanching extending from the ligation point down to the apex. Subsequently, the thoracic cavity and skin were closed with 6-0 polypropylene suture. To prevent surgery-related infections, animals received s.c. endofloxacin at a dosage of 5 mg/kg, with a total volume of 20 µl/10 g body weight. Upon completion of the surgical procedure, which typically lasted about 20 min, the supply of isoflurane was reduced. Animals were observed until reflexes occurred, and then promptly extubated from the oxygen flow rate of 1 l/min. Depending on the experiment, mice were sacrificed on day 1, 3, 7, or 28 after ligation.

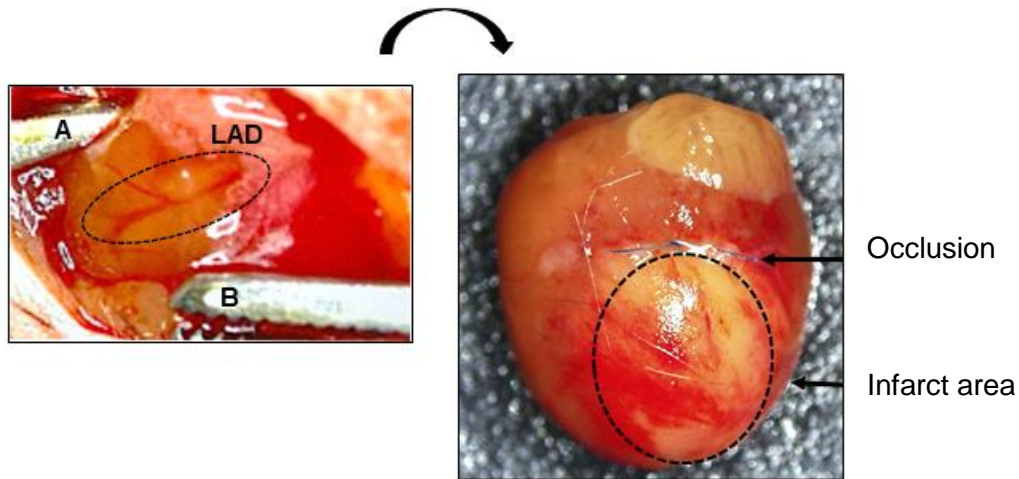


Figure 7: Representative images of mice hearts during/after MI induction by left anterior descending artery (LAD) ligation. Left site: LAD is encircled by a dotted line. The ligation was initiated at the upper edge of the image (**A**) using surgical thread and closed below the LAD (**B**). Right site: Infarcted heart *ex vivo*.

3.2.3.5 Scoring and analgesia

Analgesia was administered every 8 h using buprenorphine diluted in 0.9% NaCl solution (s.c. 0.1 mg/kg) over a total duration of 3 days post-surgery. The treatment was continued in response to any perception of pain. Animals were monitored daily, and their health status was assessed using a score sheet approved by LANUV. Mice with severe signs of pain and distress were excluded from the study and euthanized by cervical dislocation.

3.2.3.6 Verification of infarcts by transthoracic echocardiography

To verify a successful ligation of the LAD, transthoracic echocardiography was performed with a preclinical Imaging System for small animal research (Fujifilm, Vevo 3100). Mice were transferred to a chamber and continuously exposed with 2% isoflurane and an oxygen flow rate of 1 l/min to keep them under anaesthesia. Afterwards mice were placed on a temperature-controlled platform to prevent hypothermia caused by the ultrasound gel and to ensure physiological heart and respiratory rates. Ultrasound gel was applied to the depilated skin of the chest of the mice. After locating the heart with a MX550d transducer, imaging was performed to verify MI. For a successful ligation of the LAD, a slowed heartbeat was observed on the left ventricle, starting under the atrium and ending at the apex. Upon this recognition, the skin was cleaned from the gel, isoflurane was reduced, and once the mice exhibited signs of reflexes, they were returned to the cage for further analysis.

3.2.3.7 Cardiac plasma collection

After initial anaesthesia (3% isoflurane, oxygen flow rate of 1 l/min) mice were placed in a supine position on a small experimental plate with continuously maintained under anaesthesia (1.8% - 2% isoflurane, oxygen flow rate of 1 l/min). The extremities were extended and immobilized to induce stretching of the mice. The skin was incised in the middle of the abdominal area, and the sternum was immobilized using a clamp to maximally open the abdominal cavity. To achieve an optimal view of the heart, the ligament located at the lower edge of the diaphragm and attached to the liver, was carefully cut off. As soon as the beating heart was detected, blood was collected using a 1 ml syringe with a 30 G needle and slowly isolated without any interruption. After approximately 800 µl of blood were isolated, it was transferred into MiniCollect® EDTA tubes. The blood samples were centrifuged at 3000 × g for 10 min at RT. Subsequently, the plasma was collected and immediately transferred to a freezer at -80°C for storage and further experiments.

3.2.3.8 Enzymatic digestion of infarcted mouse hearts

Following cardiac plasma collection, hearts underwent perfusion with isotonic 0.9% NaCl solution to clear residual blood. Subsequently, the atria of the heart were removed and the entire heart, including infarct and border zone, was enzymatically digested. For this, heart tissue was minced in small pieces and incubated with collagenase type II (450 U/ml), hyaluronidase (60 U/ml), and DNase I (60 U/ml) for 50 min at 37°C in DMEM, low glucose medium without any supplements. After vortexing for 30 sec, cells were triturated and filtered through a pre-wetted 40 µm cell strainer with HBB buffer to remove cell clumps and collected in a 50 ml falcon tube. The filter was rinsed with 10 ml of HBB buffer and cell suspension were transferred to a 15 ml falcon tube and centrifuged at 400 × g for 5 min at 4°C. Afterwards supernatants were removed and the cell pellet was resuspended in 1 ml of FACS buffer. For red blood cells lysis cell suspension were incubating for 30 sec in 3 ml of RBC lysis buffer. Followed by the addition of 10 ml of HBSS. Cells were centrifuged at 400 × g for 5 min at 4°C and resuspended in MACS or FACS buffer, respectively.

3.2.3.9 Isolation of cardiac monocytes / macrophages (Mo/M ϕ) and cardiac fibroblast (CFs)

Cardiac Mo/M ϕ or CFs were isolated from enzymatically digested hearts by magnetic activated cell sorting (MACS). Cells from two enzymatically digested hearts (approximately 1.5×10^6 cells/heart) were pooled and incubated with Fc blocking antibody (1 μ g/ 1×10^6 cells in 100 μ l) for 10 min on ice. Cell suspensions were further incubated with anti-Ly6G-biotin antibody (1:50) for 10 min at 4°C, washed twice with 1 ml of MACS buffer, followed by centrifugation at $400 \times g$ for 5 min at 4°C. Cells were resuspended in 80 μ l MACS buffer and incubated with 20 μ l anti-biotin microbeads for 20 min at 4°C before negative selection using autoMACS. Neutrophil-depleted cell suspensions were further incubated with biotin-labelled anti-CD11b antibody (1:50) for 10 min at 4°C, washed twice in MACS buffer, centrifuged at $400 \times g$ for 5 min at 4°C and incubated with anti-biotin microbeads for 20 min at 4°C, as previously described. Cardiac Mo/M ϕ were separated by positive selection using magnetic columns. Freshly isolated cells were centrifuged and cell pellets were stored at -80°C until further processing.

For isolation of CFs, cell suspensions depleted for Ly6G and CD11b were cultivated as described earlier in section 3.2.1.3.

3.2.4 Molecular biology

3.2.4.1 RNA isolation and quantification

Total RNA was extracted using RNeasy Mini Kit (Qiagen) or Tri Reagent (Sigma Aldrich) according to the manufacturer's instructions for cell lysates or heart tissue, respectively. Before RNA extraction for heart tissue, frozen sections (19 mg – 31 mg) were homogenized using a Precellys 24 Touch homogenizer and zirconium oxide beads. To achieve this, tissue sections were placed into a 1 ml tube pre-filled with 800 μ l of TRIzol™ Reagent along with approximately 10 zirconium oxide beads. Homogenization was carried out at 6500 rpm for 20 sec, followed by a 5-sec pause, and this cycle was repeated three times. The supernatant was transferred into a new tube and further procedure was carried out according to the manufacturer's instructions.

For RNA isolation from tissue samples embedded in paraffin, the RNA was extracted using the FFPE RNeasy Qiagen Kit following the manufacturer's instructions.

RNA quality was evaluated by measuring the absorption at 260 nm and 280 nm as well as 260 nm and 230 nm using NanoDrop spectrophotometer. The purity of RNA was assessed by calculating the ratio of A_{260}/A_{280} and A_{260}/A_{230} with 2 being pure RNA. Ratios below 2 or above 2 were indicative of protein or genomic DNA contamination, respectively.

3.2.4.2 DNA removal from RNA samples

To remove contaminating DNA, the isolated RNA was treated with DNase following the protocol outlined in the DNA-free™ DNA Removal Kit. Briefly, RNA samples were combined with DNase Buffer and rDNase, followed by an incubation period of 25 min at 37°C. Subsequently, DNase was inactivated by an inactivation Reagent, incubated for 2 min at RT, and then centrifuged at 10.000 \times g for 1.5 min. The RNA-containing supernatant was carefully transferred to a new tube. RNA concentration was quantified using NanoDrop spectrophotometer.

3.2.4.3 Bulk RNA sequencing

Whole transcriptome analysis was conducted on infarcted hearts from WT mice, WT mice treated with BB-Cl-amidine, and PAD4^{-/-} at days 1, 3, and 7 post-MI. RNA extraction was performed using the RNeasy Mini kit, followed by treatment with the DNA-free kit as previously described. Following this, the samples (100 ng/μl in a volume of 20 μl, with A₂₆₀/A₂₈₀ ratios ranging between 1.96 and 2.12, and A₂₆₀/A₂₃₀ ratios ranging between 1.83 and 2.14) were sent to the Center of Genomics Cologne (CCG) for further analysis. Further procedure was performed by the scientific staff at CCG. In brief, RNA integrity was initially verified with RNA Integrity Number (RIN) values >7.0. Libraries were generated following the Illumina Stranded TruSeq RNA sample preparation protocol. Starting with 500 ng of total RNA, the process included poly-A selection using poly-T oligo-attached magnetic beads to enrich mRNA, followed by fragmentation using divalent cations at an elevated temperature. The fragmented RNA underwent reverse transcription using random primers, followed by second strand cDNA synthesis using DNA Polymerase I and RNase H. Subsequent steps included end repair, A-tailing, and ligation of indexing adapters. The resulting products were purified and subjected to 15 cycles of PCR amplification to generate final cDNA libraries. After validation and quantification using Agilent Tape Station, equimolar amounts of libraries were pooled. Library quantification was performed using the Peqlab KAPA Library Quantification Kit and the Applied Biosystems 7900HT Sequence Detection System. Sequencing was conducted on an Illumina NovaSeq6000 platform using a PE100 protocol.

3.2.4.4 Affymetrix microarray analysis

RNA was obtained from freshly isolated Mo/M^φ or CFs of infarcted hearts using the RNeasy Mini kit and DNA-free kit as described in the sections above. The Mouse Clariom™ S Assay was utilized to analyze mRNA expression levels in each sample, in collaboration with the Affymetrix Facility in Cologne, headed by Prof. A. Sachinidis. Following the attainment of sufficient RNA amounts of 400 ng each, further analyses were conducted by the facility. For a short overview, RNA was converted into cDNA. The cDNA was then fragmented and labelled before hybridizing it onto the microarray chip. The chip contains probes specific to mouse genes. Following hybridization, the chip is scanned to measure the fluorescent signal intensity at each probe position, which indicates the level of gene expression. The *p*-values were calculated by Transcriptome Analysis Console (TAC version 4.0, Thermo Fisher Scientific).

3.2.4.5 cDNA synthesis

Following the guidelines provided by the High Capacity cDNA Reverse Transcription Kit, single-stranded cDNA was synthesized from total RNA. Briefly, master mix was prepared containing nuclease-free H₂O, RT buffer, dNTP Mix, random primers and reverse transcriptase. 250 ng RNA for cells and 1000 ng RNA for heart tissue in a volume of 10 µl were mixed with 10 µl master mix and reverse transcribed to cDNA using a thermocycler. The following program was used: 10 min 25°C, 120 min 37°C, 5 min 85°C. The obtained cDNA was stored at -20°C.

3.2.4.6 Real-time PCR

Real-time PCR, also known as quantitative PCR (qPCR), is performed to precisely quantitate changes in gene expression. Synthesized cDNA (0.08 – 10 ng/4 µl) was used as template in the real-time PCR reaction. All samples were run in triplicates. Using SYBR Green PCR Master Mix according to the manufacturer's recommended protocol, the amplification was conducted under the following thermal cycling conditions: 2 min 50°C, 2 min 95°C, 40 cycles of 1 sec 95°C and 30 sec 60°C, and hold at 4°C. Subsequently, the amount of double stranded amplification product was quantified based on the fluorescence emitted by intercalated SYBR Green dye. Relative gene expression levels of target genes were normalized to the endogenous control *18S rRNA* or *GAPDH*. Fold expression of target genes was determined using the $2^{-\Delta\Delta CT}$ method. All primers used in this study, to detect specific genes, are listed in Table 6.

3.2.5 Bioinformatical analysis

The bioinformatical analysis of the Bulk RNA-seq data were conducted in collaboration with Dr. Ali Abdallah from the Bioinformatics Core Facility at the CECAD Research Center, University of Cologne.

Bioinformatics analysis of microarray data was performed in collaboration with Prof. A. Sachinidis. For identification of Gene Ontology (GO) and pathway enrichment of up- and downregulated genes, the web-based DAVID 2021 tool (<https://david-d.ncifcrf.gov/>) was used. GO terms with Benjamini-corrected $p < 0.05$ were considered statistically significant.

For data visualization the web-based bioinformatics tool SRplot (SRplot -Science and Research online plot) available at (<https://www.bioinformatics.com.cn>) was used.

3.2.6 Protein biochemistry

3.2.6.1 Protein isolation from heart tissue

For protein isolation, frozen heart pieces (19 mg – 31 mg) were placed in RIPA buffer with protease inhibitor cocktail and phosphatase inhibitor cocktail. By using the Precellys® 24 Touch homogenizer and 5 - 8 zirconium oxide beads, hearts here homogenized at 6500 rpm for 20 sec, followed by a 5-sec break, repeated three times. After centrifugation by 16.000 × g for 10 min at 4°C, supernatants were collected and stored by -80°C for further analysis.

3.2.6.2 Quantification of protein concentration

Total protein concentration of heart tissue was determined by performing a bicinchoninic acid (BCA) assay following manufacturer's instructions. The BCA Protein Assay operates by utilizing the reduction of Cu^{2+} to Cu^{1+} by proteins in an alkaline medium, followed by the sensitive detection of the cuprous cation (Cu^{1+}). In brief, samples (diluted 1:6) were loaded onto a 96-well plate together with a BSA standard (range 0 - 2 $\mu\text{g}/\mu\text{l}$), followed by the addition of BCA Working Reagent. After incubating for 25 min at 37°C, the absorbance at 562 nm was measured using the VICTOR X3 microplate reader.

3.2.6.3 SDS-PAGE

The SDS-PAGE technique is employed for protein separation based on molecular size. This is achieved by a two-layer system: a porous stacking gel to facilitate the formation of distinct proteins and a separating gel for sorting proteins. For this, 30 or 40 µg protein was mixed with Laemmli Buffer and 5% mercaptoethanol and further incubated at 95°C for 7 min. Tubes were placed on ice and samples were loaded onto a 10% sodium dodecyl sulfate-polyacrylamide gel. Electrophoresis was carried out with 60 V for 20 min followed by 130 V for approximately 60-90 min.

Table 16: Composition of used gels for western blot.

Stacking gel (V/gel)	10% Separating gel (V/gel)
650 µl 30% Acrylamide	2.5 ml 30% Acrylamide
3 ml Ampuwa H ₂ O	3.125 ml Ampuwa H ₂ O
1.25 ml 4 x Stacking gel buffer (pH 6.8)	1.875 ml 4 x Separating buffer (pH 8.8)
10 µl TEMED	10 µl TEMED
25 µl 10% APS	25 µl 10% APS

3.2.6.4 Western blot

After SDS-PAGE, samples were transferred to a nitrocellulose membrane using a Trans-Blot Turbo transfer system (Bio-Rad) for 1 h at 23 V according to the manufacturer's instructions using blotting buffer. To confirm protein transfer, the nitrocellulose membrane was stained with Ponceau S solution for 2 to 3 min. Membranes were washed in TBST before blocking in TBST containing 5% milk powder. Membranes were incubated with primary antibodies directed against TGF-β1, collagen I, collagen III and citrullinated histone H3 in 5% milk powder in TBST or for Smad2, p-Smad2, β-Actin, GAPDH, p-MLKL in 5% BSA in TBST overnight at 4°C. After four washing steps with TBST, membranes were incubated with HRP-conjugated polyclonal goat anti-rabbit IgG in TBST for 1 h at RT in the dark. Chemiluminescence was detected using Pierce ECL detection reagent or UptiLight HRP Blot chemiluminescence ECL substrate and ChemiDoc XRS+. Densitometric analysis was performed using Image Lab software (version 6.1.0, Bio-Rad Laboratories).

3.2.6.5 Cardiac troponin t type 2 quantification

Cardiac troponin levels in plasma samples were quantified by Mouse cTnT ELISA Kit from Elabscience according to manufacturer's instructions. Shortly, a biotinylated detection antibody specific for mouse cTnT and an anti-biotin antibody were added to each well and allowed to incubate. Following washing to remove unbound components, substrate solution was added. The enzyme-substrate reaction was stopped by the addition of sulfuric acid, causing the colour to turn from blue to yellow. Absorbance was measured spectrophotometrically at a wavelength of 450 nm.

3.2.6.6 Total collagen quantification

Total collagen content in heart tissue were quantified using the Total collagen Assay Kit (Perchlorate-Free) from Abcam according to manufacturer's instructions. For a brief overview, samples and standards were hydrolyzed with concentrated NaOH to break down collagen into hydroxyproline. After cooling and neutralizing with HCl, samples were centrifuged. The samples were dried, and an oxidation mix was added to oxidize hydroxyproline. A developer solution was introduced to form a chromophore. Finally, DMAB concentrate was added, to complete chromophore development. Absorbance was measured spectrophotometrically at a wavelength of 560 nm, allowing for accurate quantification of collagen levels.

3.2.7 Cellular biology

3.2.7.1 Preparation heart tissue for histological analysis

After perfusion with isotonic 0.9% NaCl solution, the atria were removed with a straight horizontal cut along the ligature. Subsequently, hearts were fixed overnight in phosphate-buffered 4% formaldehyde before being drained overnight, dehydrated and embedded in paraffin. Following fixation, the hearts were serially sectioned (4 μm thick) by a technical assistant for subsequent histological staining.

3.2.7.2 Immunohistochemistry

After deparaffinization and rehydration steps involving two incubations in xylene for 15 min each, followed by a series of graded alcohol washes (100% ethanol for 3 min, 90% ethanol for 3 min, 70% ethanol for 3 min, 50% ethanol for 3 min), and a final rinse in tap water for 1 min, the heart sections were stained with Masson's trichrome (MTC) or Picrosirius Red.

For the MTC staining procedure, slides were first fixed overnight with Bouin's solution, followed by three washes with distilled water. MTC staining was performed according to manufacturer's recommendations. Briefly, Weigert's hematoxylin solution was applied for 5 min to stain the nuclei. After different washing steps muscle fibers were stained red using Biebrich scarlet-acid fuchsin. Collagen fibers were stained blue with aniline blue for 5 min, and excess stain was removed using a weak 1% acidic solution for a short incubation time. Slides were then incubated for 30 sec in 100% ethanol, followed by a 10-min incubation in xylene, before being mounted.

For Picrosirius Red staining the sections were stained with Picrosirius Red solution for 1 h at RT. Following staining, picrosirius red dye binds specifically to collagen fibers and by rinsing the sections afterwards in acidified water (0.5% acetic acid) for 2 min the contrast helps to distinguishing collagen fibers from other tissue components. The stained sections were dehydrated using graded alcohols, cleared in xylene, and mounted with a suitable medium.

Image acquisition was performed using an Eclipse Ti-U 100 microscope and NIS-Element software package (Nikon). Image J software was used to define collagen content in heart tissue sections.

3.2.7.3 Immunofluorescence

All paraffin-embedded heart tissue sections underwent sequential steps including deparaffinization involving two incubation steps in xylene for 15 min each, rehydration using graded alcohols (100% 3 min, 90% 3 min, 70% 3 min, 50% 3 min and 1 min tap water), and antigen retrieval utilizing citrate buffer for 2 h at 60 °C.

To detect histone H3 citrullination, heart tissue sections were permeabilized using permeabilization buffer at RT for 5 min. Subsequently, the sections were blocked in a buffer solution composed of TBS with 5% goat serum and 0.1% TritonX-100 for 1 h at RT. Specific antibody staining was carried out overnight at 4°C using rabbit anti-Histone H3 (citrulline R2+R8+R17) antibody (diluted 1:200 in blocking buffer), followed by incubation with goat anti-rabbit Alexa Fluor 488-conjugated antibody (diluted 1:1.000 in TBS containing 1% BSA and 0.1% Triton X) for 1 h at RT. DAPI counterstaining was applied for 10 min at RT and slides were mounted in fluorescence mounting medium.

For the identification of NETs, tissue sections were permeabilized as previously described, followed by a blocking step using blocking buffer (TBS + 0.05% TritonX-100 and 5% donkey serum) for 1 h at RT. Subsequently, sections were incubated overnight at 4°C with rabbit anti-Histone H3 (citrulline R2+R8+R17) antibody (1:200) and goat anti-MPO antibody (1:200) in blocking buffer. Following this, three washing steps were performed with TBS + 0.05% TritonX-100, followed the incubation with donkey anti-goat Alexa Fluor 488 (1:800) and donkey anti-rabbit Alexa 555 (1:800) secondary antibodies in blocking for 1.5 h buffer at RT in the dark. After three additional washing steps, slides were further washed with distilled water, incubated with DAPI for 10 min and mounted in fluorescence mounting medium.

For α -SMA staining, tissue sections underwent permeabilization by incubating the sections in permeabilization buffer at RT for 5 min. Slices were blocked with 5% goat serum and 0.3% TritonX-100 in PBS for 1 h. Following this, sections were incubated overnight at 4°C with rabbit anti-mouse α -SMA antibody (1:1000) in staining buffer (PBS + 1% BSA + 0.1% TritonX-100). After five washing steps with PBS, sections were incubated with goat anti-rabbit Alexa 488 antibody (1:1000) in staining buffer for 1.5 h at RT and subsequently mounted in fluorescence mounting medium with additional DAPI staining.

Image acquisition was performed using an Eclipse Ti-U 100 microscope and NIS-Element software package (Nikon). Image J software was used to define the number of positive cells per square millimeter of the infarct area or positive signal of specific antibody per infarct area.

3.2.7.4 Assessment of cell death

Apoptotic cell death was assessed using the Elabscience One-step TUNEL Assay Kit according to the manufacturer's instructions. After deparaffinization and rehydration as previously described, the slides were washed three times with PBS. Permeabilization of tissue sections was achieved using Proteinase K for 20 min at 37°C. Subsequently, assay-specific solutions were applied to detect cleaved DNA fragments, indicative of apoptosis. Nuclei were counterstained with DAPI.

Image acquisition was carried out using the Eclipse Ti-U 100 microscope and analysis was performed using the NIS-Element software package and Image J software, respectively. Image J software was utilized to quantify the number of positive cells per square millimeter of the infarct area.

3.2.7 Flow cytometry

Before any measurements were performed, compensation was conducted using compensation beads (ArC Amine Reactive Compensation Bead Kit and BD™ CompBeads) according to manufacturer's instructions.

To determine immune cell recruitment in infarcted heart tissue, hearts were collected, minced and enzymatically digested as previously described. For incubation with fluorochrome-conjugated antibodies, 1×10^5 cells/100 μ l were used. Live/dead staining was performed using Ghost Dye™ Violet 510 for 30 min on ice. After washing with FACS buffer 4°C, cells were incubated with Fc blocking antibody (0.1 μ g/ 1×10^6 cells in 100 μ l) for 10 min on ice. Afterwards, cells were stained for 30 min on ice with fluorochrome-conjugated antibodies selected to identify different immune cell populations (see Table 3). To establish the background fluorescence signal in a sample stained with fluorochrome-conjugated antibodies, Fluorescence Minus One (FMO) controls were employed. These controls involve staining the sample with all antibodies except for the one of interest, enabling the determination of specific fluorescence signals and background noise. After one washing step with FACS buffer and centrifugation at $400 \times g$ for 5 min at 4°C, cells were resuspended in 300 μ l FACS buffer for final analysis. Data were acquired on FACS Canto II flow cytometer. Data analysis was performed using with FlowJo Software v10.9.1 (Tree Star).

3.2.8 Statistics

All data are presented as means \pm SEM. Statistical analyses were conducted using GraphPad Prism version 10 (GraphPad Software, San Diego, CA, USA). Prior to analysis, the data were assessed for normal distribution using the Shapiro-Wilk test. For variables that were not normally distributed, the Mann-Whitney U test was employed for unpaired comparisons and otherwise by normal distribution t-test were used. Differences among more than two groups were evaluated using the Kruskal-Wallis test or one-way ANOVA, followed by Tukey's post-hoc test. Two-way ANOVA with Tukey's post-hoc test was utilized for comparisons involving two independent variables. Survival differences were determined using the log-rank test. Detailed information regarding the sample sizes (n) of both, biological samples and animals, used in the study can be found in the figure legends. Otherwise, each dot represents one mouse. A p-value < 0.05 was considered statistically significant.

4. Results

To date, whether PAD4 plays a role in regulating inflammation and resolution in CVDs such as MI remains largely unexplored. To investigate the functional role of PAD4 in MI, the following experimental set-up, focusing on the early, acute, pro-inflammatory phase (Day 1 – Day 3) and the late immune response (Day 7) post-MI was designed (**Fig. 8**). MI was induced by permanent ligation of the LAD in 9-12-week-old male WT mice as well as in mice lacking the *Padi4* gene ($PAD4^{-/-}$). Additionally, WT mice were subjected to daily injections of the pan-PAD inhibitor BB-CI-Amidine (WT + BB-CI) to pharmacologically inhibit PAD activity.

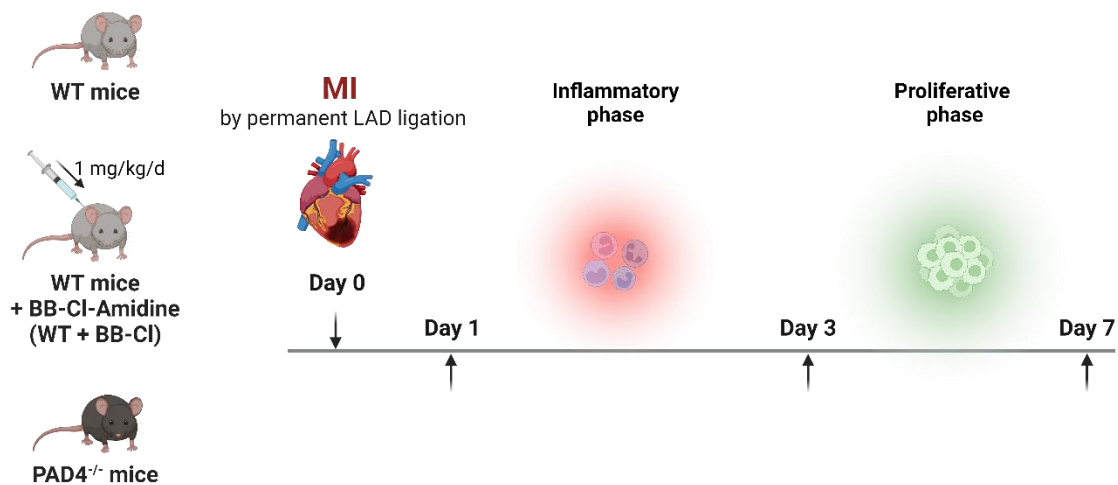


Figure 8: Experimental setup for MI induction and post-MI analyses. MI was induced by a permanent ligation of the LAD in 9-12-week-old male WT mice and mice with constitutive *Padi4* ablation ($PAD4^{-/-}$). For pharmacological PAD inhibition, WT mice received daily injections with the pan-PAD inhibitor BB-CI-Amidine (WT + BB-CI). Analyses on day 1 and 3 post-MI primarily focus on the acute, pro-inflammatory phase, whereas days 3-7 post-MI are intended to examine the transition to the anti-inflammatory phase. Graphic created with BioRender.

4.1 Increased PAD4 activity after MI in mice and humans

To investigate the role of PAD4 post-MI and its clinical relevance, the expression of *Padi4* was analysed under baseline conditions and at days 1, 3 and 7 after LAD ligation in mice and in *post-mortem* cardiac tissue from patients with MI and individuals without evidence of infarction. In mice, *Padi4* expression was significantly upregulated during the pro-inflammatory phase at day 3 and peaked at day 7 post-MI when compared to baseline expression levels (**Fig. 9A**). Analysis in *post-mortem* cardiac tissue from patients revealed strong upregulation of *Padi4* in the ischemic, infarcted left ventricle (LV), compared to non-ischemic tissue of the right ventricle (RV) and to individuals who died from non-cardiovascular causes (**Fig. 9B**). Furthermore, citrullination of histone 3 (citH3) was observed in the infarct and peri-infarct region in mice at day 1 post-MI, indicating an increased PAD4 enzymatic activity (**Fig. 9C**). Besides, citH3 was

noted in the infarcted, human LV, arguing for a functional role of PAD4-mediated citrullination in cardiac ischemia (**Fig. 9D**).

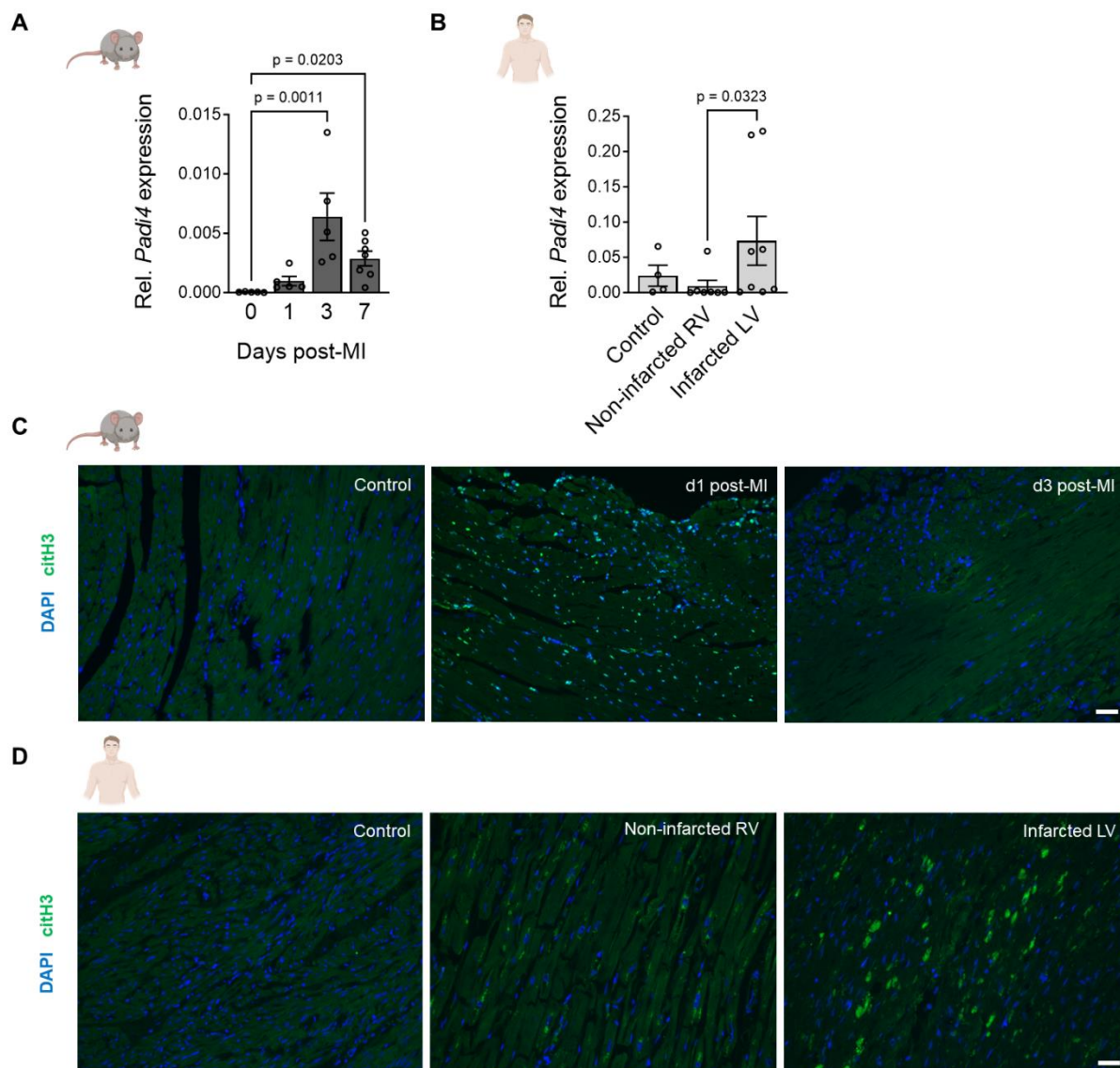


Figure 9: *Padi4* expression and PAD4-mediated citrullination post-MI in murine and human hearts. (A) Relative gene expression of *Padi4* in mice under baseline conditions and at days 1, 3, and 7 post-MI (n = 5-7) (B) *Post-mortem* analysis of *Padi4* expression in infarcted and non-infarcted cardiac tissue of acute MI patients (n = 8) as well as healthy controls (n = 4). (C) Representative immunofluorescence showing in mice the distribution of citrullinated histone 3 (citH3) with DAPI staining in the infarcted area. Scale bar, 50 μm. (D) Representative immunofluorescence images of citH3 in *post mortem* human heart tissue in healthy controls, non-infarcted RV and infarcted LV. Scale bar, 50 μm. Data are presented as means ± SEM. Kruskal-Wallis test with Dunn's post-hoc test was used to assess differences between the groups (in A and B).

4.2 Comparative consequences of genetic or pharmacological PAD4 inhibition on the early pro-inflammatory immune response post-MI (days 1 - 3)

4.2.1. Decreased PAD4-mediated citrullination and NETs formation with BB-CI-Amidine

To elucidate which PAD isoforms are expressed in cardiac tissue, the levels of *Padi1*, *Padi2*, *Padi3*, *Padi4*, and *Padi6* was examined in murine hearts under baseline conditions. Of note, only *Padi2* and *Padi4* were detected in hearts of WT and PAD4^{-/-} mice, without significant alterations (**Fig. 10A**). Daily treatment of WT mice with the pan-PAD inhibitor BB-CI-Amidine for seven days had no observable toxic effects. This was shown by a 100% survival rate in WT + BB-CI mice (**Fig. 10B**).

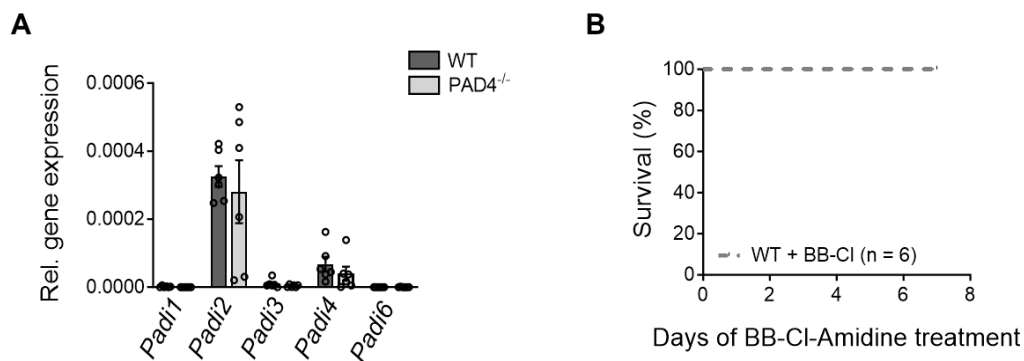


Figure 10: *Padi* gene expression and effects of BB-CI-Amidine treatment in mice without surgery. (A) Relative expression of *Padi* genes encoding for different PAD isoforms in WT and PAD4^{-/-} hearts under baseline conditions (n = 6). **(B)** WT mice were daily treated with BB-CI-Amidine (1 mg/kg/d) for up to 7 days. Kaplan-Meier survival curves of WT + BB-CI mice (n = 6).

To investigate the abundance of citH3 post-surgery, protein levels in infarcted cardiac tissue of WT, PAD4^{-/-} and WT + BB-CI mice at days 1 and 3 were quantified. Decreased citH3 levels were observed on both time points in WT + BB-CI and PAD4-deficient mice when compared to untreated WT mice (**Fig. 11A, B**). No significant differences were noted between WT + BB-CI and PAD4^{-/-} mice (**Fig. 11A, B**). However, the reduction in citH3 levels suggests an impaired enzymatic activity of PAD4 in both, inhibitor-treated and PAD4-deficient mice.

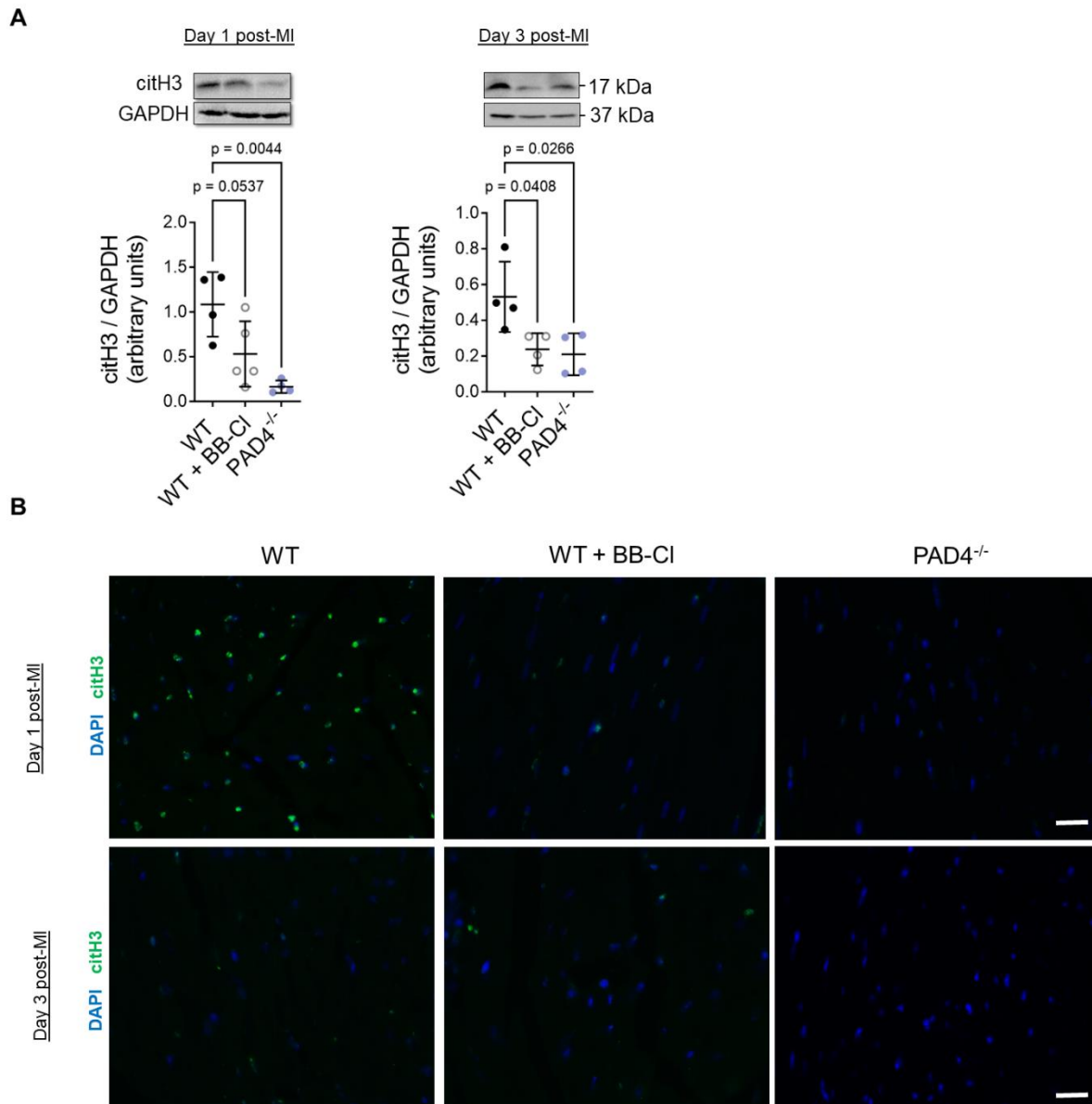


Figure 11: CitH3 protein levels post-MI in mice. (A) Protein was extracted from heart tissue of WT, PAD4^{-/-}, and WT + BB-CI mice at days 1 and 3 post-MI to quantify citH3 by western blot. Representative western blots are shown (n = 4-5). (B) Immunofluorescence staining showing citH3 (green) and nuclei counterstained with DAPI (blue) at days 1 and 3 post-MI. Scale bar, 20 μ m. Data are presented as means \pm SEM. Ordinary one-way ANOVA with Tukey's multiple comparisons test was used to assess differences between the groups.

Because citH3 is essential for NETs formation, the appearance of NETs was investigated post-surgery. As indicated by absent co-localization of MPO and citH3, no NETs were detected in both PAD4^{-/-} mice and WT + BB-CI mice on day 1 (Fig. 12A) and 3 (Fig. 12B) post-MI. Notably, only the WT mice exhibited pronounced NETs formations on the first day post-MI (Fig. 12A), with no NETs formation being observable on day 3 (Fig. 12B).

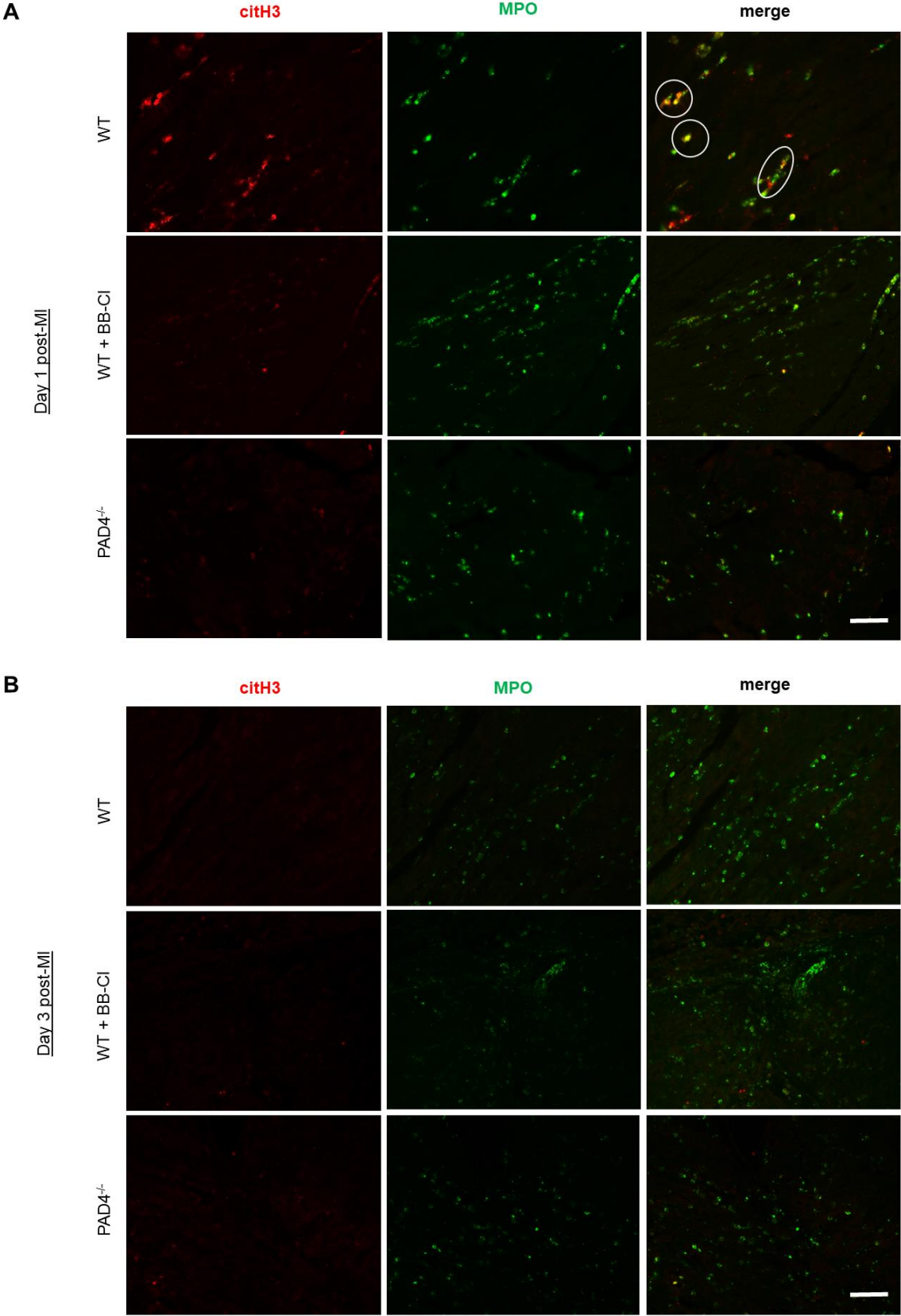


Figure 12: NETs formation in PAD4-deficient, WT + BB-CI and WT mice post-MI. Representative immunofluorescence staining for citH3 (red) and myeloperoxidase (MPO, green) at days 1 and 3 post-MI. NETs were identified as double positive yellow structures (white circle). Scale bar, 50 μ m.

4.2.2. Induction of massive cardiac damage by pharmacological PAD inhibition in the acute phase

To investigate cardiac damage and the extent of cell death following the acute phase post-MI, both systemic and local inflammatory responses were examined. After surgery, cardiac troponin (cTnT) levels, which serve as clinical biomarker for cardiac damage, were noted to be elevated in plasma of WT + BB-CI and PAD4^{-/-} mice compared to WT mice on day 1 post-MI. On day 3 post-MI, significantly higher cTnT levels were quantified in PAD4-deficient mice compared to WT + BB-CI mice but both of them exhibited no alterations compared to WT mice (**Fig. 13A**). Furthermore, both PAD4^{-/-} and WT + BB-CI mice exhibited reduced levels of cell necroptosis, as indicated by decreased levels of phosphorylated mixed lineage kinase domain-like protein (pMLKL) on day 1 post-MI. On day 3 post-MI, PAD4-deficient mice displayed again significantly lower levels of pMLKL in comparison to both, WT mice with and without inhibitor treatment. In contrast, WT + BB-CI mice exhibited significantly higher levels of this marker compared to both other groups (**Fig. 13B**). In addition, apoptosis was analysed by TUNEL assay. Treatment with the inhibitor led to increased cell apoptosis in WT mice at day 1 and 3 post-MI, as evidenced by elevated levels of cleaved DNA fragments. In contrast, PAD4^{-/-} mice exhibited significantly lower number of apoptotic, TUNEL positive cells (**Fig. 13C**).

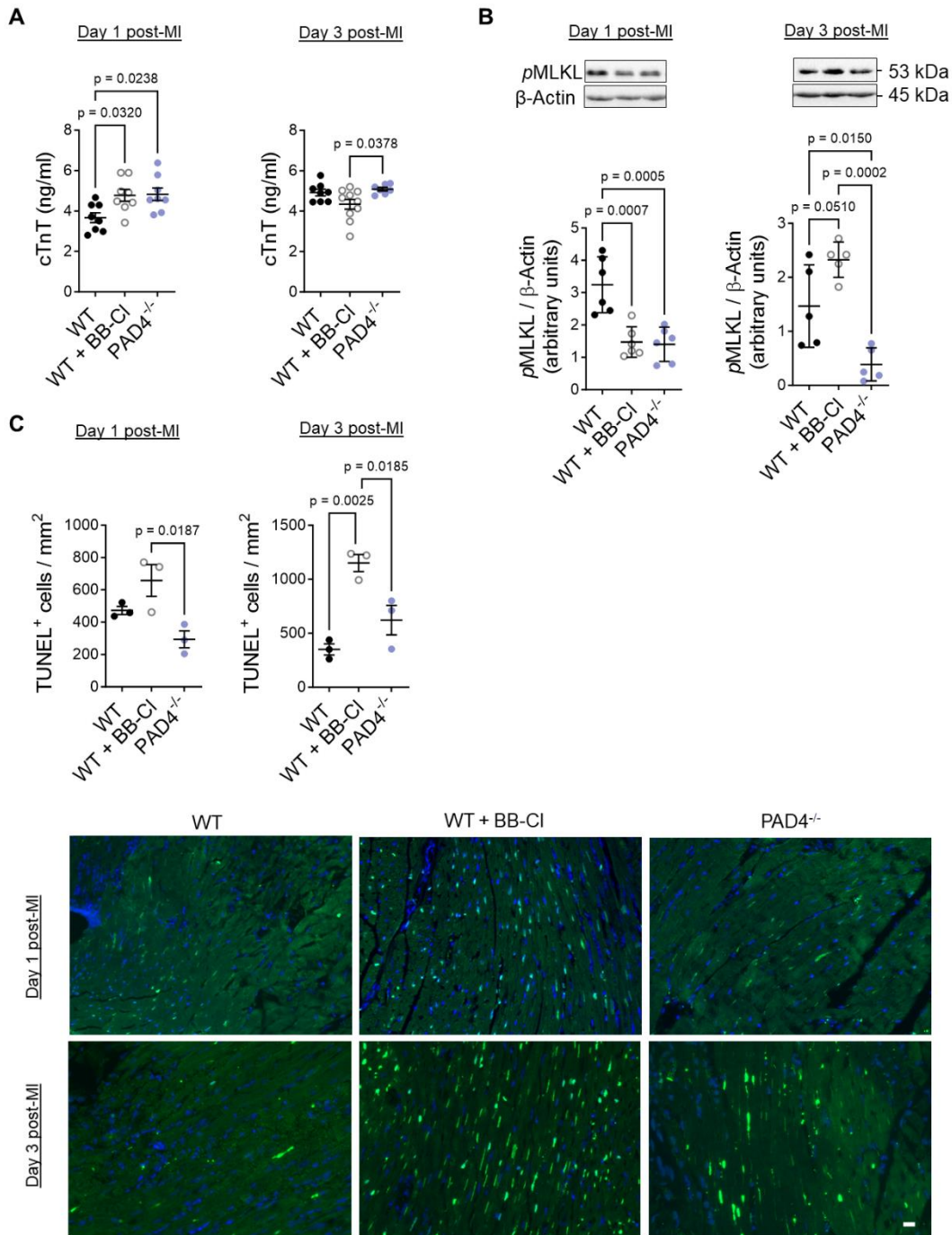


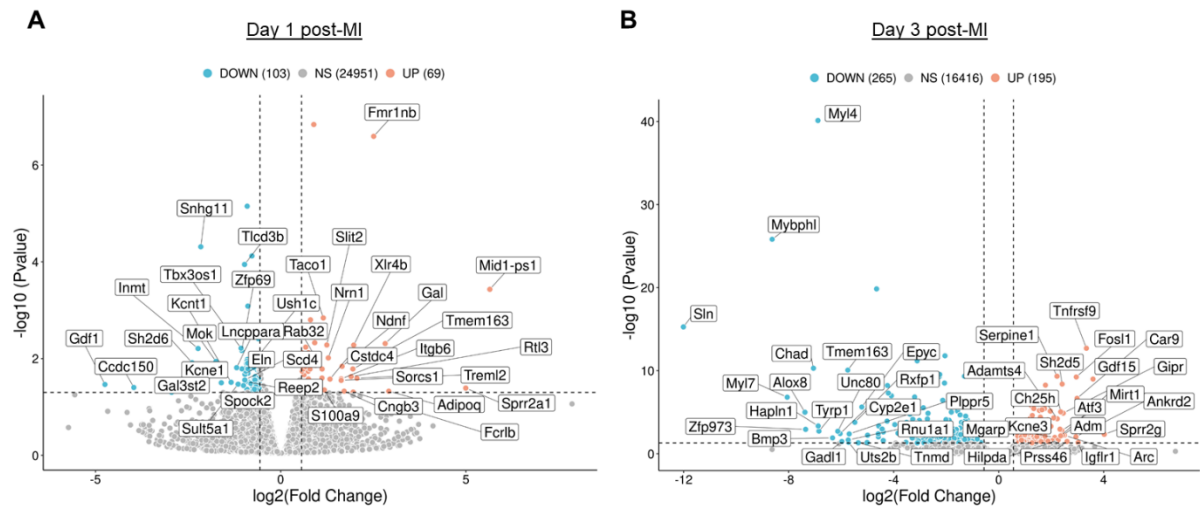
Figure 13: Impact of genetic or pharmacological PAD4 inhibition on cell death. (A) Blood plasma samples were obtained in all groups at days 1 and 3 post-MI and cTnT levels were quantified by ELISA (n = 6-10). (B) Proteins were isolated from heart tissue of WT, PAD4^{-/-} and WT + BB-CI mice at days 1 and 3 post-MI to quantify pMLKL abundance, presented by representative western blots (n = 5). (C) Immunofluorescence images and quantification of TUNEL-positive cells were performed in infarcted hearts of WT, PAD4^{-/-} and WT + BB-CI mice at days 1 and 3 post-MI (n = 3). Nuclei were counterstained using DAPI. Scale bar, 20 μm. Data are presented as means ± SEM. One-way ANOVA with Tukey's post-hoc test or Kruskal-Wallis test with Dunn's post-hoc test was used for statistical analysis.

4.2.3. Enhanced inflammatory gene expression in WT + BB-CI mice

To understand alterations in inflammation-related pathways, bulk RNA sequencing (RNA-seq) analysis of infarct and remote regions at day 1 and 3 post-MI was performed in all three groups. Analysis revealed 69 significantly upregulated and 103 downregulated genes at day 1 (**Fig. 14A**), as well as 195 upregulated and 265 downregulated genes at day 3 (**Fig. 14B**) in WT + BB-CI mice compared to WT mice. Notably, a significant upregulation of *Trem2* (Triggering receptor expressed on myeloid cells like 2), a receptor expressed on immune cells (Wang et al. 2023), and *Adipoq* (Adiponectin), a hormone secreted by adipose tissue (Khoramipour et al. 2021), at day 1 post-MI was observed. Additionally, *Mok* (MAPK/MAK/MRK kinase), encoding a kinase involved in signalling pathways regulating cell proliferation, differentiation, and survival (Zhang and Liu 2002), exhibited a significant downregulation (**Fig. 14A**). Particularly on day 3 post-MI genes like *Ankrd2* (Ankyrin repeat domain 2) and *Serpine1* (serpin family E member 1), whose expression is associated with cardiac diseases and fibrosis (Bean et al. 2014; Kubota et al. 2021), were significantly upregulated in WT + BB-CI mice (**Fig. 14B**).

On the other hand, at day 1 post-MI, PAD4^{-/-} mice exhibited 255 significantly upregulated and 279 downregulated genes (**Fig. 13C**), while at day 3 post-MI, there were 203 upregulated and 162 downregulated genes (**Fig. 13D**) in comparison to WT controls. In this context, it was observed that several genes, including *Chil3* (Chitinase-like 3), *Cxcl13* (Chemokine (C-X-C motif) ligand 13), and *Cfd* (Complement factor D), were significantly downregulated on day 1 post-surgery. These genes have been associated with inflammation process within the cardiovascular system (Yu et al. 2024; Wang et al. 2022; Barratt and Weitz 2021). On day 3 post-MI, *Cfd* remained among the top downregulated genes, consistent with its role in activating the complement cascade during inflammation. This cascade is involved in recruiting immune cells, releasing inflammatory mediators, and activating tissue responses (Barratt and Weitz 2021; Vandendriessche et al. 2021).

WT + BB-CI vs. WT



PAD4^{-/-} vs. WT

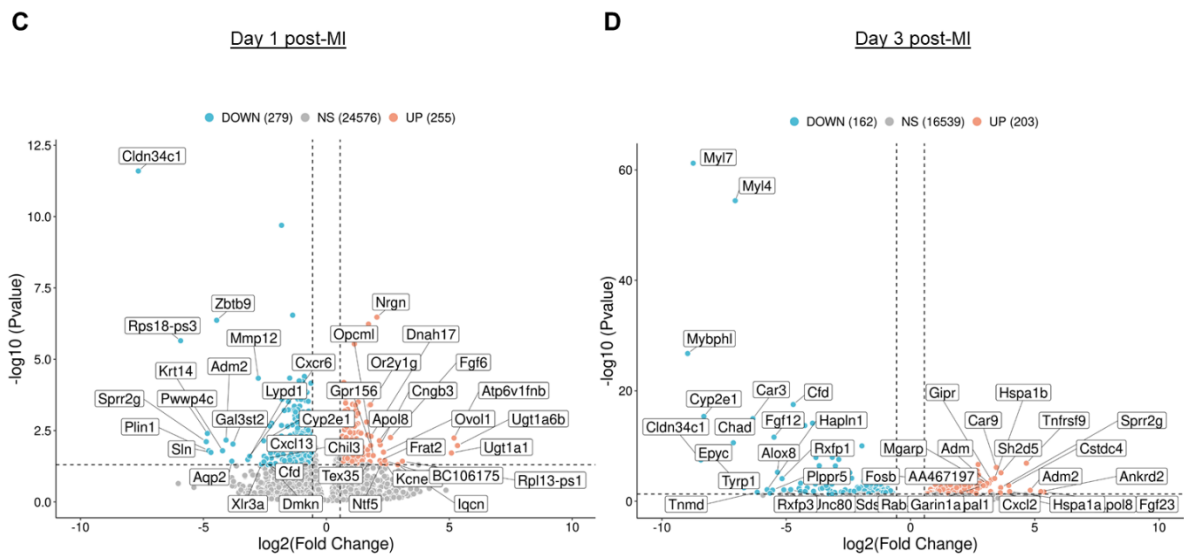


Figure 14: Bulk RNA-seq analysis of infarcted hearts on day 1 and 3 post-MI. Volcano plots illustrating differentially expressed genes in WT + BB-CI mice compared to WT on day 1 (A) and day 3 (B) post-MI and PAD4^{-/-} compared to WT on day 1 (C) and day 3 (D) post-MI. Top 20 up- and downregulated genes with adjusted p-value < 0.05 and log₂ Fold Change > 0.56 are highlighted.

Detailed analysis of the expression levels of significantly regulated genes unveiled a heightened inflammatory response in WT + BB-CI mice compared to WT mice on both, day 1 and day 3 post-MI. This was evidenced by a significant upregulation of *Il6*, the surface marker *Ly6c1*, typically found on monocytes, and *Gal* on day 1 post-MI (**Fig. 15A**) as well as *Gdf15*, *Tnfrsf9* and *Mirt1* on day 3 post-MI (**Fig. 15B**). Moreover, on day 3 post-MI, a significant decrease of genes encompassing the ECM like *Col6a6* as well as genes encoding proteins associated with myofilament structures and predicted to be involved in cardiac muscle contraction, including *Mybphl*, *MyI7* and *MyI4* was observed in WT + BB-CI mice (**Fig. 15B**). There was also a significant decrease in *Fgf12* and *Wif1* in mice included in the inhibitor group on day 3 post-MI. On the contrary, PAD4^{-/-} mice exhibited a substantial downregulation of genes encoding for chemokines and receptors on day 1 after surgery. For instance, a significant downregulation of *Cxcr6*, *Ccr2*, *Ccl7* and *Ccl2* was observed. Additionally, significant downregulation of *Gdf15* was detected in PAD4^{-/-} mice whereas it was upregulated in WT + BB-CI on day 3 post-MI (**Fig. 15C**). Interestingly, on day 3 after permanent ligation, both, PAD4^{-/-} and WT + BB-CI mice, displayed a significant downregulation of *Mybphl*, *MyI7*, and *MyI4*, implying regulation by PAD4 (**Fig. 15D**). However, genes encoding for fibroblast growth factors like *Fgf23*, *Fgf6* were significantly upregulated in PAD4^{-/-} mice whereas they were downregulated in WT + BB-CI. Beside this, a decrease in the gene *Cidec*, involved in cell death (Song et al. 2022), was observed in mice lacking the *Padi4* gene on day 3 after ligation (**Fig. 15D**). Furthermore, sequencing analysis revealed a downregulation of *Padi4* gene expression in PAD4-deficient mice and elevated mRNA levels of *Il4ra* on day 3 post-MI (**Fig. 15D**).

		A			
		Gene	Log ₂ Fold Change	Adjusted p-value	Description
WT + BB-CI vs. WT	Day 1 post-MI	<i>Gdf1</i>	-4.744387665	0.034237256	growth differentiation factor 1
		<i>Kcne1</i>	-1.603978096	0.031606926	potassium voltage-gated channel, member 1
		<i>Kcnt1</i>	-1.339403932	0.030864902	potassium channel, subfamily T, member 1
		<i>Eln</i>	-0.966212783	0.021094869	elastin
		<i>Smad6</i>	-0.722613397	0.029956383	SMAD family member 6
		<i>Fgfr3</i>	-0.695946367	0.027624816	fibroblast growth factor receptor 3
		<i>Acta2</i>	-0.592199991	0.024926831	actin alpha 2, smooth muscle
		<i>Gal</i>	+2.81961968	0.004888029	galanin and GMAP prepropeptide
		<i>Il6</i>	+1.01069758	0.032591976	interleukin 6
		<i>Ly6c1</i>	+0.6514495	0.043869131	lymphocyte antigen 6 complex
		B			
		Gene	Log ₂ Fold Change	Adjusted p-value	Description
WT + BB-CI vs. WT	Day 3 post-MI	<i>Mybphl</i>	-8.627303857	1.51156E-26	myosin binding protein H-like
		<i>Myl7</i>	-8.052991791	1.56005E-07	myosin, light polypeptide 7, regulatory
		<i>Myl4</i>	-6.883514287	7.57066E-41	myosin, light polypeptide 4
		<i>Fgf12</i>	-4.235956697	6.04978E-09	fibroblast growth factor 12
		<i>Wif1</i>	-3.822389591	5.75803E-07	Wnt inhibitory factor 1
		<i>Col6a6</i>	-3.37910397	1.7254E-05	collagen, type VI, alpha 6
		<i>Gdf15</i>	+3.592517087	1.01622E-09	growth differentiation factor 15
		<i>Tnfrsf9</i>	+3.340681347	2.0016E-13	tumor necrosis factor receptor superfamily, member 9
		<i>Mirt1</i>	+2.361780582	0.007027615	myocardial infarction associated transcript 1
				C	
Gene	Log ₂ Fold Change			Adjusted p-value	Description
PAD4 ^{-/-} vs. WT	Day 1 post-MI	<i>Cxcr6</i>	-3.118221712	0.025134195	chemokine (C-X-C motif) receptor 6
		<i>Mmp12</i>	-2.768648793	4.63705E-05	matrix metalloproteinase 12
		<i>Mmp24</i>	-2.128653905	0.017970856	matrix metalloproteinase 24
		<i>Gdf15</i>	-1.709249855	0.000625091	growth differentiation factor 15
		<i>Ccr2</i>	-1.416204733	0.039630795	chemokine (C-C motif) receptor 2
		<i>Ccl7</i>	-1.295107609	0.000635855	chemokine (C-C motif) ligand 7
		<i>Ccl2</i>	-1.259471549	0.0105916	chemokine (C-C motif) ligand 2
		<i>Fgf6</i>	+2.608530556	0.005556297	fibroblast growth factor 6
		<i>Col6a6</i>	+1.677921808	0.014747125	collagen, type VI, alpha 6
				D	
Gene	Log ₂ Fold Change			Adjusted p-value	Description
PAD4 ^{-/-} vs. WT	Day 3 post-MI	<i>Mybphl</i>	-8.962708894	1.79886E-27	myosin binding protein H-like
		<i>Myl7</i>	-8.739152429	6.1477E-62	myosin, light polypeptide 7, regulatory
		<i>Myl4</i>	-7.048747166	3.73632E-55	myosin, light polypeptide 4
		<i>Cidec</i>	-4.419573536	0.000551014	cell death-inducing DFFA-like effector c
		<i>Padi4</i>	-2.483865926	0.028587086	peptidyl arginine deiminase, type IV
		<i>Col4a6</i>	-1.75042235	0.005062508	collagen, type IV, alpha 6
		<i>Fgf23</i>	+5.371063891	0.020726298	fibroblast growth factor 23
		<i>Il4ra</i>	+1.190764827	0.037535399	interleukin 4 receptor, alpha

Figure 15: Differential gene expression in infarcted hearts on day 1 and 3 post-MI in WT + BB-CI and PAD4^{-/-} mice compared to WT mice. Selected regulated genes displayed with log₂ Fold Change and adjusted p-value < 0.05, comparing WT + BB-CI versus WT mice on day 1 (A) and day 3 (B), as well as PAD4^{-/-} versus WT mice on day 1 (C) and day 3 (D) post-MI.

The comparison between WT + BB-CI and PAD4-deficient mice on day 1 post-MI is also noteworthy. *Cxcr6* exhibited significant upregulation in WT + BB-CI mice (**Fig. 16**), whereas a significant downregulation was noted in PAD4^{-/-} mice. Similar trends were observed on day 3 post-MI for *Fgf23*, *Col6a6*, and *Mirt*, with all of them showing downregulation under treatment (**Fig. 16**) and upregulation in deficient mice. Notably, *Padi4* was the only isoform detected in NGS data and exhibited a significant upregulation on day 3 post-MI after inhibition of PADs by BB-CI-Amidine (**Fig. 16**), suggesting a role in the processes post-MI.

Gene	Log ₂ Fold Change	Adjusted p-value	Description
Day 1 post-MI			
<i>Cxcr6</i>	+3.388118463	0.015936099	chemokine (C-X-C motif) receptor 6
Day 3 post-MI			
<i>Fgf23</i>	-3.401126591	8.32776E-05	fibroblast growth factor 23
<i>Mirt</i>	-2.559205102	0.025159235	myocardial infraction associated transcript
<i>Col6a6</i>	-1.974295537	0.005356372	collagen, type VI, alpha 6
<i>Padi4</i>	+2.131810602	0.009795449	peptidyl arginine deiminase, type IV

Figure 16: Gene expression variation in infarcted hearts at day 1 and 3 post-MI in WT + BB-CI compared to PAD4^{-/-} mice. Selected differentially expressed genes displayed with log₂ Fold Change and adjusted p-value, comparing WT + BB-CI versus PAD4^{-/-} mice on day 1 and 3 post-MI.

To assess the biological functions of the differentially expressed genes across the groups, functional annotation and Gene Ontology (GO) enrichment analysis were performed. The most statistically significant terms related to biological processes (BP), cellular components (CC), and molecular functions (MF) were examined in detail (**Fig. 17**). WT + BB-CI mice displayed increased expression of genes coding for potassium ion channels and subunits like *Kcnq1*, *Kcnj5*, *Kcna7*, *Kcnj2*, *Kcnj12*, and *Kcnk13* compared to untreated WT mice. Specifically, these genes are involved in membrane repolarization during the action of cardiac muscle cells. This pathway as well as pathways associated with potassium ion transport are upregulated in WT + BB-CI mice on day 1 after permanent ligation. Additionally, on day 1 as well as on day 3 after surgery, an increased expression of genes involved in positive regulation of cell death, response to stress, hypoxia, and oxygen levels was observed. Furthermore, a significant number of pathways affecting the extracellular matrix, such as extracellular matrix organization, extracellular region, extracellular matrix, and collagen-containing extracellular matrix was found to be downregulated after treatment with BB-CI-Amidine. These results indicate a decrease in heart stability after PAD inhibition (**Fig. 17**).

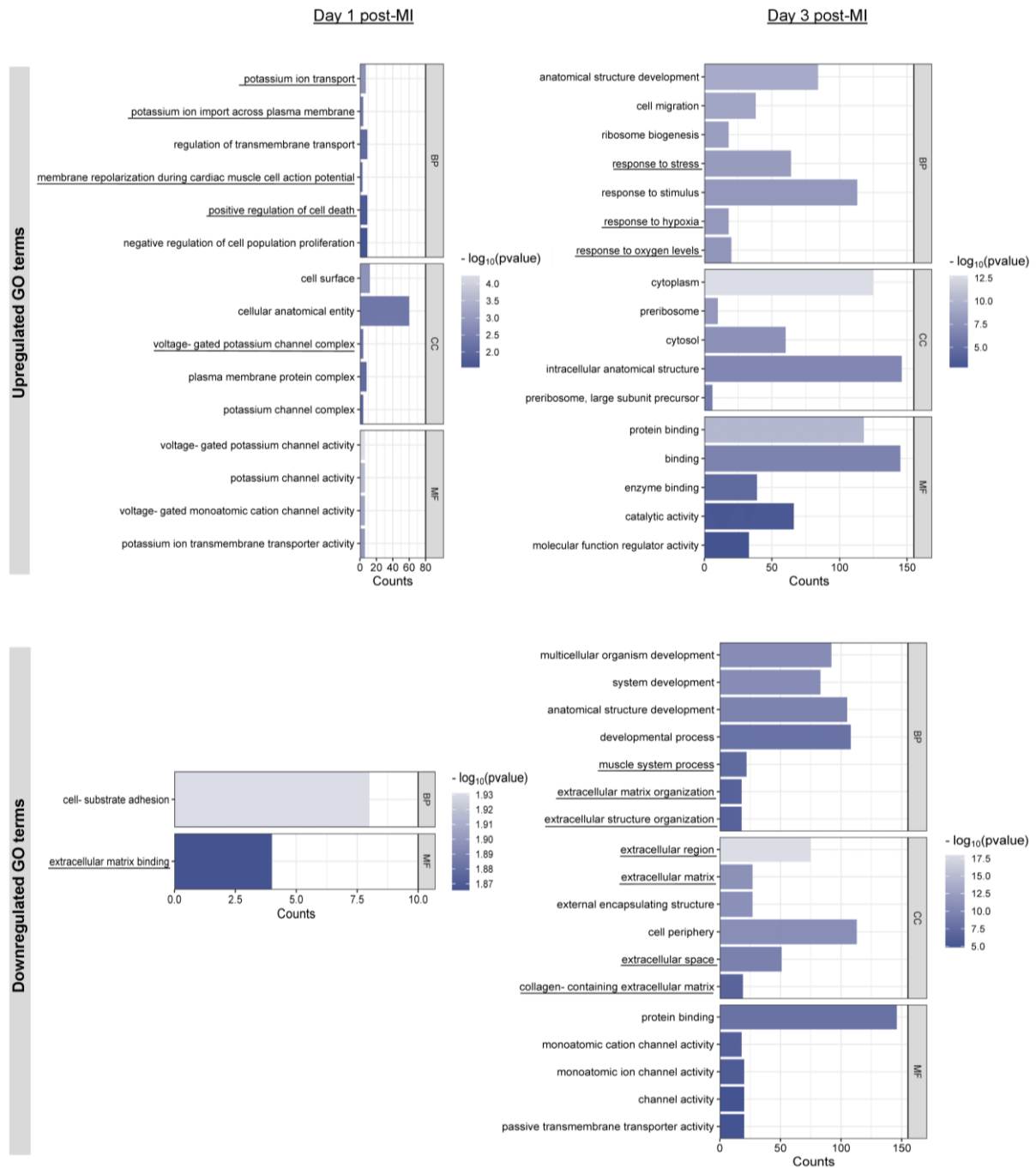


Figure 17: GO term analysis of RNA-seq data from WT + BB-CI mice hearts on day 1 and 3 post-MI compared to WT. Selected GO terms ranged under the top 10 with significant p-values of upregulated and downregulated genes based on biological processes (BP), cellular components (CC), and molecular functions (MF) were identified in WT + BB-CI mice on day 1 and 3 post-MI.

GO enrichment analysis of differentially expressed genes revealed that PAD4-deficient mice, starting from the acute phase post-MI (day 1), exhibit a significantly reduced expression of genes associated with myeloid leukocyte migration, immune system processes and granulocyte migration compared to WT mice. Similar to the observations in WT + BB-CI mice, terms associated with the ECM, such as collagen-containing extracellular matrix, extracellular

matrix organisation and extracellular region were found to be significantly downregulated on day 3 after surgery (**Fig. 18**).

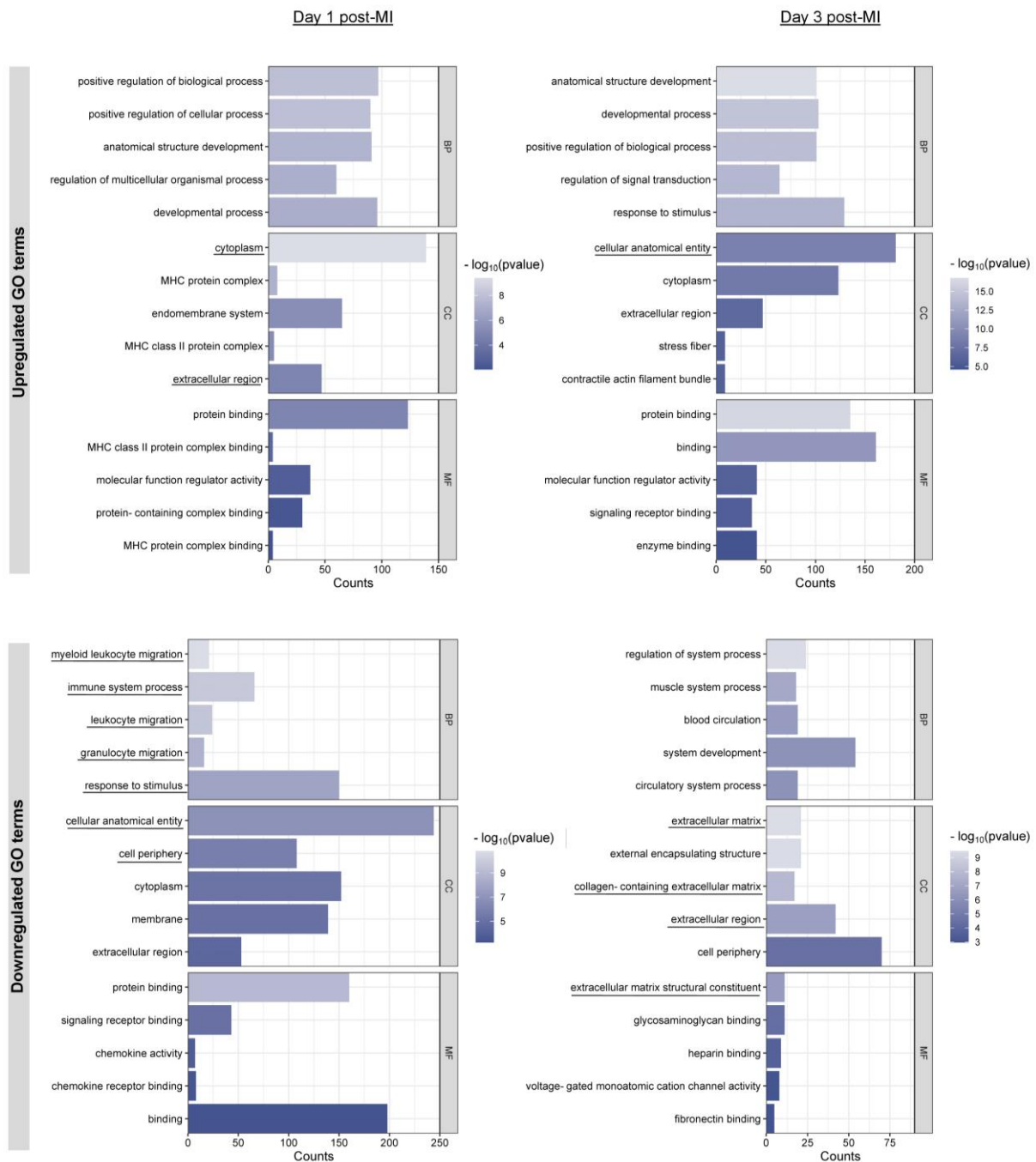


Figure 18: GO term analysis of RNA-seq data from $PAD4^{-/-}$ hearts on day 1 and 3 post-MI compared to WT. Selected GO terms under the top 10 with significant p-values of upregulated and downregulated genes based on biological processes (BP), cellular components (CC), and molecular functions (MF) were identified in $PAD4^{-/-}$ mice on days 1 and 3 post-MI.

4.2.4. Suppression of myeloid cell recruitment by PAD inhibition

The results above indicate altered immune responses in mice with genetic or pharmacological PAD4 inhibition post-MI. To investigate immune cell recruitment post-MI, single-cell suspensions from enzymatically digested hearts were analysed by flow cytometry. A gating strategy was created to identify cardiac myeloid cells, macrophages, and neutrophils (**Fig. 19A**). Remarkably, at day 1 after occlusion, there was a significant decrease in cardiac myeloid cells (CD45⁺CD11b⁺) in PAD4^{-/-} mice compared to WT mice (**Fig. 19B**). Similar effects were found after pharmacological PAD inhibition on day 1 and 3 post-MI.

Detailed analysis of immune cells revealed that WT + BB-CI mice exhibited a reduced number of infiltrated neutrophils (CD45⁺CD11b⁺Ly6G⁺) on day 1 post-MI compared to WT and PAD4^{-/-} mice (**Fig. 19B**). Conversely, PAD4^{-/-} mice displayed a higher count of neutrophils compared to both groups on this day. The level of neutrophils did not differ on day 3 after surgery. Despite the relative number of myeloid cells decreasing after PAD inhibition, the relative number of macrophages (CD45⁺CD11b⁺Ly6G⁻F4/80⁺) was higher on day 1 post-MI compared to WT mice and those lacking the *Padi4* gene, indicating an overall weaker, yet more macrophage-pronounced inflammatory response. However, no differences of macrophages were found on day 3 post-MI between the groups.

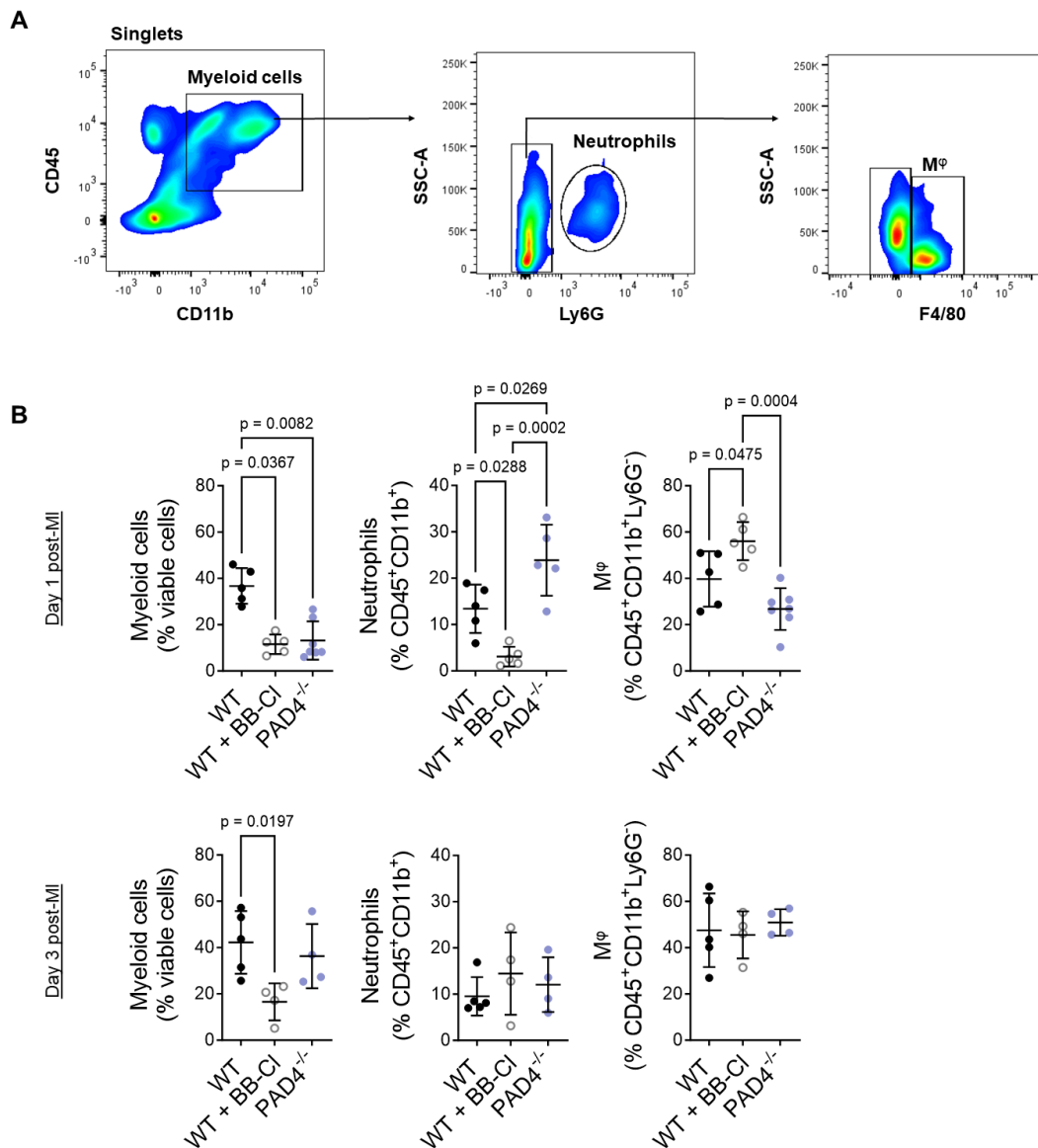


Figure 19: Effects of pharmacological inhibition of PADs and *Padi4* ablation on immune cells recruitment during the inflammatory phase post-MI. (A) Gating strategy for myeloid cells (CD45⁺CD11b⁺), neutrophils (CD45⁺CD11b⁺Ly6G⁺), and macrophages (CD45⁺CD11b⁺Ly6G⁻F4/80⁺) (B) FACS analysis showing the percentage of myeloid cells, neutrophils, and macrophages in all three groups (n = 3-7 mice per group). Data are presented as means ± SD. One-way ANOVA with Tukey's post-hoc test or Kruskal-Wallis test with Dunn's post-hoc test was used for statistical analysis.

4.2.5. Increased risk of cardiac rupture following pharmacological PAD inhibition post-MI

In the context of bulk RNA-seq analyses, it was shown that the ECM appears to be influenced in mice with compromised PAD4 activity. To investigate the potential effects on heart stability and survival rate, the hearts of WT and PAD4-deficient mice as well as those treated with the pan-PAD inhibitor were examined for total collagen content in the inflammatory phase post-MI. A significant reduction in total collagen content was found in WT + BB-CI mice on day 1 post-MI in comparison to WT mice. However, with no significant changes, the total collagen content was also reduced in PAD4^{-/-} mice on day 1 and 3 post-MI (**Fig. 20A**). Interestingly, WT + BB-CI mice showed a notable rise in the heart-to-body weight ratio on both time points in comparison to WT and PAD4^{-/-} mice (**Fig. 20B**). These findings indicate a volume overload of the heart in these mice. Moreover, it was observed that hearts of WT + BB-CI mice become balloon-like in size on the first day after permanent ligation (**Fig. 20C**). Ultimately, upon autopsy following the demise of inhibitor-treated mice, blood was noticed in the thoracic cavity of the animals, indicating a ventricular rupture. Kaplan-Meier analysis revealed a significantly lower 7-day survival rate among WT + BB-CI mice compared to both WT and PAD4^{-/-} mice, as illustrated in **Fig. 20D** with only a 20% survival rate.

Considering this aspect, animals treated with the inhibitor BB-CI-Amidine from the day of surgery onwards were excluded from subsequent analyses.

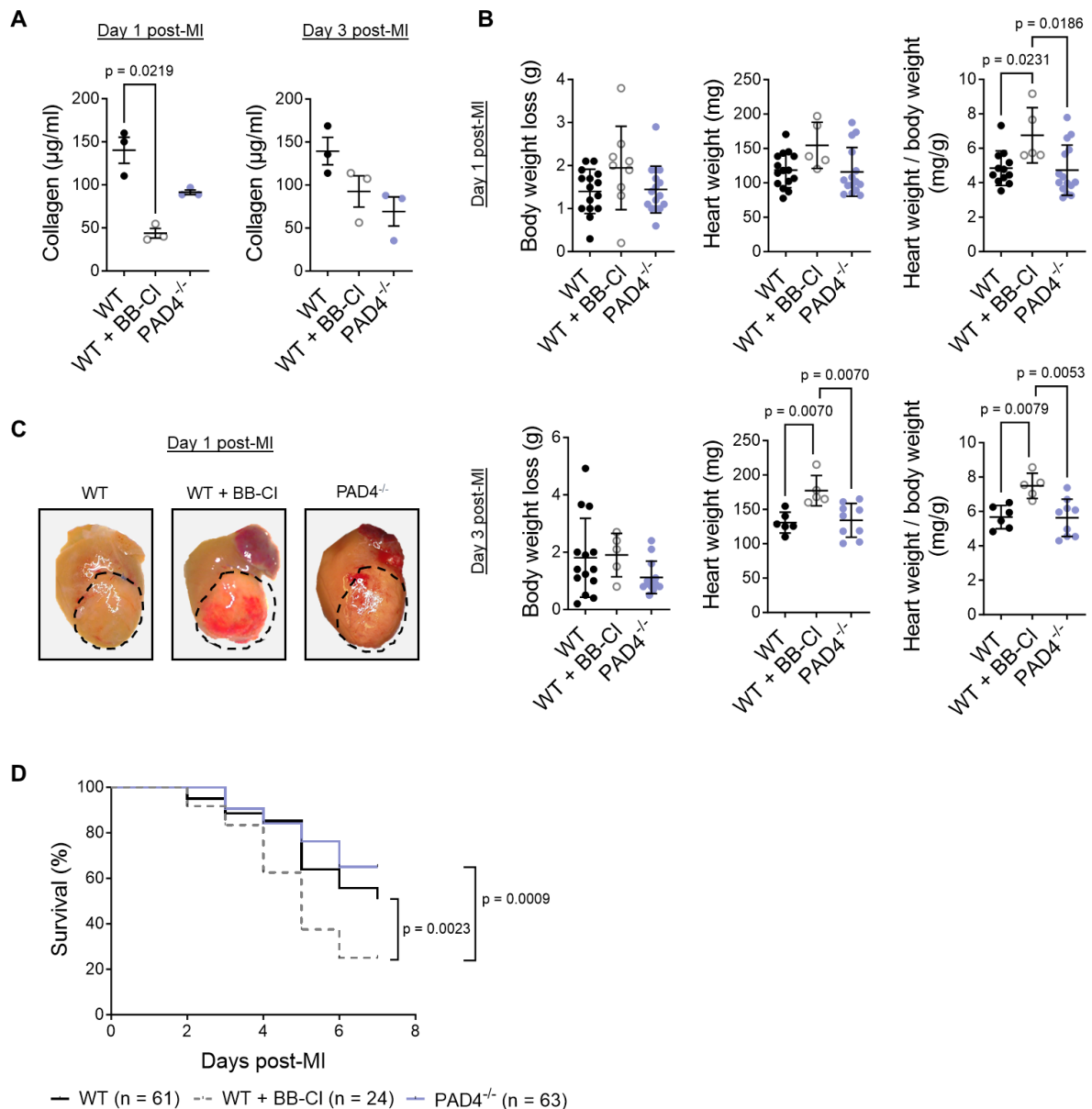


Figure 20: Impact of pharmacological inhibition of PAD and *Padi4* deficiency on cardiac collagen, body weight, heart weight and survival. (A) Quantification of total cardiac collagen of heart lysates in WT, WT + BB-CI and PAD4^{-/-} mice (n = 3). **(B)** Monitoring of body and heart weights in WT, WT + BB-CI and PAD4^{-/-} mice until day 3 post-MI. Calculation of the heart to body weight ratio (n = 5-16). **(C)** Representative macroscopic heart images of each group, highlighting the infarct area on day 1 post-MI. **(D)** Kaplan-Meier survival curves of WT, WT + BB-CI and PAD4^{-/-} mice included in the 7-days group. Log-rank (Mantel-Cox) test was used to compare survival curves. Data are presented as means \pm SEM. One-way ANOVA with Tukey's post-hoc test was used to access differences between the groups.

4.3 Influence of genetic PAD4 inhibition on the anti-inflammatory phase post-MI (day 7)

4.3.1. Attenuation of pro-inflammatory gene expression by PAD4 deficiency

Considering the significance of PAD4 in regulating immune responses and its survival-protective effects compared to pan-PAD inhibition post-surgery, additional examinations were performed on day 7 post-MI. To investigate whether loss of PAD4 affects cardiac regeneration after permanent LAD ligation, bulk RNA-seq analysis was performed on day 7 after surgery.

Transcriptome analyses revealed a significant reduction in genes associated with inflammatory responses and cardiac inflammation in PAD4^{-/-} mice compared to WT mice. Volcano plots illustrate 198 downregulated and 159 upregulated genes at day 7 post-MI in mice lacking the *Padi4* gene (**Fig. 21A**). Interestingly, several downregulated genes in PAD4^{-/-} mice, such as chemokines, MMPs and fibrotic genes were detected (**Fig. 21B, C**). Particularly, *Ccl9* exhibited a significant reduction in gene expression. Additionally, *Padi4* was significantly downregulated in PAD4-deficient mice, consistent with the observations from day 3 post-MI (**Fig. 21B**). Also of interest, the significant downregulation of *Cxcl2*, *Ccr1*, *Cxcl3*, *Tnfsf11* and *Il33*, all of which being associated with pathways contributing to immune system processes and inflammatory responses (**Fig. 21C**). Consequently, these pathways were downregulated that time point post-MI (**Fig. 21D**). Besides, reduced expression levels of inflammatory genes were confirmed by Real-Time PCR as shown for *Il6*, *Il12*, *Tnfa*, *Mpo*, *Ccl2* and *Ccr2*. These results indicate a less inflammatory microenvironment in PAD4^{-/-} hearts on day 7 post-MI (**Fig. 21D**).

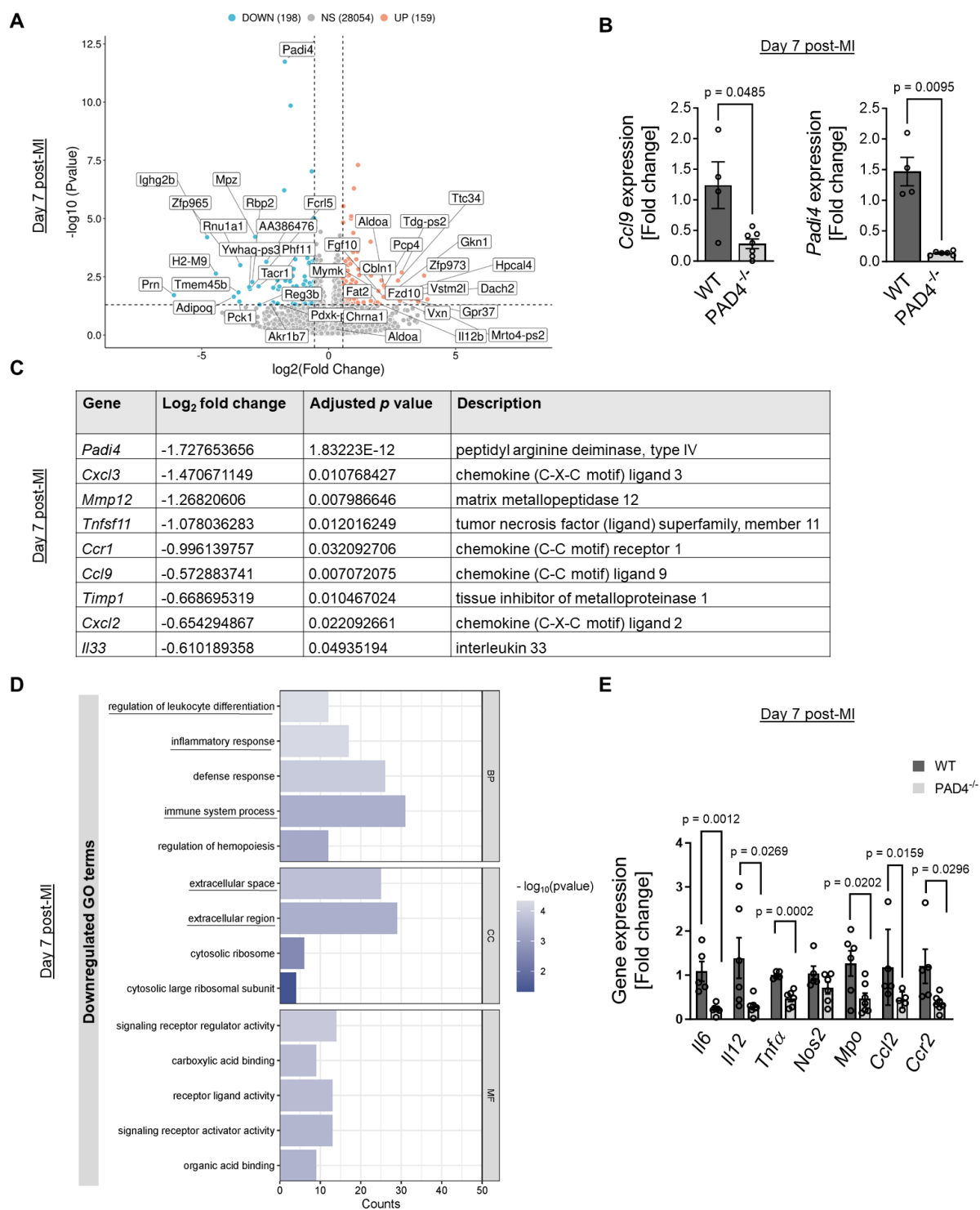


Figure 21: Bulk RNA-seq and gene expression analysis in *PAD4*^{-/-} hearts at day 7 post-MI. (A) Volcano plots of differentially expressed genes highlighting selected up- and downregulated genes with adjusted p-value < 0.05 and log₂FC > 0.56 in WT and *PAD4*^{-/-} mice (n = 5) **(B)** Real-time PCR analysis of *Ccl9* and *Padi4* in the infarcted area/border zone of WT and *PAD4*^{-/-} mice (n = 4-7). **(C)** Selected differentially expressed genes displayed with log₂ Fold Change and adjusted p-value < 0.05, comparing *PAD4*^{-/-} vs. WT mice. **(D)** The top 5 GO terms with the most significant p-values of downregulated genes based on biological process (BP), cellular component (CC) and molecular function (MF) were identified and displayed. **(E)** Real-time PCR analysis of selected inflammatory genes in the infarcted area/border zone of both groups (n = 5-6). Data are presented as means ± SEM. Student's unpaired t-Test or Mann Whitney test were used to assess significant differences between two groups.

4.3.2. Reduced count of cardiac macrophages ($M\phi$) in PAD4-deficient mice

Due to the significant downregulation of *Ccl2* and *Ccr2* (**Fig. 21E**), key regulators for the infiltration of monocytes/macrophages as well as other chemokines and inflammation-related genes, in the tissue of PAD4-deficient mice, it is likely that the inflammatory response is compromised. Thus, immune cell dynamics following MI, focusing on the recruitment to the infarcted tissue were investigated on day 7 post-MI.

A gating strategy was designed to identify myeloid cells, recruited myeloid cells, macrophages ($M\phi$), and recruited $M\phi$ (**Fig. 22A**). FACS analysis showed a significant increase in the percentage of myeloid cells ($CD45^+CD11b^+$) in mice lacking the *Padi4* gene compared to WT. While the percentage of recruited myeloid cells ($CD45^+CD11b^+CCR2^+$) did not differ between the groups, there was a significant decrease in the mean fluorescent intensity (MFI) in $PAD4^{-/-}$ mice post-surgery compared to WT (**Fig. 22B**). Moreover, a reduced percentage of $M\phi$ ($CD45^+CD11b^+F4/80^+$) was observed in mice lacking *Padi4* compared to WT mice. While the percentage of recruited $M\phi$ ($CD45^+CD11b^+F4/80^+CCR2^+$) did not show significant differences between the groups, there was a notable tendency for a decrease in MFI in $PAD4^{-/-}$ mice (**Fig. 22B**).

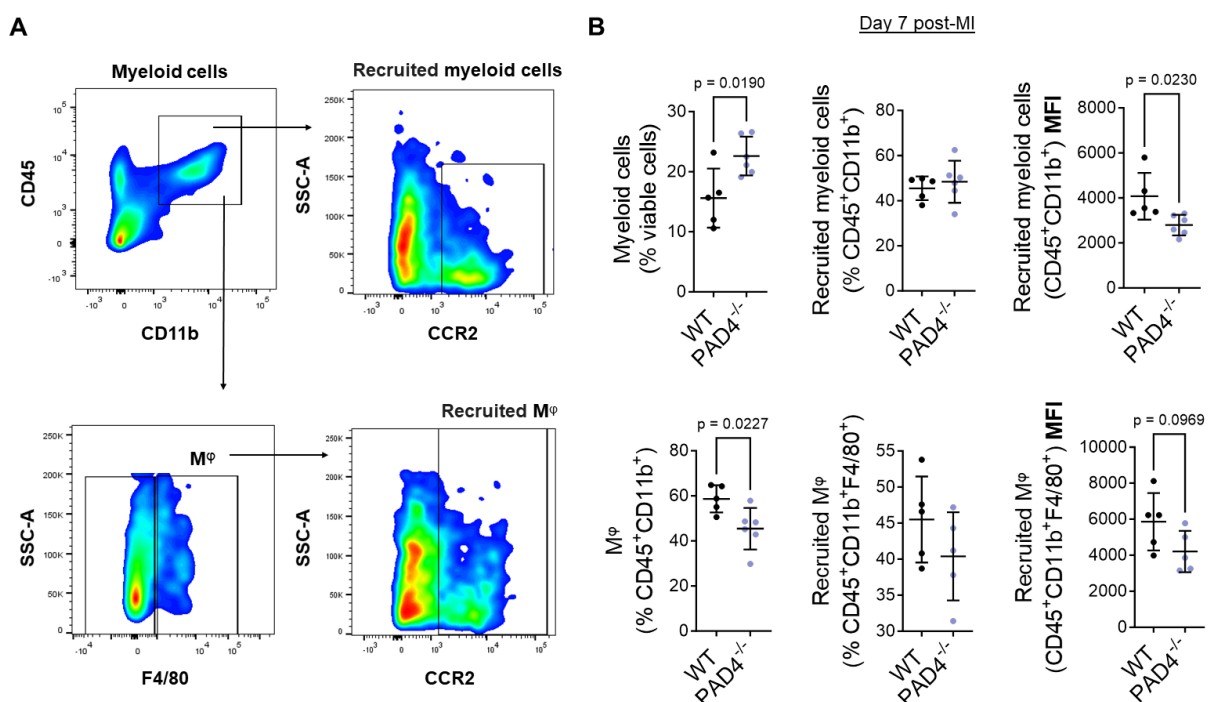


Figure 22: Impact of PAD4 on cardiac immune cell recruitment on day 7 post-MI. (A) Gating strategy for the identification of myeloid cells ($CD45^+CD11b^+$), recruited myeloid cells ($CD45^+CD11b^+CCR2^+$), macrophages ($M\phi$) ($CD45^+CD11b^+F4/80^+$) and recruited $M\phi$ ($CD45^+CD11b^+F4/80^+CCR2^+$) in infarcted hearts of WT and $PAD4^{-/-}$ mice. **(B)** The percentage and mean fluorescence intensity (MFI) of cardiac myeloid cells and cardiac $M\phi$ of enzymatically digested hearts was quantified by flow cytometry in WT and $PAD4^{-/-}$ mice ($n = 5-6$). Data are presented as means \pm SEM. Student's unpaired t-test or Mann Whitney test were used to assess differences between the groups.

4.3.2. Less inflammatory phenotype observed in PAD4^{-/-} M ϕ

Based on previous findings indicating a decreased macrophage count and a tendency towards reduced expression levels of *Ccr2* on day 7 post-MI, the potential phenotypic disparities were investigated in isolated cardiac monocytes/macrophages (Mo/M ϕ) from PAD4^{-/-} and WT mice.

Real-time PCR analysis of freshly isolated cardiac Mo/M ϕ from PAD4^{-/-} mice revealed significantly reduced expression levels of inflammatory genes such as *Il6*, *Nos2*, *Tnfa* compared to WT mice (**Fig. 23A**). However, whereas *Tgfb* expression was notably reduced in these cells, *Il10* expression was upregulated. Furthermore, FACS analysis demonstrated an elevated expression of CD206, a surface marker associated with M2-like macrophages, on PAD4^{-/-} Mo/M ϕ compared to WT Mo/M ϕ (**Fig. 23B**).

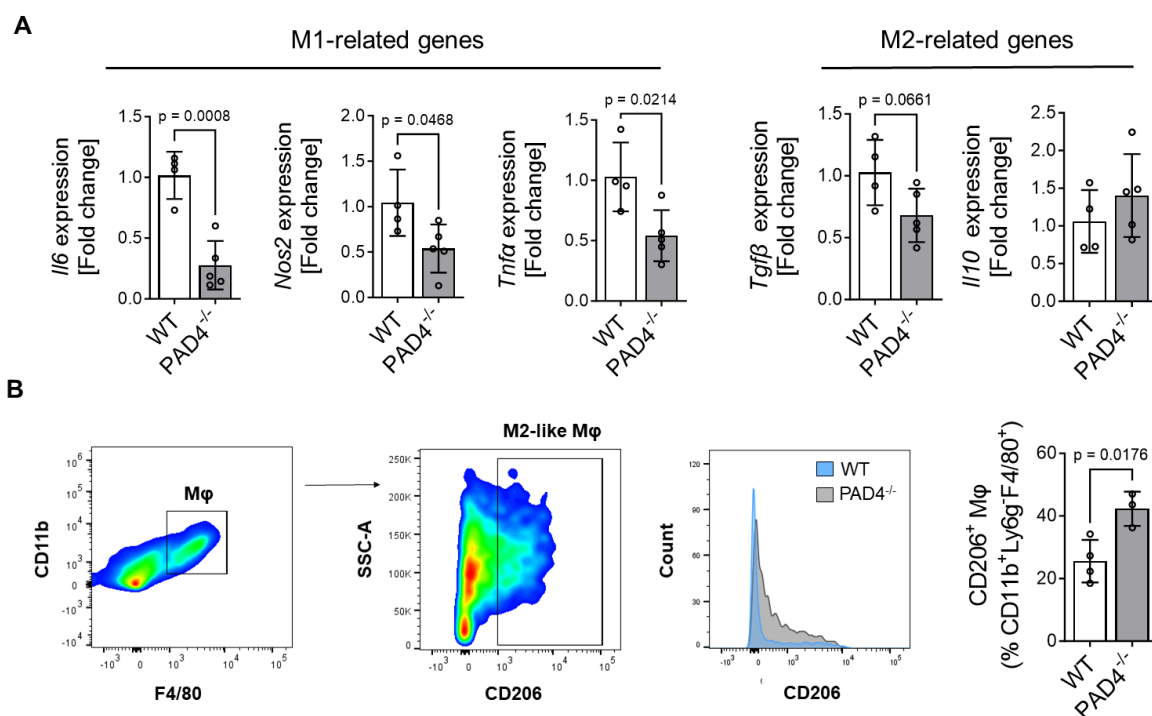


Figure 23: Phenotypic differences in cardiac monocytes/macrophages (Mo/M ϕ) from PAD4^{-/-} and WT mice on day 7 post-MI. (A) Real-time PCR analysis of selected M1 or M2-related genes in Mo/M ϕ from PAD4^{-/-} and WT mice. **(B)** Gating strategy for identifying CD206⁺ M ϕ (M2-like M ϕ) by flow cytometry **(C)** Quantification of reparative, CD206⁺ M ϕ in CD11b⁺F4/80⁺ isolated cells from infarcted WT and PAD4^{-/-} mice hearts. Data are presented as means \pm SEM. Student's unpaired t-Test or Mann-Whitney test were used to assess differences between two groups.

Subsequently, the transcriptome of Mo/M ϕ from PAD4^{-/-} and WT mice was examined using Affymetrix microarrays. Fold change analysis using fold change (FC) > 2 or < -2 and *p* value < 0.05 revealed 246 up- and 355 downregulated genes in Mo/M ϕ from PAD4-deficient mice compared to Mo/M ϕ from WT mice. Interestingly, genes like *I11 α* (Interleukin-1 alpha) (log₂FC -13.56), *Chil3* (Chitinase-3-like protein 3) (log₂FC -12.41) and *Ccr2* (log₂FC -2.35) were significantly reduced in Mo/M ϕ from PAD4-deficient mice (**Fig. 24A**). However, there was also a significant reduction of *Arg1* (Arginase 1) (log₂FC -11.31) in mice lacking the *Padi4* gene. Moreover, a downregulation of genes not highlighted here, encoding for chemokines including *Ccl9* (log₂FC -2.64), *Ccl5* (log₂FC -2.5), *Ccl6* (log₂FC -2.36) and chemokine receptors such as *Ccr1* (log₂FC -4.84) was observed in PAD4^{-/-} Mo/M ϕ . This downregulation affects pathways related to cell migration, inflammatory response, which were also downregulated on day 7 post-MI (**Fig. 24B**). Mo/M ϕ from PAD4-deficient mice also showed a downregulation of genes regulating endocytosis and phagocytosis, suggesting a reduced potential to clear DAMPs and cellular debris (**Fig. 24B**). GO term analysis further revealed a significant upregulation of a negative regulation of Wnt- and TGF β receptor pathway signalling in PAD4-deficient Mo/M ϕ (**Fig. 24B**). Both pathways are closely associated with the regulation of fibrosis and modulation of inflammation. With respect to the upregulation of a negative regulation of TGF β receptor pathway, the expression of *Smad7* (log₂FC +3.27), a key inhibitory regulator of TGF β signalling was increased in cardiac Mo/M ϕ of PAD4^{-/-} mice. A tendency towards increased *Smad7* expression in Mo/M ϕ of PAD4^{-/-} mice was also observed by performing Real-Time PCR, however, although results did not reach statistical significance (**Fig. 24C**).

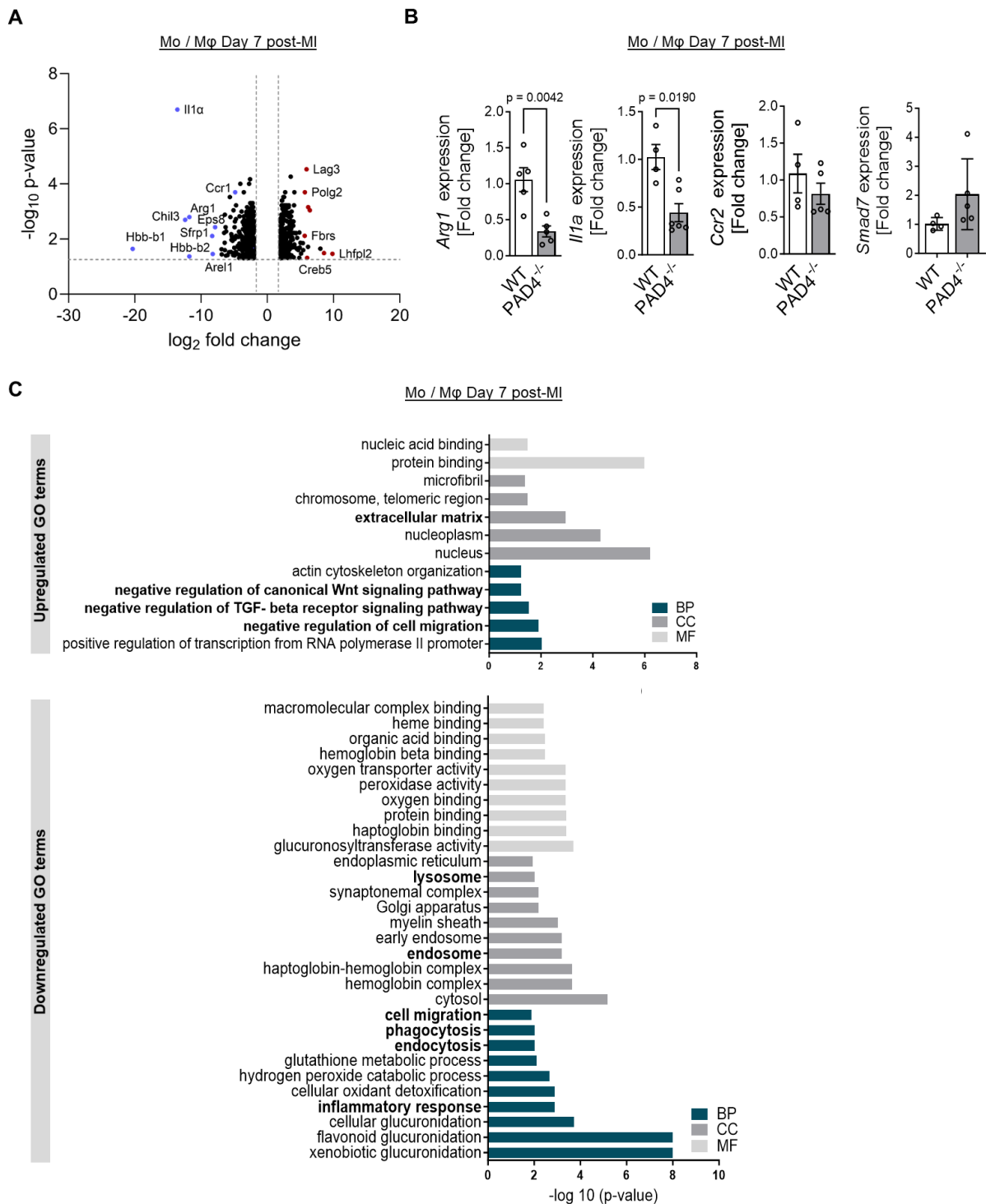


Figure 24: Transcriptomic alterations in cardiac Mo/M ϕ from PAD4^{-/-} mice on day 7 post-MI. (A) Bar plots displaying the top 15 of differentially expressed genes in PAD4^{-/-} Mo/M ϕ . (B) Top10 of significantly enriched GO terms in biological processes (BP), cellular compartments (CC) and molecular functions (MF). (C) Selected identified downregulated genes were confirmed by Real-time PCR (n = 3-5). Data are presented as means \pm SEM. Student's unpaired t-Test was used to assess differences between two groups.

Analysis so far suggests that the cardiac PAD4-deficient Mo/M ϕ exhibit a predominantly anti-inflammatory phenotype on day 7 post-MI. To investigate whether the observed shift towards an anti-inflammatory phenotype in cardiac macrophages is attributed to PAD4 deficiency, bone marrow-derived macrophages (BMDMs) were isolated from PAD4^{-/-} and WT mice. BMDMs were differentiated into macrophages and stimulated with Lipopolysaccharides (LPS) and IFN γ to induce a pro-inflammatory M1-like phenotype *in vitro*. M1 polarization was blunted in PAD4-deficient cells, as shown by significantly reduced *Ii6*, *Ii12* and *Nos2* expression (**Fig. 25A**). In addition, less nitrite in supernatants of PAD4^{-/-} M1-like macrophages was detected indicating reduced iNOS activity. Notably, similar results were obtained in BMDMs polarized in the presence of the pan-PAD inhibitor Cl-Amidine (**Fig. 25B**), suggesting that the regulation of genes characteristic for M1-like macrophages is under the control of PAD4. Additionally, M1-like macrophages from PAD4^{-/-} mice exhibited improved efferocytosis capacity; in fact, they showed enhanced uptake of apoptotic Jurkat cells compared to WT M1-like macrophages (**Fig. 25C**).

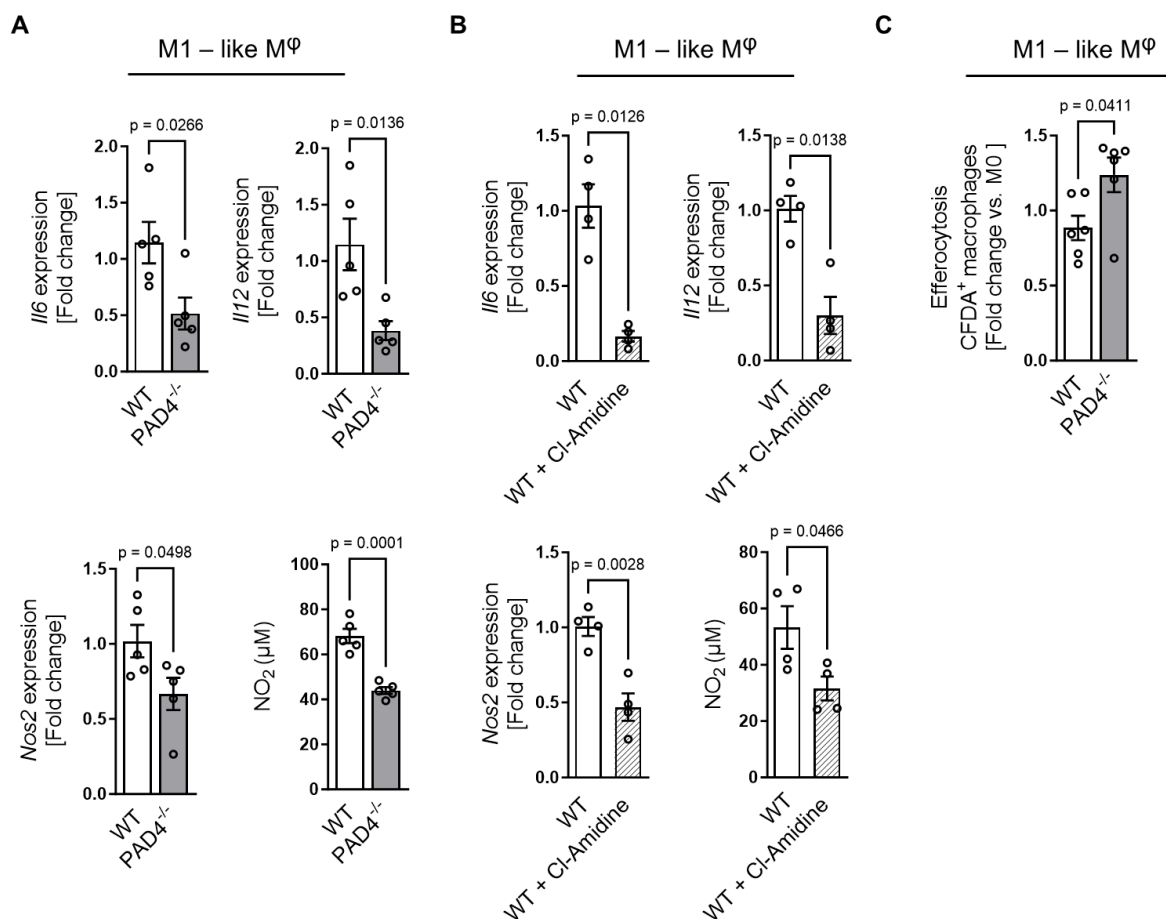


Figure 25: Role of PAD4 in inflammation-related macrophage polarization and function. Bone marrow-derived WT and PAD4^{-/-} macrophages were stimulated with LPS and IFN γ to induce pro-inflammatory M1-like macrophages. **(A)** Fold change expression of selected inflammatory genes in M1-like WT and PAD4^{-/-} macrophages. Nitrite levels in culture supernatants were quantified by Griess assay (n = 5). **(B)** Fold change expression of selected inflammatory genes in WT M1-like macrophages and WT macrophages polarized toward M1-like phenotype in the presence of the pan-PAD inhibitor Cl-Amidine (200 μ M). Nitrite levels in culture supernatants were quantified by Griess assay (n = 4). **(C)** Flow cytometry analysis for quantification of efferocytosis capacity of macrophages polarized toward a M1-like phenotype (n = 5-6). Data are shown as means \pm SEM. Student's unpaired t-Test or Mann-Whitney test was used to assess differences between two groups.

4.3.3. Diminished fibrotic pathways in cardiac fibroblasts (CFs) as a result of PAD4 deficiency

Cardiac regeneration is closely associated with the level of fibrosis that occurs as a result of the multifaceted pro-inflammatory immune response. Based on the findings showing that the inflammatory process and the integrity of the ECM are altered by the loss of PAD4, it is highly likely that PAD4 regulates the function of CFs during cardiac regeneration. To prove this assumption, CFs were isolated from hearts of PAD4-deficient and WT mice on day 7 post-MI, cultured up to passage 1, and subjected to microarray analysis. By employing a \log_2FC difference of ± 2 in conjunction with a significance threshold of p -value set at 0.05, 1782 differentially expressed genes were identified in CFs from PAD4^{-/-} mice compared to controls. Being the most regulated gene, the downregulation of *Lum* (lumican) (\log_2FC -62.63) is of interest, given the important role in regulating collagen fibrillogenesis in connective tissues (Mohammadzadeh et al. 2019). This observation aligns with a decrease in the expression of dermatopontin (*Dpt*) (\log_2FC -45.25), the second most downregulated gene in CFs from PAD4^{-/-} mice. Moreover, *Dad1* (\log_2FC +14.56), responsible for encoding the defender against apoptotic cell death, exhibited an upregulation in CFs from PAD4^{-/-} mice (**Fig. 26A**). The most notable changes among downregulated GO terms associated with biological process were linked with genes involved in DNA replication, cell cycle and ECM assembly (**Fig. 26B**). Interestingly, besides the top 10 downregulated pathways shown in Fig. 26, many identified down-regulated genes also participate in the regulation of canonical and non-canonical Wnt signalling pathways. Array analysis revealed downregulation of genes related to the Wnt signaling pathway, such as *Fzd1* (Frizzled Class Receptor) and *Tgfr1*, as well as genes linked to cell proliferation like *Pdgfra* (Platelet-derived growth factor receptor alpha), in mice lacking the *Padi4* gene. Using Real-time PCR, the downregulation of *Fzd1* and *Pdgfra* was confirmed, while *Tgfr1* showed a trend towards downregulation without statistical significance. (**Fig. 26C**). However, an increase of genes coding for ribosomes and translation machinery was observed in CFs from PAD4^{-/-} mice post-MI (**Fig. 26B**), indicating an enhanced ability of these cells to produce proteins.

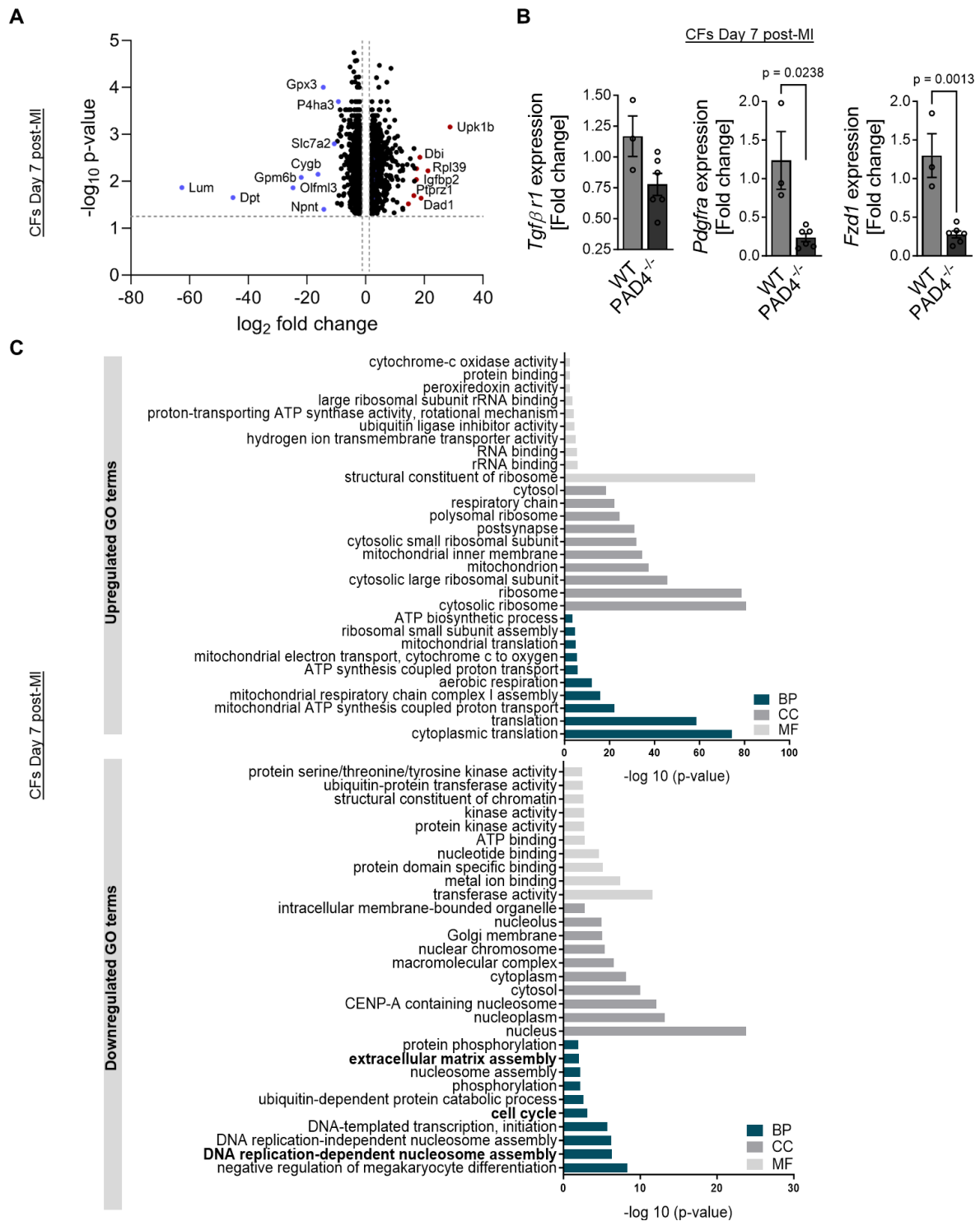


Figure 26: Transcriptomic alteration in CFs from $PAD4^{-/-}$ mice on day 7 post-MI. (A) CFs were isolated post-MI and cultured up to P1. Bar plots illustrate the top 15 up- and down-regulated genes in $PAD4^{-/-}$ mice CFs. (B) Top 10 of significantly enriched GO terms in biological process (BP), molecular function (MF) and cellular component (CC). (C) Gene expression levels of selected downregulated genes identified through microarray analysis were confirmed by Real-time PCR ($n = 3-5$). Data are shown as means \pm SEM. Student's unpaired t-Test or Mann-Whitney test were used to assess differences between two groups.

4.3.4. Reduction of cardiac fibrosis after PAD4 ablation in mice

CFs showed selected downregulated genes implicated in the fibroblast to myofibroblast transition and cardiac fibrosis. Consequently, the remodelling processes, including fibrosis, were investigated on day 7 post-MI in the hearts of PAD4^{-/-} and WT mice. Analysis of fibrotic genes in heart tissue from both WT and PAD4-deficient mice using Real-Time PCR revealed a significant reduction of *Col1α1*, *Acta2* and *MMP2* expression levels in the infarct/peri-infarct region of PAD4^{-/-} mice compared to WT mice (**Fig. 27A**). However, whereas the *Tgfβ* expression did not differ between the two groups, TGF-β protein levels were significantly diminished at this day post-MI in mice lacking *Padi4* (**Fig. 27B**). In addition, reduced protein levels of phosphorylated Smad2 (*pSmad2*), a direct downstream target of TGF-β receptor 1 activation, were detected in PAD4^{-/-} mice when compared to controls (**Fig. 27B**), suggesting that the TGF-β signalling pathway is less activated in PAD4^{-/-} mice. Moreover, reduced levels of collagen type I (Col I) and elevated levels of collagen type III (Col III) were observed in the cardiac tissue of PAD4^{-/-} mice. Consequently, the ratio of Col I / Col III was significantly decreased in these mice. Since PAD4-deficient mice showed lower cardiac expression of genes commonly known as myofibroblast marker such as *Acta2* (**Fig. 27A**), α-SMA⁺ cells in hearts of PAD4^{-/-} mice and controls at day 7 post-MI were quantified. Consistently, the number of α-SMA⁺ cells in the infarct/peri-infarct region was lower in hearts of PAD4^{-/-} mice compared to controls (**Fig. 27C**). In line, analysis of heart tissue sections stained with Sirius red and Masson trichrome showed a significant reduction in fibrotic area in mice lacking *Padi4* (**Fig. 27D**).

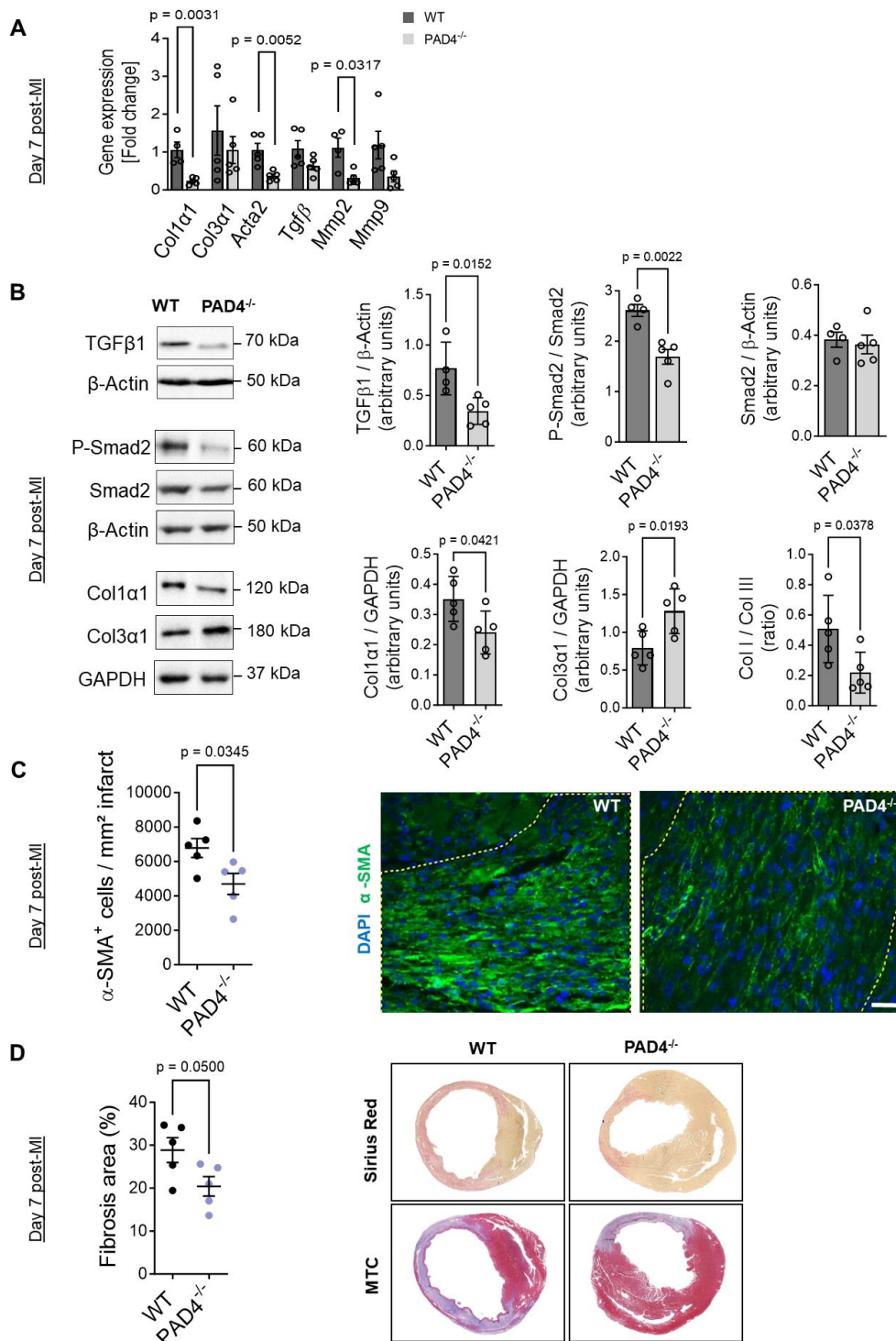


Figure 27: Effect of PAD4 on cardiac fibrosis on day 7 post-MI. (A) Expression levels of fibrosis-related genes in the infarcted area/border zone from WT and PAD4^{-/-} mice (n = 4-5). **(B)** Protein levels of TGFβ, p-Smad2, Smad2, Col1α1 and Col3α1 in infarcted hearts. GAPDH or β-actin served as the normalization control. Representative Western blots are illustrated (n = 4-5). **(C)** Immunofluorescence staining showing the distribution of α-SMA positive cells (green), with nuclei counterstained using DAPI (blue). Quantification of α-SMA positive cells within the infarcted area post-MI (n = 5) Scale bar, 20 μm. **(D)** Representative images depict Sirius Red and Masson's trichrome (MTC)-stained sections of heart tissue post-MI. Quantification of fibrotic area within the infarcted hearts (n = 5). Data are shown as means ± SEM. Student's unpaired t-Test or Mann-Whitney test was used to assess differences between two groups.

4.4 PAD4 deficiency and pharmacological pan-PAD inhibition starting at day 7 post-MI limits maladaptive cardiac remodelling

The results shown above indicate that PAD4 deficiency extenuate inflammation and cardiac fibrosis, possibly by regulating the phenotypes of cardiac macrophages and fibroblasts. However, considering that reduction of collagens can counteract adverse cardiac remodelling, such an effect could potentially lead to beneficial long-term outcomes following infarction and improve survival rates. To assess the translational significance of pan-PAD inhibitors in mitigating adverse cardiac remodelling and subsequent heart failure post-MI, WT and PAD4^{-/-} mice underwent LAD ligation as previously described. Treatment with BB-CI-Amidine in WT mice was started on day 7 post-MI (WT + BB-CI (d7)) and continued with daily injections until day 28 post-MI (**Fig. 28A**). Keeping in mind that treatment with BB-CI-Amidine in the initial phase post-MI significantly increases the inflammatory response and mice mortality, the treatment with the inhibitor was started after resolution of inflammation (day 7). At that time point, reduced immune cell recruitment in WT mice, a hallmark for the anti-inflammatory process, was observed (**Fig. 18 and 21**).

Interestingly, the expression of the *Padi4* gene remained elevated on day 28 post-MI in WT mice compared to its baseline conditions, highlighting the pivotal role of PAD4 in the remodelling process following MI (**Fig. 28B**). In WT + BB-CI (d7) mice, no differences were observed in *Col1a1* expression compared to both other groups, but there was a significant increase in *Col3a1* expression compared to both. Moreover, more mRNA levels of *Acta2* were found in WT + BB-CI (d7) compared to PAD4-deficient mice (**Fig. 28C**). Similarly, to PAD4^{-/-} mice, treatment with BB-CI-Amidine starting at day 7 resulted in a substantial reduction in collagen abundance and of the fibrotic area at day 28 post-MI when compared to untreated WT (**Fig. 28D**). Importantly, PAD4 ablation in mice significantly improved 28-day survival compared to WT mice and similar improvements in survival were observed in the WT + BB-CI (d7) group (**Fig. 28E**).

To summarize, initial pharmacological inhibition of PADs during the first 7 days promotes cardiac rupture and inflammation. Inhibiting PADs, including PAD4, at a later stage improves long-term survival in mice by minimizing excessive deposition of ECM and scar formation post-MI.

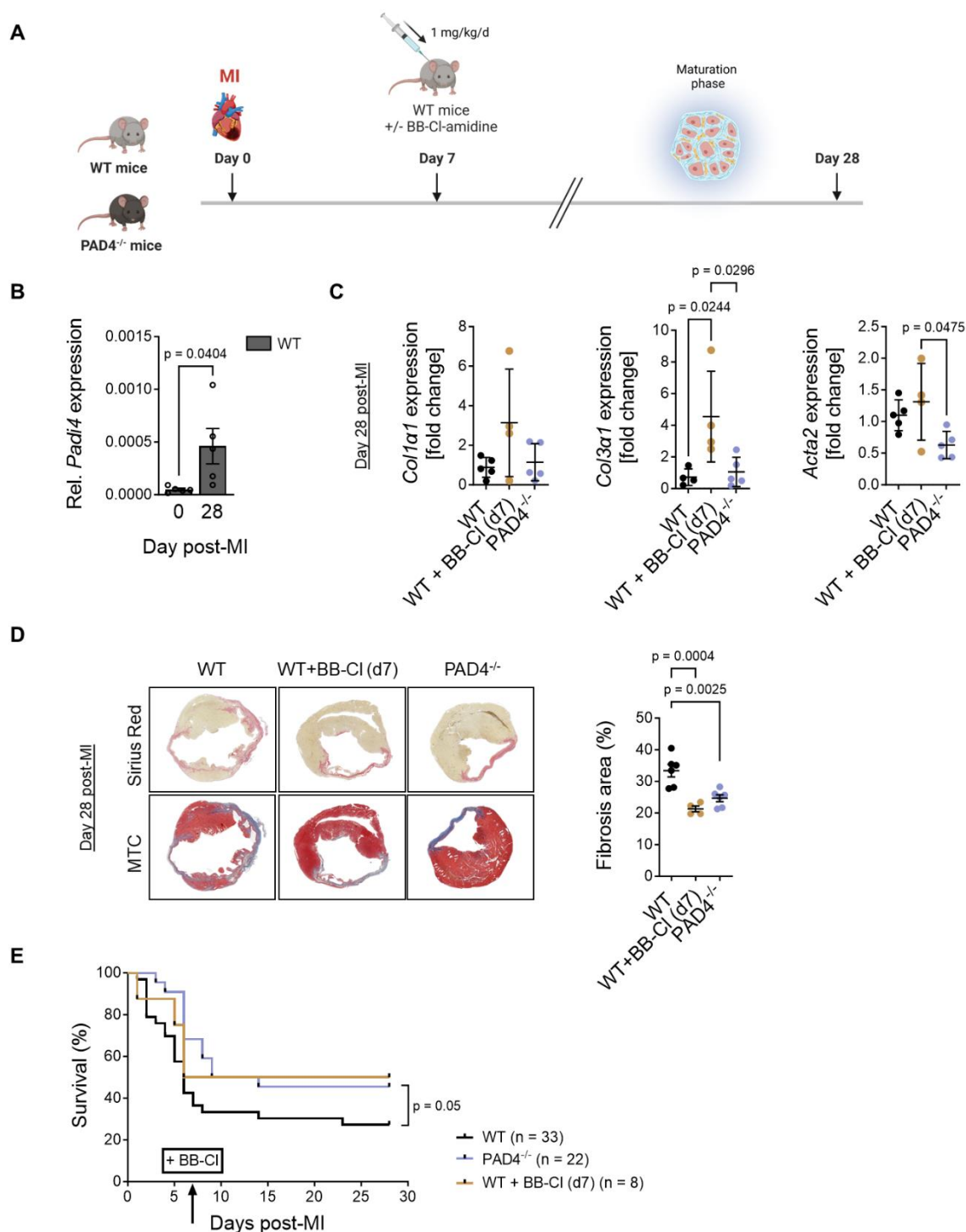


Figure 28: Impact of pharmacological PAD Inhibition initiated at day 7 and PAD4 deficiency on cardiac remodelling and long-term survival. (A) Experimental Setup. MI was induced by permanent ligation of LAD in all three groups and some WT mice were daily treated with the pan-PAD inhibitor BB-CI-Amidine (1 mg/kg/d) starting at day 7 until day 28 post-MI. **(B)** Expression of *Padi4* under baseline conditions and post-MI in WT mice (n = 5). **(C)** mRNA levels of fibrosis-related genes in infarcted LV analysed by Real-time PCR (n = 4-5). **(D)** Representative images of Sirius Red and Masson's trichrome (MTC) stained sections of heart tissue post-MI. Quantification of fibrotic area (n = 4-5). **(E)** Kaplan-Meier survival analysis for WT, PAD4^{-/-}, and WT +BB-CI (d7) mice. Data shown as means ± SEM. Mann-Whitney test or One-way ANOVA with Tukey's post-hoc test or Kruskal-Wallis test with Dunn's post-hoc test was used for statistical analysis. Graphic created with BioRender.

5. Discussion

The management of HF post-MI represents a significant challenge due to limited options for risk assessment and pharmacological treatment. Despite timely and urgent revascularization and subsequent treatment strategies, the occurrence of HF is persistently increasing, with an expected surge of 46% by the year 2030 (Heidenreich et al. 2013). Not only the European Society of Cardiology, but also the American Heart Association has recognized HF prevention as an urgent public health priority (Heidenreich et al. 2022; Roth et al. 2020). It is widely known that inflammation and the development of fibrosis influence each other and play a fundamental role in the pathogenesis of HF. Targeting fibrosis and thereby inducing tissue regeneration specifically poses a significant challenge, as achieving these objectives represents the optimal therapeutic goal for post-MI treatment (Travers et al. 2022). In this study, genetic ablation of *Padi4* was found to ameliorate cardiac remodelling by reducing inflammation and fibrosis, thus improving survival rates. Additionally, pharmacological inhibition of PADs, after the resolution of inflammation, also demonstrated a reduction in fibrosis, thus preventing HF prevalence and revealing an advantage for survival.

Given the association of PAD4 with diverse cardiac diseases, the expression of *Padi4* surged in mice across all experimental time points (days 1, 3, 7, and 28) post-MI compared to its baseline levels. In addition, highlighting its exclusive role, *Padi4* was the only isoform detectable in bulk RNA-seq analysis of cardiac tissue post-MI, and it was significantly upregulated after treatment with the pan-PAD inhibitor BB-CI-Amidine. Moreover, the upregulation of *Padi4* was not only confined to the experimental mice model, it was also conspicuously evident in MI patients underlying its clinical relevance. Upregulation of *Padi4* after MI coincided with an increase in citrullination of histone H3, indicating calcium-dependent activation of PAD4 in the ischemic tissue. However, although citH3 is essential for NETs formation, in this study, these structures were only detectable on day 1 post-MI in WT mice, but not at later stages. Du et al. showed NETs formation on day 3 post-MI by co-localization of NE signals with spread DAPI patterns (Du et al. 2020). The process of histone 3 (H3) citrullination, imperative for NETs formation, was not addressed. Several studies, focusing directly on NETs formation, used models of ischemia/reperfusion (I/R), revealing significant endothelial damage, ROS production, and elevated Ca^{2+} concentrations (Ge et al. 2015; Kivit et al. 2024; Lewis et al. 2015). The highest Ca^{2+} concentration or Ca^{2+} overload occurs directly post-MI in the acute phase, ensuring the highest detectability for NETs formation. This is due to ischemia, which affects the function of ion pumps, such as the Na^+/K^+ -ATPase and the Ca^{2+} -ATPase of the sarcoplasmic reticulum (Bögeholz et al. 2012; Baumeister and Quinn 2016). The intracellular sodium concentration increases, enhancing the activity of the $\text{Na}^+/\text{Ca}^{2+}$

exchanger, which transports calcium into the cells to compensate for the excess sodium. Finally, studies indicate that it is quite important to balance the membrane potential as fast as possible, to control excitation-contraction coupling in cardiomyocytes, preserving cardiac function and preventing cell apoptosis. (Bagur and Hajnóczy 2017; Berridge et al. 2003; Sutanto et al. 2020). Since PAD4 activity is highly dependent on Ca^{2+} concentration, this could explain why NETs formation or citrullination of H3 is difficult to detect on day 3 or later on.

To the current knowledge, moderate inflammation is crucial for the subsequent healing process, but excessive inflammation is associated with worsened cardiac outcomes and increased fibrosis (Frangogiannis 2015). Whenever PAD4 was genetically or pharmacologically inhibited, there were significant transcriptomic changes in the cardiac tissue post-MI regarding inflammation. For example, after pan-PAD inhibition, a heightened immune response and upregulation of pathways linked to the positive regulation of oxidative stress, response to stress, hypoxia, and oxygen levels were observed by GO term analysis in these mice. A recent publication has demonstrated that GDF-15, whose expression was significantly upregulated in WT + BB-Cl mice, serves as an inflammatory and oxidative stress biomarker, with emerging research suggesting its potential involvement in myocardial fibrosis (Dominguez-Rodriguez et al. 2011). GDF-15 was detectable as a marker of left ventricular remodelling and could function as an integrative biomarker of HF in patients experiencing acute MI (Leancă et al. 2022; Dominguez-Rodriguez et al. 2011). Interestingly, this marker was significantly downregulated in PAD4-deficient mice. Thus, indicating that WT+BB-Cl mice showing increased tendency for HF conditions. Moreover, inflammatory cytokines such as TNF- α and IL-6, both of which showed significantly upregulated RNA levels in inhibitor-treated mice, are strongly associated with adverse LV remodelling (Schumacher and Naga Prasad 2018; Mohan et al. 2017; Hartupee and Mann 2013). In addition, shortly after ischemic injury, these cytokines are released and play crucial roles in regulating apoptosis (Fanola et al. 2017; Fontes et al. 2015; Tian et al. 2015). Here, after pharmacological inhibition of PADs, pathways linked to the positive regulation of cell death were noted to be upregulated. Cardiac troponin, released by necrotic cardiomyocytes, is an established clinical marker for cardiac damage (Jaffe et al. 1996; Potter et al. 2022). In this study, both WT mice treated with BB-Cl and PAD4^{-/-} mice exhibited elevated levels of this marker following MI compared to WT mice, suggesting increased death of cardiac cells in these mice. In contrast, Du et al. reported that pharmacological PAD4 inhibition with GSK484 led to reduced cTnT levels post-MI (Du et al. 2020). It should be noted that GSK484 is a selective and reversible inhibitor of PAD4. In contrast, BB-Cl-Amidine inhibits multiple PAD isoforms, including PAD2, whose expression was detectable in cardiac tissue. Anyhow, preliminary data from our research group indicated that despite elevated cTnT levels on the first day post-MI, PAD4^{-/-} mice did not exhibit a significantly larger infarct size in the early phase post-MI. More importantly, these mice

demonstrated a better recovery, as verified by improved cardiac function at later stages (day 21) (Eghbalzadeh et al. 2019).

In this context, the infarct size in PAD4-deficient mice does not appear to be notably larger at the first days (day 1 - 3) post-MI compared to WT mice in this study. This may be evidenced by the observation of reduced levels of *pMLKL*, a marker for cell necroptosis (a form of inflammation-induced cell death triggered by TNF α), in the heart tissue of PAD4-deficient mice. In contrast, BB-CI-treated mice exhibited significantly higher levels of *pMLKL*. Supportive, elevated levels of cardiac *Tnfa* were found in mice treated with BB-CI but not in PAD4^{-/-} mice. However, necroptosis is associated with the release of DAMPs, subsequently triggering an inflammatory response and affecting the extent of fibrosis, as these processes are closely connected. Several studies have shown increased protein expression of *pMLKL* in the myocardium following ischemic injury in mice, indicating that RIPK1/RIPK3-dependent pathways, including MLKL/*pMLKL*, contribute to worsened cardiac outcomes and increased fibrosis (Guo et al. 2022; Wu et al. 2021b; Piamsiri et al. 2021). Together with this, higher levels of cleaved DNA fragments were detected in inhibitor-treated mice at day 1 and 3 post-MI compared to PAD4-deficient and WT mice, may correlating with extended infarct area (Piamsiri et al. 2021).

Myeloid cells, including macrophages and neutrophils, are essential for phagocytizing dead cells and damaged ECM. This process promotes cardiac healing and reduces the extent of cardiac damage, thereby mitigating cardiac fibrosis (Duncan et al. 2020; Kain and Halade 2020). FACS analysis in this study showed a significant reduction in myeloid cell counts in mice treated with BB-CI and PAD4^{-/-} on day 1 post-MI compared to WT. Additionally, there was no increase in myeloid cell count at day 3 post-MI in inhibitor-treated mice compared to WT. In light of this, on day 1 post-MI, the predominantly cell population in PAD4^{-/-} mice was characterized by neutrophils, whereas in WT + BB-CI mice, the most detected cells were characterized as macrophages. Interestingly, the neutrophil recruitment was markedly impaired in inhibitor-treated mice on day 1, indicating an immune response imbalance in these mice. These results let suggests that PADs or PAD2, rather than PAD4, may be involved in myeloid chemotaxis in general, as *Padi2* was detectable in heart tissue of these mice. Additionally, one study by Horibata et al., demonstrated that PAD2 depletion (lentiviral shRNA-mediated depletion) inhibits cell migration and invasion of mammary tumor cells, as shown by wound healing and single cell tracking assays (Horibata et al. 2017). Moreover, they showed, that BB-CI-Amidine treatment suppresses cell migration and enhances cell adhesion in this cancer cell line (Horibata et al. 2017). Alternatively, other PADs could also be necessary for chemotaxis, as there is no clear indication reported in the literature on this topic.

Despite this fact the predominantly cell population was characterized as macrophages in WT + BB-CI mice. RNA-seq analysis of infarcted cardiac tissue from these mice revealed increased mRNA levels of inflammation-associated genes such as *Il6*, *Ly6c* and *Tnfa*, which are commonly expressed by inflammatory monocytes/macrophages (Mills 2015). Studies highlighted a well-coordinated interaction between initially arriving neutrophils and infiltrating macrophages within the heart tissue, including cardiac-resident macrophages (Silvestre-Roig et al. 2020). In neutropenic mice, cardiac macrophages exhibited changes in their activation patterns, which were marked by an increased pro-inflammatory response and reduced ability to clear apoptotic cells compared to macrophages from mice with normal neutrophil levels (Silvestre-Roig et al. 2020). In addition, co-culture experiments of neutrophils with activated macrophages conducted by Marwick et al. showed a reduction in the release of inflammatory mediators by macrophages ongoing with impaired nuclear factor- κ B (NF- κ B) activation (Marwick et al. 2018). Moreover, it has been reported that following LAD ligation in mice, neutrophil depletion worsens cardiac function driving adverse remodelling and heart failure (Horckmans et al. 2017). In contrast, in mice the neutrophils or the neutrophil secretome were found to promote macrophage polarization towards a reparative M2 phenotype (Horckmans et al. 2017). Consequently, it can be hypothesized that the absence of neutrophils in mice treated with BB-CI preserves the inflammatory phenotype of macrophages, especially since *Ly6c* is recognized as a primary marker for murine infiltrating monocytes / macrophages (Ma et al. 2018; Mouton et al. 2018; Heidt et al. 2014).

Moreover, the heart-to-body weight ratio was significantly increased on days 1 and 3 post-MI in WT + BB-CI mice, and an accumulation of macrophages in the heart is associated with increased left ventricular volume and reduced diastolic function (Hulsmans et al. 2016; Bajpai et al. 2019). In general the massive infiltration of monocytes/macrophages has been linked to ventricular remodelling and fibrosis for over 20 years (Yerra and Advani 2022; Frangogiannis et al. 2002). For example, peripheral monocytosis occurs in patients with MI and correlates positively with end diastolic volume and negatively with EF, acting as an independent predictor of pump failure. Specifically, a peak number of circulating monocytes were observed in MI patients with pump failure or LV aneurysm demonstrating a negative correlation with EF and survival (Maekawa et al. 2002). Consequently, the cardioprotective role of PAD inhibition in the acute phase seems to be absent. More likely, these mice exhibited infarct expansion in conjunction with ventricular dilation. Therefore, collagen deposition during the inflammatory phase is mandatory to maintain structural integrity of the heart. As higher levels of cleaved DNA fragments and pMLKL were found in WT + BB-CI mice, the total collagen content was significantly reduced in these mice during the acute phase post-MI, indicating an instability of the heart. Investigations in a mouse model of MI showed associations between ECM deposition and a higher incidences of LV rupture (Hanna et al. 2020). Clinical investigation

evidenced that even when the heart experiences an increase in volume, it becomes dilated, potentially leading to a decrease in pumping function and the inability to adequately circulate blood throughout the body (Cohn et al. 1993; Ferreira et al. 2023). Consequently, this could explain, why WT + BB-CI mice exhibited a poor prognosis post-MI, evidenced by a mortality rate of 70%, whereas PAD4^{-/-} and WT mice experienced only a 30% mortality rate. Ultimately, different studies showed that post-MI patients with left ventricular systolic dysfunction have a higher risk of mortality or morbidity (Gheorghiade and Fonarow 2007).

Notably, the consistently and prominently downregulated genes at day 1 and 3 post-MI identified by RNA-seq analysis in infarcted hearts of PAD4^{-/-} and inhibitor-treated mice compared to WT mice were *Mybphl*, *Myl7*, and *Myl4*. Myosin subunits, such as *Myl7*, were significantly downregulated in cardiomyocytes of HF patients, as identified through human single-cell RNA transcriptome profile analysis (Zhu et al. 2022). MYL7, the regulatory light chain of myosin, plays a crucial role in myocardial contractility by hydrolyzing ATP to release energy (Kampourakis and Irving 2021). Consequently, downregulation of MYL7 suggests impaired cardiomyocyte function and heart contractility. Transthoracic echocardiography analysis conducted within our laboratory revealed impaired cardiac function in PAD4-deficient mice compared to WT on day 1 post-MI. This was characterized by diminished EF, reduced left ventricular posterior wall thickness, and decreased fractional shortening (Eghbalzadeh et al. 2019). However, these effects disappeared in later stages, with observable improvements in heart function in these mice (Eghbalzadeh et al. 2019). Nevertheless, it might indicate that a lack of PAD4 in the acute phase post-MI does not support cardiac function and could be assumed for PAD inhibition as well.

Among the similarities between WT + BB-CI and PAD4^{-/-} mice, the notable differences were observed in respect to fibroblast growth factors (FGFs). For example, comparing pharmacological inhibition of PADs to PAD4 deficiency revealed that pan-PAD inhibition led to significantly higher *Fgf23* expression compared to *Padi4* ablation. Clinical studies have shown that in MI patients with concomitant HF, significantly higher FGF23 levels were observed among non-survivors compared to survivors, and were fairly predictive for one-year mortality in patients with concomitant HF (Cornelissen et al. 2022). Moreover, a significant upregulation of *Fgf6* expression was found in PAD4^{-/-} mice. Investigations by Floss et al found that FGF6 could completely restore experimentally damaged skeletal muscle (Floss et al. 1997). The heart is also a muscle, and a study by Hu et al. demonstrated that treatment with recombinant FGF6 improved cardiac function, reduced infarct size and promoted cardiac repair in a mouse model of MI (Hu et al. 2022). Considering that different FGFs were the most striking differences between the inhibition and genetic knockout of PAD4, it can be assumed that a compensatory mechanism is present in the PAD4-deficient mouse. This is supported by numerous studies

showing a positive correlation between FGFs and improved cardiac function or angiogenesis (Itoh et al. 2016; Xie et al. 2020).

However, in the end, there was no clear advantage to blocking PAD4 during the first days post-MI, as PAD4^{-/-} mice did not exhibit any survival benefits. This data strongly suggests that inhibiting PADs generally during the initial days post-MI may not be protective, but rather deleterious. Therefore, as mentioned, the role of other PADs, such as PAD2, should be taken into consideration, since *Padi2* expression was detectable in the cardiac tissue of PAD4^{-/-} mice. In contrast to WT + BB-CI mice, where PAD2 is blocked. Although the survival rate of PAD4^{-/-} mice was not significantly higher compared to WT mice, it was significantly increased compared to inhibitor-treated mice showing increased 7-day mortality. This underscores the detrimental effect of PAD2 inhibition in mouse survival post-MI.

Likewise, the most pronounced benefits in PAD4-deficient mice manifested around day 7 post-MI, characterized by notable downregulation of cytokines, chemokines and receptors such as *Il6*, *Il12*, *Tnfa*, *Mpo*, *Ccl2*, and *Ccr2* in cardiac tissue. These downregulations impacted pathways crucial for immune cell migration and inflammatory responses, with continued downregulation evident on day 7 post-MI. CCL2 and CCR2 are key regulators for the infiltration of monocytes / macrophages (Mo/M ϕ), associated with a predominantly pro-inflammatory phenotype and pronounced immune response. FACS analysis in this study showed that the percentage of macrophages was significantly reduced on day 7 post-MI and a clear tendency for a decrease in CD45⁺CD11b⁺F4/80⁺CCR2⁺ cells in PAD4^{-/-} mice was observable. The literature clearly indicates that CD11b⁺F4/80⁺ cells in general and specifically CD11b⁺F4/80⁺CCR2⁺ cells, are associated with increased inflammation, enhanced recruitment of monocytes, infarct expansion, reduced cardiac function, and excessive fibrosis (Bajpai et al. 2019; Boniakowski et al. 2018). Thus, a recently published study demonstrated that global CCR2 KO in mice or administration of the specific CCR2 inhibitor RS102895, reduced infarct size and downregulated inflammatory mediators after I/R injury (Shen et al. 2024). However, cardiac macrophages (CD11b⁺F4/80⁺ cells) demonstrate a broader transcriptional diversity *in vivo* than conventionally depicted by the M1/M2 paradigm (Ma et al. 2018; Mouton et al. 2018). Despite this variability, the presence or absence of CCR2 consistently serves as a reliable marker for macrophage origin and phenotype. Genetic fate mapping studies have elucidated that CCR2 expression distinguishes monocyte-derived cardiac macrophages (CD11b⁺F4/80⁺CX3CR1⁻CCR2⁺) from those originating from yolk sac progenitors in mice (Martini et al. 2019; Epelman et al. 2014). Using genetic fate mapping, long-term parabiosis and RNA sequencing two resident macrophage populations (MHC-II^{low}CCR2⁻ and MHC-II^{hi}CCR2⁻), along with one monocyte-derived macrophage population (MHC-II^{hi}CCR2⁺) and one monocyte population (MHC-II^{low}CCR2⁺) were identified in the adult mouse heart.

Significantly, in the context of injury, the adult heart selectively recruits monocytes and MHC-II^{hi}CCR2⁺ monocyte-derived macrophages, (Dick et al. 2019).

As the MFI in cardiac tissue showed a reduction of CD45⁺CD11b⁺F4/80⁺CCR2⁺ cells, isolated PAD4^{-/-} Mo/M ϕ at day 7 post-MI exhibited reduced expression levels of *Ccr2*, along with decreased levels of *Il6*, *Nos2*, *Tnfa*, *Il1a*, *Ccl9*, *Ccl5*, *Ccl6*, and *Ccr1*. These markers are all contributors to inflammation, indicating a less inflammatory phenotype of these cells. However, the shift towards a less inflammatory phenotype could be attributed to PAD4 deficiency, because PAD4^{-/-} M1-like BMDM showed reduced *Ccr2*, *Il6*, *Il12*, and *Nos2* expression. Similar results were observed in the presence of the pan-PAD inhibitor Cl-Amidine, suggesting that the regulation of genes characteristic for M1-like macrophages is under the control of PAD4. In line, a study by Cheng et al. who demonstrated that BMDM and THP-1 macrophages infected with an adenovirus vector for overexpression of PAD4 showed an increase in the M1 markers such as *Ccr7*, *Ccl2* and *Tnfa*, indicating modulation of M1 polarization by PAD4 (Cheng et al. 2021). Moreover, it has been published by Sun et al. that citrullination of NF- κ B promotes its nuclear translocation and the expression of IL-1 β and TNF- α (Sun et al. 2017). Accordingly, the absence of PAD4 may prevent citrullination of NF- κ B and nuclear translocation, potentially explaining the downregulation of inflammatory genes observed in PAD4^{-/-} Mo/M ϕ .

Besides, the function of efferocytosis capacity was markedly improved in PAD4^{-/-} M1 polarized BMDM *in vitro*. These functions are important for clearing debris and apoptotic cells as an early response after inflammation (van der Laan et al. 2014; Duncan et al. 2020). Although it has not been tested *in vivo*, it is vital for limiting the release of DAMPs and clearing cell debris during the acute phase after MI, thereby reducing the extent of cardiac damage, infarct area and resulting fibrosis. Gene ontology analysis at day 7 post-MI from PAD4^{-/-} Mo/M ϕ showed a significant downregulation of pathways related to endocytosis and phagocytosis, indicating a non-inflammatory or less M1-like macrophage proliferation. But *Tgf β* levels, often associated with M2-like macrophages, were not upregulated in PAD4-deficient mice, in contrast it was almost significantly downregulated on this day post-MI.

Despite this fact, PAD4^{-/-} Mo/M ϕ showed upregulated CD206 expression, still suggesting polarization towards a reparative M2 phenotype (Nawaz et al. 2017; Mouton et al. 2018; Bajpai et al. 2019; Li et al. 2022; Mills 2015). Supporting this, a decrease in CD45⁺CD11b⁺F4/80⁺CCR2⁺ cells was observed in hearts of PAD4^{-/-} mice. Willenborg et al. demonstrated that CD11b⁺F4/80⁺CCR2^{-/low} Ly6c^{-/low} macrophages exhibited the highest gene expression of CD206 at day 4 or 14 after injury, as isolated from skin wound tissue (Willenborg et al. 2012). Beyond that, studies have shown that reparative macrophages regulate cardiac fibroblast activation, thereby reducing cardiac fibrosis. M2b macrophages, significantly suppressed the proliferation and migration of cardiac fibroblasts, the expression of fibrosis-

related proteins like collagen I and α -SMA, and differentiation into cardiac myofibroblasts (Jung et al. 2017; Yue et al. 2020). Furthermore, after transplantation of M2b macrophages in a rat model of I/R, improved cardiac function and reduced cardiac fibrosis were observed (Yue et al. 2020). In accordance with that study, a recent study demonstrated that in co-culture settings of BMDMs with CFs *in vitro*, treatment with recombinant CCL2 stimulated macrophages to release TGF- β and facilitated the release of collagen I by fibroblasts, thereby promoting the transformation of CFs into myofibroblasts. This effect was attenuated in BMDMs from CCR2^{-/-} mice (Shen et al. 2024). As outlined above, isolated cardiac PAD4^{-/-} Mo/M ϕ on day 7 post-MI showed significantly less *Ccr2* expression and could therefore explain the reduced *Tgfb* expression observed in these cells too. Moreover, whereas the significant upregulation of inhibitory *Smad7* could not be confirmed by PCR, these findings might indicate a negative regulation of TGF- β cascade and fibrotic pathways in these Mo/M ϕ subsets.

CFs generate a network of extracellular protein fibers and connecting proteins that contribute to the structural integrity of tissues. However, excessive collagen deposition can have serious consequences for heart function and tissue elasticity (Kong et al. 2014; Hanna and Frangogiannis 2019). PAD4-deficient CFs isolated on day 7 post-MI exhibited reduced expression of *Pdgfra* and a recent study has elucidated that PDGFR α ⁺ CFs serve as the main contributors to the synthesis of type 1 collagen. Furthermore the deletion of these PDGFR α ⁺ cells resulted in an improved cardiac function after LAD-ligation in mice (Kuwabara et al. 2022). Yue et al. demonstrated that M2b macrophage treatment *in vitro* inhibited PDGFR kinase activation in CFs and since PAD4^{-/-} Mo/M ϕ showed similar anti-inflammatory characteristics on day 7 post-MI, potentially explaining the reduced activation of pro-fibrotic signaling pathways in CFs from PAD4-deficient mice (Yue et al. 2020). Thus, impaired PDGFR activation in CFs could result in reduced fibrotic area. Additionally, the significant downregulation of the pro-inflammatory cytokine *Il6* in PAD4^{-/-} hearts, as well as in isolated PAD4^{-/-} Mo/M ϕ at day 7 post-MI, could contribute to a reduced fibrotic area, as this cytokine is well-established in cardiac fibrosis (Meléndez et al. 2010). Sarkar et al. demonstrated that IL-6 treatment increased collagen gene expression in cultured CFs (Sarkar et al. 2004). Furthermore, IL-6 promoted the production of TGF- β 1 and the phosphorylation of Smad3, which in turn facilitated the transformation of CFs into collagen-producing myofibroblasts (Ma et al. 2012). Heart tissue from mice lacking the *Padi4* gene showed decreased TGF- β levels and impaired Smad2 activation at day 7 post-MI. Correspondingly, type 1 collagen was significantly lower, along with a reduced abundance of α -SMA⁺ cells, leading to a reduced fibrosis area. The reduced gene expression of *Tgfb* in PAD4^{-/-} Mo/M ϕ may provide an explanation for the reduced TGF- β levels observed in hearts of mice lacking the *Padi4* gene. These cells are considered the main producers of TGF- β , a crucial growth factor that promotes fibrosis. (Lafuse et al. 2020, Frangogiannis 2012, 2015). Besides, a well-documented fact is that TGF- β has a positive

feedback loop, thereby regulating itself. It utilizes several pathways to support its autoinduction. Consequently reduced TGF- β levels in cardiac tissue are expected to dampen *Tgf β* expression (Hariyanto et al. 2021). Anyhow, the reduced TGF- β levels observed in PAD4^{-/-} mice align with recent data showing decreased TGF- β levels in mice treated with the non-covalent specific PAD4 inhibitor JBI-589 (Heger et al. 2023). This suggests a broader influence of PAD4 on TGF- β production.

The effect of *Padi4* ablation on CF characteristics, as assessed by microarrays, showed additionally downregulation of *Tgfbr1* and *Fzd1*, both implicated in fibroblast-to-myofibroblast transition and fibrosis (Laeremans et al. 2010). Pathways related to fibrosis or transdifferentiation of CFs, such as extracellular matrix assembly, cell cycle, and DNA replication, were significantly downregulated in these cells. Yet, prior investigations conducted within our laboratory have demonstrated that the deficiency of PAD4 in CFs impedes TGF- β -induced transdifferentiation into myofibroblasts *in vitro*. Moreover, PAD4^{-/-} CFs did not upregulate *Col1a1* and *Acta2* expression after TGF- β treatment (Akboua et al. 2021), indicating impaired activation of TGF- β signalling. Nonetheless, reduction of TGF- β receptors encoding genes in CFs in combination with reduced cardiac levels of TGF- β apparently contribute to impaired myofibroblast abundance in PAD4^{-/-} mice. This assumption is also supported by the fact, that the ratio of type I collagen to type III collagen was significantly lower in PAD4^{-/-} mice on day 7 post-MI compared to WT, and higher ratios are strongly associated with adverse remodelling and HF in both humans and mice (Graziani et al. 2018; Hassanein et al. 2023).

Considering the critical role of the TGF- β /SMADs signaling pathway post-MI, interventions using drugs such as simvastatin have been observed to reduce TGF- β expression thereby improving ventricular remodelling in mice. Moreover, the antihypertensive drug valsartan significantly decreased the expression of TGF- β /SMADs, HIF-1 α and fibrosis-related proteins in rats after MI, leading to significant improvements in cardiac function, infarct size, wall thickness, and myocardial vascularization in ischemic heart conditions (Wu et al. 2021). Finally, in clinical practice, Statins, angiotensin-converting enzyme inhibitors (ACEIs), and angiotensin receptor antagonists (ARBs), which inhibit this pathway as well, have shown promising outcomes in patients with MI (Bonanni et al. 2023; Zhang et al. 2022). But, despite their efficacy, there is still a lack of comprehensive understanding and therefore concerns regarding potential side effects. Because of that, PAD4, through its direct or indirect effects on TGF- β , presents a promising therapeutic target and opens new avenues for research.

Taken together, targeting of PAD4 at later stages could be a promising strategy to protect the infarcted heart from adverse remodelling and excessive collagen deposition. *Padi4* was still significantly upregulated on day 28 after surgery and affects pro-fibrotic pathways in CFs.

Specific inhibition of PAD4 after the resolution of inflammation might be better than blocking during the acute inflammation, as other studies indicated that completely suppressing inflammation is not protective (Hörner et al. 2004; Murphy and Weaver 2018). A balanced activation of pro-inflammatory and anti-inflammatory immune responses appeared to have a crucial impact on mortality rates. For example, the total depletion of monocytes and infiltrating macrophages during the first week following myocardial injury in mice was associated with enhanced heart rupture and increased mortality (Bajpai et al. 2019). Besides, expanding the focus from the heart to the entire body, inflammation is crucial for fighting and eliminating infectious agents. Therefore, targeting inflammation in any medical context, including MI, might enhance susceptibility to infections by disrupting the body's defense mechanisms. Moreover, even when viewed objectively, on day 1 and 3 after experimental MI induction, PAD4^{-/-} mice exhibited less inflammatory immune response, indicated by reduced cell apoptosis, decreased infiltration of myeloid cells, macrophages, and inflammatory markers in cardiac tissue. Despite this, there were no notable differences in survival rates between PAD4^{-/-} and WT mice up to day 7 post-MI, suggesting that these effects do not confer a significant advantage.

Finally, treatment with the pan-PAD inhibitor BB-CI starting at day 7 demonstrated a reduction in collagen content and reduced fibrotic area, resulting in an improved survival curve on day 28 post-MI. These effects were also demonstrated for PAD4^{-/-} mice, being in line with previously published data (Eghbalzadeh et al. 2019; Martinod et al. 2017; Heger et al. 2023). The idea for reducing fibrosis by inhibition of PAD4 is not new. It was reported in collagen-induced arthritis (CIA) (Willis et al. 2017). Treatment with the PAD4-selective inhibitor GSK199, was sufficient to prevent CIA and resulted in decreased paw inflammation, joint destruction and a substantially reduced deposition of collagen in the joints (Willis et al. 2017). In accordance, a recent study by Heger et al. who demonstrated prevention of hypertrophic cardiomyopathy, fibrosis and diastolic HF after inhibition of PAD4 with JBI-589 (Heger et al. 2023). However, whereas this study cannot clearly ascertain whether inflammation influences fibrosis or if it occurs independently, it indicated that even if inflammation occurs in the acute phase in WT mice (day 1 – day 7), the fibrotic area is reduced after treatment with a pan-PAD inhibitor beginning at day 7 post-MI. It nearly proposes that diminished levels of pro-fibrogenic TGF- β , and reduced abundance of collagen-producing myofibroblasts in the absence of PAD4 activity substantially contribute to improve cardiac regeneration post-MI.

In summary, these findings demonstrate that a lack of PAD4 offers protection against cardiac remodelling by shifting the phenotype of macrophages, influencing pro-fibrotic pathways in CFs, thereby reducing fibrosis and improving long-term survival. The inhibition of PADs, especially PAD4, after the acute inflammation process is an effective clinical strategy to prevent adverse remodelling in HF patients.

6. Conclusion and remarks

This study demonstrates for the first time that PAD4 deficiency prevents maladaptive cardiac remodelling and improves long-term survival by mitigating the inflammatory response through modulating inflammation and pro-fibrotic pathways in macrophages or CFs, respectively. Moreover, targeting PADs, including PAD4, after the resolution of acute inflammation offers a clinical strategy for improving the prognosis for HF.

Summarizing the key findings (**Fig. 29**), it is evident that PAD4 regulates the expression of pro-inflammatory and pro-fibrotic genes, therefore affecting overall survival in mice. *In vitro* studies showed that PAD4 influences the characteristics of M1-like macrophages through the upregulation of inflammatory genes (*Il6*, *Nos2*, and *Il12*). After MI, the recruitment of myeloid leukocyte migration is strictly regulated by PADs, including PAD4, as it was significantly downregulated in the absence of PADs. Moreover, the local inflammation in heart tissue and positive regulation of cell death (μ MLKL and DNA fragmentation) were markedly upregulated in pan-PAD inhibitor-treated mice during the first days (1 – 3) post-MI. This was accompanied by a reduced content of total collagen and heart stability, leading to a high risk of death at day 7 post-MI.

In mice with genetic *Padi4* ablation, less inflammation in cardiac tissue and fewer macrophages were observed on the first day as well as on day 7 post-MI. On day 7, the reduced abundance of myofibroblasts, impaired TGF- β /SMAD signaling and collagen type I production resulted in less cardiac fibrosis. Additionally, isolated CFs from PAD4-deficient mice showed downregulation of pro-fibrotic genes involved in ECM assembly (*Pdgfra*, *Fzd1* and *Tgfbr1*). Of note, isolated macrophages from these mice exhibited a reparative phenotype on day 7 post-MI, evidenced by higher expression of CD206 and lower expression of inflammatory genes (*Il6*, *Nos2*, *Tnfa*), providing a less inflammatory microenvironment. In the end, both, treatment with the inhibitor starting as soon as the inflammation is resolved (after day 7), and *Padi4* knockout resulted in reduced abundance of fibrosis and improved survival of mice on day 28 post-MI.

Although global *Padi4* knockout in mice has a significant impact on the survival rate and the development of fibrosis, it does not clearly indicate whether reduced inflammation in macrophages supports the anti-fibrotic phenotype of fibroblasts, or if reduced fibrosis occurs independently. Further studies are needed to examine the impact of Mo/M ϕ - or CFs-restricted *Padi4* ablation, respectively. Furthermore, the broad-spectrum of PAD inhibitor BB-CI-Amidine fails to elucidate the pivotal role of PAD4, particularly in light of the emergence of newly potent and selective PAD4 inhibitors such as JBI-589. Even if the results of this study yield equivalent

findings regarding fibrosis as JBI-589, recent documentation highlights the sensitivity and efficacy of JBI-589 for PAD4.

However, this work supports recent studies that present PAD4 as a key mediator of inflammation and HF development in heart tissue. Therefore, it is indispensable to unravel the molecular mechanism of PAD4 function and regulation in different cell types especially in light of inflammatory events, such as MI.

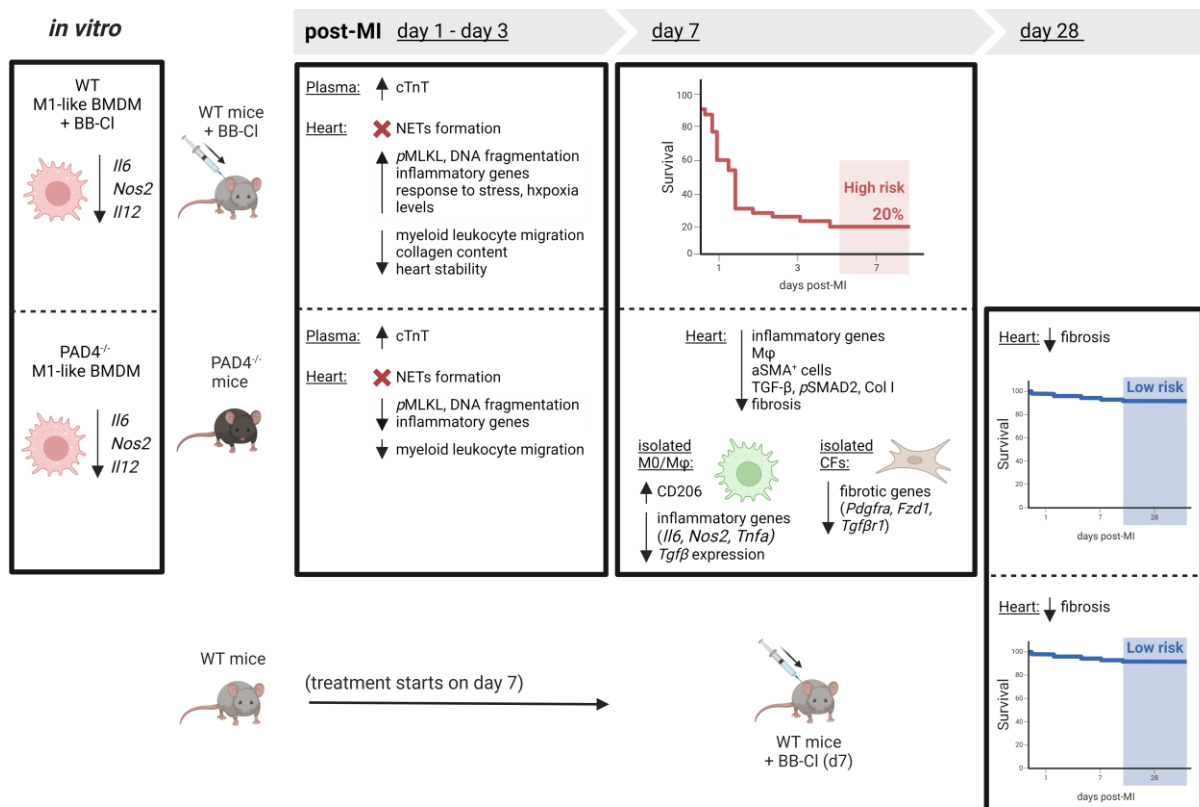


Figure 29: Schematic summary of the experimental study and main results. Inhibiting PAD4 protects against post-MI remodelling, mitigates inflammation, and diminishes fibrotic areas in cardiac tissue by altering macrophage phenotypes and affecting pro-fibrotic pathways in cardiac fibroblasts. Finally, it promotes long-term survival in mice. Graphic created with BioRender.

List of figures

Figure 1: Anatomy of the human heart.	10
Figure 2: Multifaceted immune response post-MI.	12
Figure 3: Characteristics of the initial inflammatory immune response post-MI.	14
Figure 4: Characteristics of the reparative process post-MI.	17
Figure 5: PAD-dependent citrullination.	21
Figure 6: Structure and calcium binding sites of PAD4.	22
Figure 7: Representative images of mice hearts during/after MI induction by left anterior descending artery (LAD) ligation.	40
Figure 8: Experimental setup for MI induction and post-MI analyses.	53
Figure 9: <i>Padi4</i> expression and PAD4-mediated citrullination post-MI in murine and human hearts.	54
Figure 10: <i>Padi</i> gene expression and effects of BB-CI-Amidine treatment in mice without surgery.	55
Figure 11: CitH3 protein levels post-MI in mice.	56
Figure 12: NETs formation in PAD4-deficient, WT + BB-CI and WT mice post-MI.	57
Figure 13: Impact of genetic or pharmacological PAD4 inhibition on cell death.	59
Figure 14: Bulk RNA-seq analysis of infarcted hearts on day 1 and 3 post-MI.	61
Figure 15: Differential gene expression in infarcted hearts on day 1 and 3 post-MI in WT + BB-CI and PAD4 ^{-/-} mice compared to WT mice.	63
Figure 16: Gene expression variation in infarcted hearts at day 1 and 3 post-MI in WT + BB-CI compared to PAD4 ^{-/-} mice.	64
Figure 17: GO term analysis of RNA-seq data from WT + BB-CI mice hearts on day 1 and 3 post-MI compared to WT.	65
Figure 18: GO term analysis of RNA-seq data from PAD4 ^{-/-} hearts on day 1 and 3 post-MI compared to WT.	66
Figure 19: Effects of pharmacological inhibition of PADs and <i>Padi4</i> ablation on immune cells recruitment during the inflammatory phase post-MI.	68
Figure 20: Impact of pharmacological inhibition of PAD and <i>Padi4</i> deficiency on cardiac collagen, body weight, heart weight and survival.	70
Figure 21: Bulk RNA-seq and gene expression analysis in PAD4 ^{-/-} hearts at day 7 post-MI.	72
Figure 22: Impact of PAD4 on cardiac immune cell recruitment on day 7 post-MI.	73
Figure 23: Phenotypic differences in cardiac monocytes/macrophages (Mo/M ϕ) from PAD4 ^{-/-} and WT mice on day 7 post-MI.	74
Figure 24: Transcriptomic alterations in cardiac Mo/M ϕ from PAD4 ^{-/-} mice day 7 post-MI.	76
Figure 25: Role of PAD4 in inflammation-related macrophage polarization and function.	78
Figure 26: Transcriptomic alteration in CFs from PAD4 ^{-/-} mice on day 7 post-MI.	80
Figure 27: Effect of PAD4 on cardiac fibrosis on day 7 post-MI.	82
Figure 28: Impact of pharmacological PAD Inhibition initiated at day 7 and PAD4 deficiency on cardiac remodelling and long-term survival.	84
Figure 29: Schematic summary of the experimental study and main results.	96

List of tables

Table 1: Overview of used instruments.	26
Table 2: Overview of used consumables.	26
Table 3: Overview of used chemicals.	27
Table 4: Overview of used mediums for cell culture.	28
Table 5: Overview of used cytokines and stimulating/growth factors in cell culture.	28
Table 6: Overview of used enzymes.	29
Table 7: Overview of inhibitors and drugs	29
Table 8: Overview of Sets and Kits used in this study.	29
Table 9: Overview of monoclonal antibodies used for flow cytometry.	30
Table 10: Overview of products and antibodies used for autoMACS separation.	30
Table 11: Overview of antibodies used for western blot.	30
Table 12: Overview of antibodies used for immunofluorescence.	30
Table 13: Overview of staining solutions used in this study.	31
Table 14: Overview of Buffers used in this study.	31
Table 15: Primer sequences. Fwd, forward primer. Rev, reverse primer.	33
Table 16: Composition of used gels for western blot.	47

List of abbreviations

α	alpha
β	beta
γ	gamma
ADIs	anti-citrullinated protein antibodies
AGEs	advanced glycation end products
BM	bone marrow
BDMD	bone marrow derived macrophages
BB-CI	BB-CI-Amidine (pan inhibitor of peptidylarginine deiminases)
BP	biological process
CCG	Cologne Center for Genomics
CCL2	chemokine (C-C motif) ligand 2
CCR2	C-C chemokine receptor type 2
CC	cellular component
Ca ²⁺	calcium ions
CD11b	integrin alpha-M
CD45	receptor-type tyrosine-protein phosphatase C
CD206	mannose receptor C type 1
CFs	cardiac fibroblasts
CFSE	carboxyfluorescein succinimidyl ester
cDNA	complementary DNA
CMs	cardiomyocytes
Col I	collagen type I
Col III	collagen type III
CO ₂	carbon dioxide
COVID-19	coronavirus SARS-CoV-2
cTnT	cardiac troponin T
CVDs	cardiovascular diseases
DAMPs	damage-associated molecular patterns
DMSO	dimethyl sulfoxide
ECM	extracellular matrix
EDTA	ethylenediaminetetraacetic acid

ELISA	enzyme-linked immunosorbent assay
EF	ejection fraction
FACS	fluorescence-activated cell sorting
FCS	fetal calf serum
FC	fold change
FGF	fibroblast growth factors
Fig.	figure
FSC	forward scatter
FMO	Fluorescence Minus One
F4/80	eGF-like module-containing mucin-like hormone receptor-like 1
GM-CSF	granulocyte-macrophage colony-stimulating factor
GO	gene ontology
H	hour
H1	histone protein 1
H3	histone protein 3
HF	heart failure
ICAM-1	intercellular adhesion molecule 1
IFN- γ	interferon gamma
IL-1 α	interleukin 1 alpha
IL-1 β	interleukin 1 beta
IL-4	interleukin 4
IL-6	interleukin 6
IL-10	interleukin 10
IL-13	interleukin 13
IL-12	interleukin 12
iNOS	inducible nitric oxide synthase
I/R	ischemia/reperfusion
LAD	left anterior descending artery
LCx	left circumflex artery
LV	left ventricle
Ly6G	lymphocyte antigen 6 complex locus G6D
Ly6C	lymphocyte antigen 6 family member C1
MACS	magnetic-activated cell sorting

List of abbreviations

mg	milligrams
MI	myocardial infarction
ml	milliliters
mm	millimeters
MIP-1 α	macrophage inflammatory protein 1 alpha
MHC II	myosin heavy chain II
MFI	mean fluorescence intensity
MF	molecular function
MLKL	mixed lineage kinase domain-like protein
M0/M ϕ	monocytes/macrophages
MMPs	matrix metalloproteinases
MTC	masson's trichrome staining
MPO	myeloperoxidase
NE	neutrophil elastase
NETs	neutrophil extracellular traps
NF- κ B	nuclear factor kappa B
ng	nanograms
NLS	nuclear localization signal
NO	nitric oxide
Nos2	nitric oxide synthase 2
pMLKL	phosphorylated mixed lineage kinase domain-like protein
pSMAD2	phosphorylated SMAD2
PADs	peptidylarginine deiminases
PAD4	peptidylarginine deiminase type 4
PAD4 ^{-/-}	peptidylarginine deiminase type 4 deficiency
PBS	phosphate-buffered saline
PCI	percutaneous coronary intervention
PCR	polymerase chain reaction
PFA	paraformaldehyde
PDGFRA	platelet-derived growth factor receptor alpha
PRRs	pattern recognition receptors
PTM	post-translational modification
post-MI	post myocardial infarction

RA	rheumatoid arthritis
RIPK1/3	receptor-interacting protein kinase 1 or 3
RNA	ribonucleic acid
RNA-seq	RNA sequencing
ROS	reactive oxygen species
RV	right ventricle
RT	room temperature
rpm	rounds per minute
SD	standard deviation
SDS	sodium dodecyl sulfate
SMA	smooth muscle actin
sec	seconds
SEM	standard error of mean
SSC	side scatter
TGF- β	transforming growth factor beta
TNF- α	tumor necrosis factor alpha
U	units
V	volts
VEGF	vascular endothelial growth factor
WT	wild type
μ g	micrograms
μ l	microliters
μ m	micrometers
<i>in vitro</i>	in the lab
<i>in vivo</i>	in the living organism

Bibliography

- Akboua, Hanane; Eghbalzadeh, Kaveh; Keser, Ugur; Wahlers, Thorsten; Paunel-Görgülü, Adnana (2021): Impaired non-canonical transforming growth factor- β signalling prevents profibrotic phenotypes in cultured peptidylarginine deiminase 4-deficient murine cardiac fibroblasts. In: *Journal of cellular and molecular medicine* 25 (20), S. 9674–9684. DOI: 10.1111/jcmm.16915.
- Al-U'datt, Doa'a G. F.; Allen, Bruce G.; Hiram, Roddy; Alrabadi, Nasr (2021): Current knowledge into the role of the peptidylarginine deiminase (PAD) enzyme family in cardiovascular disease. In: *European journal of pharmacology* 891, S. 173765. DOI: 10.1016/j.ejphar.2020.173765.
- Arita, Kyouhei; Hashimoto, Hiroshi; Shimizu, Toshiyuki; Nakashima, Katsuhiko; Yamada, Michiyuki; Sato, Mamoru (2004): Structural basis for Ca(2+)-induced activation of human PAD4. In: *Nature structural & molecular biology* 11 (8), S. 777–783. DOI: 10.1038/nsmb799.
- Arita, Kyouhei; Shimizu, Toshiyuki; Hashimoto, Hiroshi; Hidaka, Yuji; Yamada, Michiyuki; Sato, Mamoru (2006): Structural basis for histone N-terminal recognition by human peptidylarginine deiminase 4. In: *Proceedings of the National Academy of Sciences of the United States of America* 103 (14), S. 5291–5296. DOI: 10.1073/pnas.0509639103.
- Bagur, Rafaela; Hajnóczky, György (2017): Intracellular Ca²⁺ Sensing: Its Role in Calcium Homeostasis and Signaling. In: *Molecular cell* 66 (6), S. 780–788. DOI: 10.1016/j.molcel.2017.05.028.
- Bajpai, Geetika; Bredemeyer, Andrea; Li, Wenjun; Zaitsev, Konstantin; Koenig, Andrew L.; Lokshina, Inessa et al. (2019): Tissue Resident CCR2- and CCR2+ Cardiac Macrophages Differentially Orchestrate Monocyte Recruitment and Fate Specification Following Myocardial Injury. In: *Circulation research* 124 (2), S. 263–278. DOI: 10.1161/circresaha.118.314028.
- Barratt, Jonathan; Weitz, Ilene (2021): Complement Factor D as a Strategic Target for Regulating the Alternative Complement Pathway. In: *Frontiers in immunology* 12, S. 712572. DOI: 10.3389/fimmu.2021.712572.
- Bashir, Samina; Sharma, Yadhu; Elahi, Asif; Khan, Farah (2016): Macrophage polarization: the link between inflammation and related diseases. In: *Inflammation research : official journal of the European Histamine Research Society ... [et al.]* 65 (1), S. 1–11. DOI: 10.1007/s00011-015-0874-1.
- Baumeister, Peter; Quinn, T. Alexander (2016): Altered Calcium Handling and Ventricular Arrhythmias in Acute Ischemia. In: *Clinical Medicine Insights. Cardiology* 10 (Suppl 1), S. 61–69. DOI: 10.4137/CMC.S39706.
- Bean, C.; Verma, N. K.; Yamamoto, D. L.; Chemello, F.; Cenni, V.; Filomena, M. C. et al. (2014): Ankr2 is a modulator of NF- κ B-mediated inflammatory responses during muscle differentiation. In: *Cell death & disease* 5 (1), e1002. DOI: 10.1038/cddis.2013.525.
- Bedford, Mark T.; Clarke, Steven G. (2009): Protein arginine methylation in mammals: who, what, and why. In: *Molecular cell* 33 (1), S. 1–13. DOI: 10.1016/j.molcel.2008.12.013.
- Bergmann, Olaf; Bhardwaj, Ratan D.; Bernard, Samuel; Zdunek, Sofia; Barnabé-Heider, Fanie; Walsh, Stuart et al. (2009): Evidence for cardiomyocyte renewal in humans. In: *Science (New York, N.Y.)* 324 (5923), S. 98–102. DOI: 10.1126/science.1164680.
- Berridge, Michael J.; Bootman, Martin D.; Roderick, H. Llewelyn (2003): Calcium signalling: dynamics, homeostasis and remodelling. In: *Nature reviews. Molecular cell biology* 4 (7), S. 517–529. DOI: 10.1038/nrm1155.

- Bicker, Kevin L.; Subramanian, Venkataraman; Chumanevich, Alexander A.; Hofseth, Lorne J.; Thompson, Paul R. (2012): Seeing citrulline: development of a phenylglyoxal-based probe to visualize protein citrullination. In: *Journal of the American Chemical Society* 134 (41), S. 17015–17018. DOI: 10.1021/ja308871v.
- Bögeholz, Nils; Muszynski, Adam; Pott, Christian (2012): The physiology of cardiac calcium handling. In: *Wiener medizinische Wochenschrift (1946)* 162 (13-14), S. 278–282. DOI: 10.1007/s10354-012-0102-3.
- Bonanni, Alice; Vinci, Ramona; d'Aiello, Alessia; Grimaldi, Maria Chiara; Di Sario, Marianna; Tarquini, Dalila et al. (2023): Targeting Collagen Pathways as an HFpEF Therapeutic Strategy. In: *Journal of clinical medicine* 12 (18). DOI: 10.3390/jcm12185862.
- Boniakowski, Anna E.; Kimball, Andrew S.; Joshi, Amrita; Schaller, Matt; Davis, Frank M.; denDekker, Aaron et al. (2018): Murine macrophage chemokine receptor CCR2 plays a crucial role in macrophage recruitment and regulated inflammation in wound healing. In: *European journal of immunology* 48 (9), S. 1445–1455. DOI: 10.1002/eji.201747400.
- Brinkmann, Volker; Reichard, Ulrike; Goosmann, Christian; Fauler, Beatrix; Uhlemann, Yvonne; Weiss, David S. et al. (2004): Neutrophil extracellular traps kill bacteria. In: *Science (New York, N.Y.)* 303 (5663), S. 1532–1535. DOI: 10.1126/science.1092385.
- Brinkmann, Volker; Zychlinsky, Arturo (2012): Neutrophil extracellular traps: is immunity the second function of chromatin? In: *The Journal of cell biology* 198 (5), S. 773–783. DOI: 10.1083/jcb.201203170.
- Camelliti, Patrizia; Borg, Thomas K.; Kohl, Peter (2005): Structural and functional characterisation of cardiac fibroblasts. In: *Cardiovascular research* 65 (1), S. 40–51. DOI: 10.1016/j.cardiores.2004.08.020.
- Chalise, Upendra; Becirovic-Agic, Mediha; Lindsey, Merry L. (2023): The cardiac wound healing response to myocardial infarction. In: *WIREs mechanisms of disease* 15 (1), e1584. DOI: 10.1002/wsbm.1584.
- Cheng, Yu; Si, Yuying; Wang, Lan; Ding, Menglei; Yu, Shanshan; Lu, Liu et al. (2021a): The regulation of macrophage polarization by hypoxia-PADI4 coordination in Rheumatoid arthritis. In: *International immunopharmacology* 99, S. 107988. DOI: 10.1016/j.intimp.2021.107988.
- Cheng, Yun-Jiu; Jia, Yu-He; Yao, Feng-Juan; Mei, Wei-Yi; Zhai, Yuan-Sheng; Zhang, Ming; Wu, Su-Hua (2021b): Association Between Silent Myocardial Infarction and Long-Term Risk of Sudden Cardiac Death. In: *Journal of the American Heart Association* 10 (1), e017044. DOI: 10.1161/JAHA.120.017044.
- Chistiakov, Dimitry A.; Orekhov, Alexander N.; Bobryshev, Yuri V. (2016): The role of cardiac fibroblasts in post-myocardial heart tissue repair. In: *Experimental and molecular pathology* 101 (2), S. 231–240. DOI: 10.1016/j.yexmp.2016.09.002.
- Cohn, J. N.; Johnson, G. R.; Shabetai, R.; Loeb, H.; Tristani, F.; Rector, T. et al. (1993): Ejection fraction, peak exercise oxygen consumption, cardiothoracic ratio, ventricular arrhythmias, and plasma norepinephrine as determinants of prognosis in heart failure. The V-HeFT VA Cooperative Studies Group. In: *Circulation* 87 (6 Suppl), VI5-16.
- Cornelissen, Anne; Florescu, Roberta; Kneizeh, Kinan; Cornelissen, Christian; Liehn, Elisa; Brandenburg, Vincent; Schuh, Alexander (2022): Fibroblast Growth Factor 23 and Outcome Prediction in Patients with Acute Myocardial Infarction. In: *Journal of clinical medicine* 11 (3). DOI: 10.3390/jcm11030601.
- Curis, E.; Nicolis, I.; Moinard, C.; Osowska, S.; Zerrouk, N.; Bénazeth, S.; Cynober, L. (2005): Almost all about citrulline in mammals. In: *Amino acids* 29 (3), S. 177–205. DOI: 10.1007/s00726-005-0235-4.

- Davidson, Sean M.; Ferdinandy, Péter; Andreadou, Ioanna; Bøtker, Hans Erik; Heusch, Gerd; Ibáñez, Borja et al. (2019): Multitarget Strategies to Reduce Myocardial Ischemia/Reperfusion Injury: JACC Review Topic of the Week. In: *Journal of the American College of Cardiology* 73 (1), S. 89–99. DOI: 10.1016/j.jacc.2018.09.086.
- Davies, Luke C.; Jenkins, Stephen J.; Allen, Judith E.; Taylor, Philip R. (2013): Tissue-resident macrophages. In: *Nature immunology* 14 (10), S. 986–995. DOI: 10.1038/ni.2705.
- Di Zhu; Lu, Yu; Wang, Yanming; Wang, Yuji (2022): PAD4 and Its Inhibitors in Cancer Progression and Prognosis. In: *Pharmaceutics* 14 (11). DOI: 10.3390/pharmaceutics14112414.
- Dick, Sarah A.; Macklin, Jillian A.; Nejat, Sara; Momen, Abdul; Clemente-Casares, Xavier; Althagafi, Marwan G. et al. (2019): Self-renewing resident cardiac macrophages limit adverse remodeling following myocardial infarction. In: *Nature immunology* 20 (1), S. 29–39. DOI: 10.1038/s41590-018-0272-2.
- Dominguez-Rodriguez, Alberto; Abreu-Gonzalez, Pedro; Avanzas, Pablo (2011): Relation of growth-differentiation factor 15 to left ventricular remodeling in ST-segment elevation myocardial infarction. In: *The American journal of cardiology* 108 (7), S. 955–958. DOI: 10.1016/j.amjcard.2011.05.028.
- Du, Mingjun; Yang, Wengang; Schull, Sebastian; Gu, Jianmin; Xue, Song (2020): Inhibition of peptidyl arginine deiminase-4 protects against myocardial infarction induced cardiac dysfunction. In: *International immunopharmacology* 78, S. 106055. DOI: 10.1016/j.intimp.2019.106055.
- Duncan, Sophia Esi; Gao, Shan; Sarhene, Michael; Coffie, Joel Wake; Linhua, Deng; Bao, Xingru et al. (2020): Macrophage Activities in Myocardial Infarction and Heart Failure. In: *Cardiology research and practice* 2020, S. 4375127. DOI: 10.1155/2020/4375127.
- Dutta, Partha; Hoyer, Friedrich Felix; Grigoryeva, Lubov S.; Sager, Hendrik B.; Leuschner, Florian; Courties, Gabriel et al. (2015): Macrophages retain hematopoietic stem cells in the spleen via VCAM-1. In: *The Journal of experimental medicine* 212 (4), S. 497–512. DOI: 10.1084/jem.20141642.
- Eghbalzadeh, Kaveh; Georgi, Leena; Louis, Theresa; Zhao, Haizhi; Keser, Ugur; Weber, Carolyn et al. (2019): Compromised Anti-inflammatory Action of Neutrophil Extracellular Traps in PAD4-Deficient Mice Contributes to Aggravated Acute Inflammation After Myocardial Infarction. In: *Frontiers in immunology* 10, S. 2313. DOI: 10.3389/fimmu.2019.02313.
- Eltzschig, Holger K.; Eckle, Tobias (2011): Ischemia and reperfusion--from mechanism to translation. In: *Nature medicine* 17 (11), S. 1391–1401. DOI: 10.1038/nm.2507.
- Endo, Fumio; Matsuura, Toshinobu; Yanagita, Kaede; Matsuda, Ichiro (2004): Clinical manifestations of inborn errors of the urea cycle and related metabolic disorders during childhood. In: *The Journal of nutrition* 134 (6 Suppl), 1605S-1609S; discussion 1630S-1632S, 1667S-1672S. DOI: 10.1093/jn/134.6.1605S.
- Engblom, Henrik; Hedström, Erik; Heiberg, Einar; Wagner, Galen S.; Pahlm, Olle; Arheden, Håkan (2009): Rapid initial reduction of hyperenhanced myocardium after reperfused first myocardial infarction suggests recovery of the peri-infarction zone: one-year follow-up by MRI. In: *Circulation. Cardiovascular imaging* 2 (1), S. 47–55. DOI: 10.1161/CIRCIMAGING.108.802199.
- Epelman, Slava; Lavine, Kory J.; Beaudin, Anna E.; Sojka, Dorothy K.; Carrero, Javier A.; Calderon, Boris et al. (2014): Embryonic and adult-derived resident cardiac macrophages are maintained through distinct mechanisms at steady state and during inflammation. In: *Immunity* 40 (1), S. 91–104. DOI: 10.1016/j.immuni.2013.11.019.

- Fanola, Christina L.; Morrow, David A.; Cannon, Christopher P.; Jarolim, Petr; Lukas, Mary Ann; Bode, Christoph et al. (2017): Interleukin-6 and the Risk of Adverse Outcomes in Patients After an Acute Coronary Syndrome: Observations From the SOLID-TIMI 52 (Stabilization of Plaque Using Darapladib-Thrombolysis in Myocardial Infarction 52) Trial. In: *Journal of the American Heart Association* 6 (10). DOI: 10.1161/JAHA.117.005637.
- Ferreira, André; Ferreira, Vera; Antunes, Miguel Marques; Lousinha, Ana; Pereira-da-Silva, Tiago; Antunes, Diana et al. (2023): Dilated Cardiomyopathy: A Comprehensive Approach to Diagnosis and Risk Stratification. In: *Biomedicines* 11 (3). DOI: 10.3390/biomedicines11030834.
- Ferreira, Roberto Muniz; Souza E Silva, Nelson Albuquerque de; Salis, Lúcia Helena Alvares (2018): Complications after elective percutaneous coronary interventions: A comparison between public and private hospitals. In: *Indian heart journal* 70 (1), S. 32–36. DOI: 10.1016/j.ihj.2017.06.012.
- Fert-Bober, Justyna; Giles, John T.; Holewinski, Ronald J.; Kirk, Jonathan A.; Uhrigshardt, Helge; Crowgey, Erin L. et al. (2015): Citrullination of myofilament proteins in heart failure. In: *Cardiovascular research* 108 (2), S. 232–242. DOI: 10.1093/cvr/cvv185.
- Floss, T.; Arnold, H. H.; Braun, T. (1997): A role for FGF-6 in skeletal muscle regeneration. In: *Genes & development* 11 (16), S. 2040–2051. DOI: 10.1101/gad.11.16.2040.
- Foey, Andrew D. (2014): Macrophages — Masters of Immune Activation, Suppression and Deviation. In: Guy Huynh Thien Duc (Hg.): *Immune Response Activation*: InTech.
- Fontes, Jillian A.; Rose, Noel R.; Čiháková, Daniela (2015): The varying faces of IL-6: From cardiac protection to cardiac failure. In: *Cytokine* 74 (1), S. 62–68. DOI: 10.1016/j.cyto.2014.12.024.
- Fox, Keith A. A.; Steg, Philippe Gabriel; Eagle, Kim A.; Goodman, Shaun G.; Anderson, Frederick A.; Granger, Christopher B. et al. (2007): Decline in rates of death and heart failure in acute coronary syndromes, 1999-2006. In: *JAMA* 297 (17), S. 1892–1900. DOI: 10.1001/jama.297.17.1892.
- Frangogiannis, Nikolaos G. (2012): Regulation of the inflammatory response in cardiac repair. In: *Circulation research* 110 (1), S. 159–173. DOI: 10.1161/CIRCRESAHA.111.243162.
- Frangogiannis, Nikolaos G. (2015): Pathophysiology of Myocardial Infarction. In: *Comprehensive Physiology* 5 (4), S. 1841–1875. DOI: 10.1002/cphy.c150006.
- Frangogiannis, Nikolaos G. (2021): Cardiac fibrosis. In: *Cardiovascular research* 117 (6), S. 1450–1488. DOI: 10.1093/cvr/cvaa324.
- Frangogiannis, Nikolaos G.; Smith, C. Wayne; Entman, Mark L. (2002): The inflammatory response in myocardial infarction. In: *Cardiovascular research* 53 (1), S. 31–47. DOI: 10.1016/S0008-6363(01)00434-5].
- Frantz, Stefan; Nahrendorf, Matthias (2014): Cardiac macrophages and their role in ischaemic heart disease. In: *Cardiovascular research* 102 (2), S. 240–248. DOI: 10.1093/cvr/cvu025.
- Fröhlich, Georg M.; Meier, Pascal; White, Steven K.; Yellon, Derek M.; Hausenloy, Derek J. (2013): Myocardial reperfusion injury: looking beyond primary PCI. In: *European heart journal* 34 (23), S. 1714–1722. DOI: 10.1093/eurheartj/ehs090.
- Funes, Samanta C.; Rios, Mariana; Escobar-Vera, Jorge; Kalergis, Alexis M. (2018): Implications of macrophage polarization in autoimmunity. In: *Immunology* 154 (2), S. 186–195. DOI: 10.1111/imm.12910.
- Gale, C. P.; Allan, V.; Cattle, B. A.; Hall, A. S.; West, R. M.; Timmis, A. et al. (2014): Trends in hospital treatments, including revascularisation, following acute myocardial infarction, 2003-2010: a multilevel and relative survival analysis for the National Institute for Cardiovascular Outcomes Research (NICOR). In: *Heart (British Cardiac Society)* 100 (7), S. 582–589. DOI: 10.1136/heartjnl-2013-304517.

- Ge, Lan; Zhou, Xin; Ji, Wen-Jie; Lu, Rui-Yi; Zhang, Yan; Zhang, Yi-Dan et al. (2015): Neutrophil extracellular traps in ischemia-reperfusion injury-induced myocardial no-reflow: therapeutic potential of DNase-based reperfusion strategy. In: *American journal of physiology. Heart and circulatory physiology* 308 (5), H500-9. DOI: 10.1152/ajpheart.00381.2014.
- Gheorghiadu, Mihai; Fonarow, Gregg C. (2007): Management of post-myocardial infarction patients with left ventricular systolic dysfunction. In: *The American journal of medicine* 120 (2), S. 109–120. DOI: 10.1016/j.amjmed.2005.08.010.
- Gray, G. A.; Toor, I. S.; Castellan, Rfp; Crisan, M.; Meloni, M. (2018): Resident cells of the myocardium: more than spectators in cardiac injury, repair and regeneration. In: *Current opinion in physiology* 1, S. 46–51. DOI: 10.1016/j.cophys.2017.08.001.
- Graziani, Francesca; Varone, Francesco; Crea, Filippo; Richeldi, Luca (2018): Treating heart failure with preserved ejection fraction: learning from pulmonary fibrosis. In: *European journal of heart failure* 20 (10), S. 1385–1391. DOI: 10.1002/ejhf.1286.
- Guccione, Ernesto; Richard, Stéphane (2019): The regulation, functions and clinical relevance of arginine methylation. In: *Nature reviews. Molecular cell biology* 20 (10), S. 642–657. DOI: 10.1038/s41580-019-0155-x.
- Guo, Xiaoyun; Chen, Yi; Liu, Qinghang (2022): Necroptosis in heart disease: Molecular mechanisms and therapeutic implications. In: *Journal of molecular and cellular cardiology* 169, S. 74–83. DOI: 10.1016/j.yjmcc.2022.05.006.
- Hagiwara, Teruki; Nakashima, Katsuhiko; Hirano, Hisashi; Senshu, Tatsuo; Yamada, Michiyuki (2002): Deimination of arginine residues in nucleophosmin/B23 and histones in HL-60 granulocytes. In: *Biochemical and biophysical research communications* 290 (3), S. 979–983. DOI: 10.1006/bbrc.2001.6303.
- Hahn, Jonas; Schauer, Christine; Czegley, Christine; Kling, Lasse; Petru, Lenka; Schmid, Benjamin et al. (2019): Aggregated neutrophil extracellular traps resolve inflammation by proteolysis of cytokines and chemokines and protection from antiproteases. In: *FASEB journal : official publication of the Federation of American Societies for Experimental Biology* 33 (1), S. 1401–1414. DOI: 10.1096/fj.201800752R.
- Hanna, Anis; Frangogiannis, Nikolaos G. (2019): The Role of the TGF- β Superfamily in Myocardial Infarction. In: *Frontiers in cardiovascular medicine* 6, S. 140. DOI: 10.3389/fcvm.2019.00140.
- Hanna, Anis; Shinde, Arti V.; Frangogiannis, Nikolaos G. (2020): Validation of diagnostic criteria and histopathological characterization of cardiac rupture in the mouse model of nonreperused myocardial infarction. In: *American journal of physiology. Heart and circulatory physiology* 319 (5), H948-H964. DOI: 10.1152/ajpheart.00318.2020.
- Hariyanto, Narendra Ichiputra; Yo, Edward Christopher; Wanandi, Septelia Inawati (2021): Regulation and Signaling of TGF- β Autoinduction. In: *International journal of molecular and cellular medicine* 10 (4), S. 234–247. DOI: 10.22088/IJMCM.BUMS.10.4.234.
- Hartupee, Justin; Mann, Douglas L. (2013): Positioning of inflammatory biomarkers in the heart failure landscape. In: *Journal of cardiovascular translational research* 6 (4), S. 485–492. DOI: 10.1007/s12265-013-9467-y.
- Hassanein, Emad H. M.; Ibrahim, Islam M.; Abd El-Maksoud, Mostafa S.; Abd El-Aziz, Mostafa K.; Abd-Alhameed, Esraa K.; Althagafy, Hanan S. (2023): Targeting necroptosis in fibrosis. In: *Molecular biology reports* 50 (12), S. 10471–10484. DOI: 10.1007/s11033-023-08857-9.
- He, Li; Liu, Ruiqi; Yue, Honghua; Zhu, Guonian; Fu, Li; Chen, Hongying et al. (2021): NETs promote pathogenic cardiac fibrosis and participate in ventricular aneurysm formation after ischemia injury through the facilitation of perivascular fibrosis. In: *Biochemical and biophysical research communications* 583, S. 154–161. DOI: 10.1016/j.bbrc.2021.10.068.

- Heger, Lukas A.; Schommer, Nicolas; Fukui, Shoichi; van Bruggen, Stijn; Sheehy, Casey E.; Chu, Long et al. (2023): Inhibition of protein arginine deiminase 4 prevents inflammation-mediated heart failure in arthritis. In: *Life science alliance* 6 (10). DOI: 10.26508/lsa.202302055.
- Heidenreich, Paul A.; Albert, Nancy M.; Allen, Larry A.; Bluemke, David A.; Butler, Javed; Fonarow, Gregg C. et al. (2013): Forecasting the impact of heart failure in the United States: a policy statement from the American Heart Association. In: *Circulation. Heart failure* 6 (3), S. 606–619. DOI: 10.1161/HHF.0b013e318291329a.
- Heidenreich, Paul A.; Bozkurt, Biykem; Aguilar, David; Allen, Larry A.; Byun, Joni J.; Colvin, Monica M. et al. (2022): 2022 AHA/ACC/HFSA Guideline for the Management of Heart Failure: A Report of the American College of Cardiology/American Heart Association Joint Committee on Clinical Practice Guidelines. In: *Circulation* 145 (18), e895-e1032. DOI: 10.1161/CIR.0000000000001063.
- Heidt, Timo; Courties, Gabriel; Dutta, Partha; Sager, Hendrik B.; Sebas, Matt; Iwamoto, Yoshiko et al. (2014): Differential contribution of monocytes to heart macrophages in steady-state and after myocardial infarction. In: *Circulation research* 115 (2), S. 284–295. DOI: 10.1161/CIRCRESAHA.115.303567.
- Horckmans, Michael; Ring, Larisa; Duchene, Johan; Santovito, Donato; Schloss, Maximilian J.; Drechsler, Maik et al. (2017): Neutrophils orchestrate post-myocardial infarction healing by polarizing macrophages towards a reparative phenotype. In: *European heart journal* 38 (3), S. 187–197. DOI: 10.1093/eurheartj/ehw002.
- Horibata, Sachi; Rogers, Katherine E.; Sadegh, David; Anguish, Lynne J.; McElwee, John L.; Shah, Pragya et al. (2017): Role of peptidylarginine deiminase 2 (PAD2) in mammary carcinoma cell migration. In: *BMC cancer* 17 (1), S. 378. DOI: 10.1186/s12885-017-3354-x.
- Hörner, C.; Bouchon, A.; Bierhaus, A.; Nawroth, P. P.; Martin, E.; Bardenheuer, H. J.; Weigand, M. A. (2004): Bedeutung der angeborenen Immunantwort in der Sepsis. In: *Der Anaesthetist* 53 (1), S. 10–28. DOI: 10.1007/s00101-003-0626-4.
- Hu, Zhicheng; Chen, Peng; Wang, Linlin; Zhu, Yu; Chen, Gen; Chen, Yunjie et al. (2022): FGF6 promotes cardiac repair after myocardial infarction by inhibiting the Hippo pathway. In: *Cell Proliferation* 55 (5). DOI: 10.1111/cpr.13221.
- Hulsmans, Maarten; Sam, Flora; Nahrendorf, Matthias (2016): Monocyte and macrophage contributions to cardiac remodeling. In: *Journal of molecular and cellular cardiology* 93, S. 149–155. DOI: 10.1016/j.yjmcc.2015.11.015.
- Humeres, Claudio; Frangogiannis, Nikolaos G. (2019): Fibroblasts in the Infarcted, Remodeling, and Failing Heart. In: *JACC. Basic to translational science* 4 (3), S. 449–467. DOI: 10.1016/j.jacbts.2019.02.006.
- Itagaki, Kiyoshi; Kaczmarek, Elzbieta; Lee, Yen Ting; Tang, I. Tien; Isal, Burak; Adibnia, Yashar et al. (2015): Mitochondrial DNA released by trauma induces neutrophil extracellular traps. In: *PLoS one* 10 (3), e0120549. DOI: 10.1371/journal.pone.0120549.
- Itoh, Nobuyuki; Ohta, Hiroya; Nakayama, Yoshiaki; Konishi, Morichika (2016): Roles of FGF Signals in Heart Development, Health, and Disease. In: *Frontiers in cell and developmental biology* 4, S. 110. DOI: 10.3389/fcell.2016.00110.
- Jaffe, A. S.; Landt, Y.; Parvin, C. A.; Abendschein, D. R.; Geltman, E. M.; Ladenson, J. H. (1996): Comparative sensitivity of cardiac troponin I and lactate dehydrogenase isoenzymes for diagnosing acute myocardial infarction. In: *Clinical chemistry* 42 (11), S. 1770–1776.
- Johansson, Saga; Rosengren, Annika; Young, Kate; Jennings, Em (2017): Mortality and morbidity trends after the first year in survivors of acute myocardial infarction: a systematic review. In: *BMC cardiovascular disorders* 17 (1), S. 53. DOI: 10.1186/s12872-017-0482-9.

- Jones, Justin E.; Causey, Corey P.; Knuckley, Bryan; Slack-Noyes, Jessica L.; Thompson, Paul R. (2009): Protein arginine deiminase 4 (PAD4): Current understanding and future therapeutic potential. In: *Current opinion in drug discovery & development* 12 (5), S. 616–627.
- Jung, Mira; Ma, Yonggang; Iyer, Rugmani Padmanabhan; Deleon-Pennell, Kristine Y.; Yabluchanskiy, Andriy; Garrett, Michael R.; Lindsey, Merry L. (2017): IL-10 improves cardiac remodeling after myocardial infarction by stimulating M2 macrophage polarization and fibroblast activation. In: *Basic research in cardiology* 112 (3), S. 33. DOI: 10.1007/s00395-017-0622-5.
- Kain, Vasundhara; Halade, Ganesh V. (2020): Role of neutrophils in ischemic heart failure. In: *Pharmacology & therapeutics* 205, S. 107424. DOI: 10.1016/j.pharmthera.2019.107424.
- Kain, Vasundhara; Prabhu, Sumanth D.; Halade, Ganesh V. (2014): Inflammation revisited: inflammation versus resolution of inflammation following myocardial infarction. In: *Basic research in cardiology* 109 (6), S. 444. DOI: 10.1007/s00395-014-0444-7.
- Kampourakis, Thomas; Irving, Malcolm (2021): The regulatory light chain mediates inactivation of myosin motors during active shortening of cardiac muscle. In: *Nature communications* 12 (1), S. 5272. DOI: 10.1038/s41467-021-25601-8.
- Kaore, Shilpa N.; Amane, Hanmant S.; Kaore, Navinchandra M. (2013): Citrulline: pharmacological perspectives and its role as an emerging biomarker in future. In: *Fundamental & clinical pharmacology* 27 (1), S. 35–50. DOI: 10.1111/j.1472-8206.2012.01059.x.
- Khoramipour, Kayvan; Chamari, Karim; Hekmatikar, Amirhosein Ahmadi; Ziyaiyan, Amirhosein; Taherkhani, Shima; Elguindy, Nihal M.; Bragazzi, Nicola Luigi (2021): Adiponectin: Structure, Physiological Functions, Role in Diseases, and Effects of Nutrition. In: *Nutrients* 13 (4). DOI: 10.3390/nu13041180.
- Kiwit, Antonia; Lu, Yuqing; Lenz, Moritz; Knopf, Jasmin; Mohr, Christoph; Ledermann, Yannick et al. (2024): The Dual Role of Neutrophil Extracellular Traps (NETs) in Sepsis and Ischemia-Reperfusion Injury: Comparative Analysis across Murine Models. In: *International journal of molecular sciences* 25 (7). DOI: 10.3390/ijms25073787.
- Knuckley, Bryan; Causey, Corey P.; Jones, Justin E.; Bhatia, Monica; Dreyton, Christina J.; Osborne, Tanesha C. et al. (2010): Substrate specificity and kinetic studies of PADs 1, 3, and 4 identify potent and selective inhibitors of protein arginine deiminase 3. In: *Biochemistry* 49 (23), S. 4852–4863. DOI: 10.1021/bi100363t).
- Knuuti, Juhani; Wijns, William; Saraste, Antti; Capodanno, Davide; Barbato, Emanuele; Funck-Brentano, Christian et al. (2020): 2019 ESC Guidelines for the diagnosis and management of chronic coronary syndromes. In: *European heart journal* 41 (3), S. 407–477. DOI: 10.1093/eurheartj/ehz425.
- Ko, Toshiyuki; Nomura, Seitaro; Yamada, Shintaro; Fujita, Kanna; Fujita, Takanori; Satoh, Masahiro et al. (2022): Cardiac fibroblasts regulate the development of heart failure via Htra3-TGF- β -IGFBP7 axis. In: *Nature communications* 13 (1), S. 3275. DOI: 10.1038/s41467-022-30630-y.
- Kologrivova, Irina; Shtatolkina, Marina; Suslova, Tatiana; Ryabov, Vyacheslav (2021): Cells of the Immune System in Cardiac Remodeling: Main Players in Resolution of Inflammation and Repair After Myocardial Infarction. In: *Frontiers in immunology* 12, S. 664457. DOI: 10.3389/fimmu.2021.664457.
- Kong, Ping; Christia, Panagiota; Frangogiannis, Nikolaos G. (2014): The pathogenesis of cardiac fibrosis. In: *Cellular and molecular life sciences : CMLS* 71 (4), S. 549–574. DOI: 10.1007/s00018-013-1349-6.
- Kubota, Masaaki; Yoshida, Yoichi; Kobayashi, Eiichi; Matsutani, Tomoo; Li, Shu-Yang; Zhang, Bo-Shi et al. (2021): Serum anti-SERPINE1 antibody as a potential biomarker of acute cerebral infarction. In: *Scientific reports* 11 (1), S. 21772. DOI: 10.1038/s41598-021-01176-8.

- Kuwabara, Jill T.; Hara, Akitoshi; Bhutada, Sumit; Gojanovich, Greg S.; Chen, Jasmine; Hokutan, Kanani et al. (2022): Consequences of PDGFR α + fibroblast reduction in adult murine hearts. In: *eLife* 11. DOI: 10.7554/eLife.69854.
- Laeremans, Hilde; Rensen, Sander S.; Ottenheijm, Harry C. J.; Smits, Jos F. M.; Blankesteyn, W. Matthijs (2010): Wnt/frizzled signalling modulates the migration and differentiation of immortalized cardiac fibroblasts. In: *Cardiovascular research* 87 (3), S. 514–523. DOI: 10.1093/cvr/cvq067.
- Lafuse, William P.; Wozniak, Daniel J.; Rajaram, Murugesan V. S. (2020): Role of Cardiac Macrophages on Cardiac Inflammation, Fibrosis and Tissue Repair. In: *Cells* 10 (1). DOI: 10.3390/cells10010051.
- Leancă, Sabina Andreea; Crișu, Daniela; Petriș, Antoniu Octavian; Afrăsânie, Irina; Genes, Antonia; Costache, Alexandru Dan et al. (2022): Left Ventricular Remodeling after Myocardial Infarction: From Physiopathology to Treatment. In: *Life (Basel, Switzerland)* 12 (8). DOI: 10.3390/life12081111.
- Lewis, Huw D.; Liddle, John; Coote, Jim E.; Atkinson, Stephen J.; Barker, Michael D.; Bax, Benjamin D. et al. (2015): Inhibition of PAD4 activity is sufficient to disrupt mouse and human NET formation. In: *Nature chemical biology* 11 (3), S. 189–191. DOI: 10.1038/nchembio.1735.
- Li, Fu Jun; Surolia, Ranu; Li, Huashi; Wang, Zheng; Liu, Gang; Kulkarni, Tejaswini et al. (2021a): Citrullinated vimentin mediates development and progression of lung fibrosis. In: *Science translational medicine* 13 (585). DOI: 10.1126/scitranslmed.aba2927.
- Li, Pingxin; Yao, Hongjie; Zhang, Zhiqiang; Li, Ming; Luo, Yuan; Thompson, Paul R. et al. (2008): Regulation of p53 target gene expression by peptidylarginine deiminase 4. In: *Molecular and cellular biology* 28 (15), S. 4745–4758. DOI: 10.1128/MCB.01747-07.
- Li, Tingting; Yan, Zhipeng; Fan, Yajie; Fan, Xinbiao; Li, Aolin; Qi, Zhongwen; Zhang, Junping (2022): Cardiac repair after myocardial infarction: A two-sided role of inflammation-mediated. In: *Frontiers in cardiovascular medicine* 9, S. 1077290. DOI: 10.3389/fcvm.2022.1077290.
- Li, Zhe; Nguyen, Tuan T.; Valaperti, Alan (2021b): Human cardiac fibroblasts produce pro-inflammatory cytokines upon TLRs and RLRs stimulation. In: *Molecular and cellular biochemistry* 476 (9), S. 3241–3252. DOI: 10.1007/s11010-021-04157-7.
- Lis-López, Lluís; Bauset, Cristina; Seco-Cervera, Marta; Cosín-Roger, Jesús (2021): Is the Macrophage Phenotype Determinant for Fibrosis Development? In: *Biomedicines* 9 (12). DOI: 10.3390/biomedicines9121747.
- Ma, Feifei; Li, Yulin; Jia, Lixin; Han, Yalei; Cheng, Jizhong; Li, Huihua et al. (2012): Macrophage-stimulated cardiac fibroblast production of IL-6 is essential for TGF β /Smad activation and cardiac fibrosis induced by angiotensin II. In: *PLoS one* 7 (5), e35144. DOI: 10.1371/journal.pone.0035144.
- Ma, Yonggang; Iyer, Rugmani Padmanabhan; Jung, Mira; Czubyrt, Michael P.; Lindsey, Merry L. (2017): Cardiac Fibroblast Activation Post-Myocardial Infarction: Current Knowledge Gaps. In: *Trends in pharmacological sciences* 38 (5), S. 448–458. DOI: 10.1016/j.tips.2017.03.001.
- Ma, Yonggang; Mouton, Alan J.; Lindsey, Merry L. (2018): Cardiac macrophage biology in the steady-state heart, the aging heart, and following myocardial infarction. In: *Translational research : the journal of laboratory and clinical medicine* 191, S. 15–28. DOI: 10.1016/j.trsl.2017.10.001.
- Ma, Yonggang; Yabluchanskiy, Andriy; Iyer, Rugmani Padmanabhan; Cannon, Presley L.; Flynn, Elizabeth R.; Jung, Mira et al. (2016): Temporal neutrophil polarization following myocardial infarction. In: *Cardiovascular research* 110 (1), S. 51–61. DOI: 10.1093/cvr/cvw024.
- Maekawa, Yuichiro; Anzai, Toshihisa; Yoshikawa, Tsutomu; Asakura, Yasushi; Takahashi, Toshiyuki; Ishikawa, Shiro et al. (2002): Prognostic significance of peripheral monocytosis after reperfused acute myocardial infarction: a possible role for left ventricular remodeling. In: *Journal of the American College of Cardiology* 39 (2), S. 241–246. DOI: 10.1016/S0735-1097(01)01721-1.

- Mao, Liqun; Mostafa, Rowann; Ibili, Esra; Fert-Bober, Justyna (2021): Role of protein deimination in cardiovascular diseases: potential new avenues for diagnostic and prognostic biomarkers. In: *Expert review of proteomics* 18 (12), S. 1059–1071. DOI: 10.1080/14789450.2021.2018303.
- Martinez, Fernando O.; Gordon, Siamon (2014): The M1 and M2 paradigm of macrophage activation: time for reassessment. In: *F1000prime reports* 6, S. 13. DOI: 10.12703/P6-13.
- Martini, Elisa; Kunderfranco, Paolo; Peano, Clelia; Carullo, Pierluigi; Cremonesi, Marco; Schorn, Tilo et al. (2019): Single-Cell Sequencing of Mouse Heart Immune Infiltrate in Pressure Overload-Driven Heart Failure Reveals Extent of Immune Activation. In: *Circulation* 140 (25), S. 2089–2107. DOI: 10.1161/CIRCULATIONAHA.119.041694.
- Martinod, Kimberly; Witsch, Thilo; Erpenbeck, Luise; Savchenko, Alexander; Hayashi, Hideki; Cherpokova, Deya et al. (2017): Peptidylarginine deiminase 4 promotes age-related organ fibrosis. In: *The Journal of experimental medicine* 214 (2), S. 439–458. DOI: 10.1084/jem.20160530.
- Marwick, John A.; Mills, Ross; Kay, Oliver; Michail, Kyriakos; Stephen, Jillian; Rossi, Adriano G. et al. (2018): Neutrophils induce macrophage anti-inflammatory reprogramming by suppressing NF- κ B activation. In: *Cell death & disease* 9 (6), S. 665. DOI: 10.1038/s41419-018-0710-y.
- Meléndez, Giselle C.; McLarty, Jennifer L.; Levick, Scott P.; Du, Yan; Janicki, Joseph S.; Brower, Gregory L. (2010): Interleukin 6 mediates myocardial fibrosis, concentric hypertrophy, and diastolic dysfunction in rats. In: *Hypertension (Dallas, Tex. : 1979)* 56 (2), S. 225–231. DOI: 10.1161/HYPERTENSIONAHA.109.148635.
- Mills, Charles Dudley (2015): Anatomy of a discovery: m1 and m2 macrophages. In: *Frontiers in immunology* 6, S. 212. DOI: 10.3389/fimmu.2015.00212.
- Mohammadzadeh, Naiyereh; Lunde, Ida G.; Andenæs, Kine; Strand, Mari E.; Aronsen, Jan Magnus; Skrbic, Biljana et al. (2019): The extracellular matrix proteoglycan lumican improves survival and counteracts cardiac dilatation and failure in mice subjected to pressure overload. In: *Scientific reports* 9 (1), S. 9206. DOI: 10.1038/s41598-019-45651-9.
- Mohan, Maradumane L.; Vasudevan, Neelakantan T.; Naga Prasad, Sathyamangla V. (2017): Proinflammatory Cytokines Mediate GPCR Dysfunction. In: *Journal of cardiovascular pharmacology* 70 (2), S. 61–73. DOI: 10.1097/FJC.0000000000000456.
- Mondal, Santanu; Thompson, Paul R. (2019): Protein Arginine Deiminases (PADs): Biochemistry and Chemical Biology of Protein Citrullination. In: *Accounts of chemical research* 52 (3), S. 818–832. DOI: 10.1021/acs.accounts.9b00024.
- Moore-Morris, Thomas; Guimarães-Camboa, Nuno; Banerjee, Indroneal; Zambon, Alexander C.; Kisseleva, Tatiana; Velayoudon, Aurélie et al. (2014): Resident fibroblast lineages mediate pressure overload-induced cardiac fibrosis. In: *The Journal of clinical investigation* 124 (7), S. 2921–2934. DOI: 10.1172/JCI74783.
- Mosser, David M. (2003): The many faces of macrophage activation. In: *Journal of leukocyte biology* 73 (2), S. 209–212. DOI: 10.1189/jlb.0602325.
- Mosser, David M.; Edwards, Justin P. (2008): Exploring the full spectrum of macrophage activation. In: *Nature reviews. Immunology* 8 (12), S. 958–969. DOI: 10.1038/nri2448.
- Mouton, Alan J.; Deleon-Pennell, Kristine Y.; Rivera Gonzalez, Osvaldo J.; Flynn, Elizabeth R.; Freeman, Tom C.; Saucerman, Jeffrey J. et al. (2018): Mapping macrophage polarization over the myocardial infarction time continuum. In: *Basic research in cardiology* 113 (4), S. 26. DOI: 10.1007/s00395-018-0686-x.
- Mouton, Alan J.; Ma, Yonggang; Rivera Gonzalez, Osvaldo J.; Daseke, Michael J.; Flynn, Elizabeth R.; Freeman, Tom C. et al. (2019): Fibroblast polarization over the myocardial infarction time continuum shifts roles from inflammation to angiogenesis. In: *Basic research in cardiology* 114 (2), S. 6. DOI: 10.1007/s00395-019-0715-4.

- Mukherjee, D.; Sen, S. (1993): Alteration of cardiac collagen phenotypes in hypertensive hypertrophy: role of blood pressure. In: *Journal of molecular and cellular cardiology* 25 (2), S. 185–196. DOI: 10.1006/jmcc.1993.1021.
- Murphy, Kenneth; Weaver, Casey (2018): Die Dynamik der angeborenen und adaptiven Immunantwort. In: Kenneth Murphy und Casey Weaver (Hg.): *Janeway Immunologie*. Berlin, Heidelberg: Springer Berlin Heidelberg, S. 581–639.
- Murray, Peter J.; Allen, Judith E.; Biswas, Subhra K.; Fisher, Edward A.; Gilroy, Derek W.; Goerd, Sergij et al. (2014): Macrophage activation and polarization: nomenclature and experimental guidelines. In: *Immunity* 41 (1), S. 14–20. DOI: 10.1016/j.immuni.2014.06.008.
- Nahrendorf, Matthias; Pittet, Mikael J.; Swirski, Filip K. (2010): Monocytes: protagonists of infarct inflammation and repair after myocardial infarction. In: *Circulation* 121 (22), S. 2437–2445. DOI: 10.1161/CIRCULATIONAHA.109.916346.
- Nakashima, Katsuhiko; Hagiwara, Teruki; Yamada, Michiyuki (2002): Nuclear localization of peptidylarginine deiminase V and histone deimination in granulocytes. In: *The Journal of biological chemistry* 277 (51), S. 49562–49568. DOI: 10.1074/jbc.M208795200.
- Nawaz, Allah; Aminuddin, Aminuddin; Kado, Tomonobu; Takikawa, Akiko; Yamamoto, Seiji; Tsuneyama, Koichi et al. (2017): CD206+ M2-like macrophages regulate systemic glucose metabolism by inhibiting proliferation of adipocyte progenitors. In: *Nature communications* 8 (1), S. 286. DOI: 10.1038/s41467-017-00231-1.
- Newton, Kim; Dixit, Vishva M. (2012): Signaling in innate immunity and inflammation. In: *Cold Spring Harbor perspectives in biology* 4 (3). DOI: 10.1101/cshperspect.a006049.
- Nichols, Melanie; Townsend, Nick; Scarborough, Peter; Rayner, Mike (2014): Cardiovascular disease in Europe 2014: epidemiological update. In: *European heart journal* 35 (42), S. 2950–2959. DOI: 10.1093/eurheartj/ehu299.
- Nishihira, Kensaku; Kuriyama, Nehiro; Kadooka, Kosuke; Honda, Yasuhiro; Yamamoto, Keisuke; Nishino, Shun et al. (2022): Outcomes of Elderly Patients With Acute Myocardial Infarction and Heart Failure Who Undergo Percutaneous Coronary Intervention. In: *Circulation reports* 4 (10), S. 474–481. DOI: 10.1253/circrep.CR-22-0048.
- Ong, Sang-Bing; Hernández-Reséndiz, Sauri; Crespo-Avilan, Gustavo E.; Mukhametshina, Regina T.; Kwek, Xiu-Yi; Cabrera-Fuentes, Hector A.; Hausenloy, Derek J. (2018): Inflammation following acute myocardial infarction: Multiple players, dynamic roles, and novel therapeutic opportunities. In: *Pharmacology & therapeutics* 186, S. 73–87. DOI: 10.1016/j.pharmthera.2018.01.001.
- Paik, W. K.; Kim, S. (1967): Enzymatic methylation of protein fractions from calf thymus nuclei. In: *Biochemical and biophysical research communications* 29 (1), S. 14–20. DOI: 10.1016/0006-291X(67)90533-5.
- Penberthy, Kristen K.; Ravichandran, Kodi S. (2016): Apoptotic cell recognition receptors and scavenger receptors. In: *Immunological reviews* 269 (1), S. 44–59. DOI: 10.1111/imr.12376.
- Piamsiri, Chanon; Maneechote, Chayodom; Siri-Angkul, Natthaphat; Chattipakorn, Siriporn C.; Chattipakorn, Nipon (2021): Targeting necroptosis as therapeutic potential in chronic myocardial infarction. In: *Journal of biomedical science* 28 (1), S. 25. DOI: 10.1186/s12929-021-00722-w.
- Potter, Julia M.; Hickman, Peter E.; Cullen, Louise (2022): Troponins in myocardial infarction and injury. In: *Australian prescriber* 45 (2), S. 53–57. DOI: 10.18773/austprescr.2022.006.
- Poznyak, Anastasia V.; Ivanova, Ekaterina A.; Sobenin, Igor A.; Yet, Shaw-Fang; Orekhov, Alexander N. (2020): The Role of Mitochondria in Cardiovascular Diseases. In: *Biology* 9 (6). DOI: 10.3390/biology9060137.

- Prabhu, Sumanth D. (2005): Post-infarction ventricular remodeling: an array of molecular events. In: *Journal of molecular and cellular cardiology* 38 (4), S. 547–550. DOI: 10.1016/j.yjmcc.2005.01.014.
- Prame Kumar, Kathryn; Nicholls, Alyce J.; Wong, Connie H. Y. (2018): Partners in crime: neutrophils and monocytes/macrophages in inflammation and disease. In: *Cell and tissue research* 371 (3), S. 551–565. DOI: 10.1007/s00441-017-2753-2.
- Quillard, Thibaut; Franck, Grégory; Mawson, Thomas; Folco, Eduardo; Libby, Peter (2017): Mechanisms of erosion of atherosclerotic plaques. In: *Current opinion in lipidology* 28 (5), S. 434–441. DOI: 10.1097/MOL.0000000000000440.
- Rehman, Ibraheem; Kerndt, Connor C.; Rehman, Afzal (2024): StatPearls. Anatomy, Thorax, Heart Left Anterior Descending (LAD) Artery. Treasure Island (FL).
- ROGERS, G. E.; Harding, H. W.; Llewellyn-Smith, I. J. (1977): The origin of citrulline-containing proteins in the hair follicle and the chemical nature of trichohyalin, an intracellular precursor. In: *Biochimica et biophysica acta* 495 (1), S. 159–175. DOI: 10.1016/0005-2795(77)90250-1.
- Roth, Gregory A.; Mensah, George A.; Fuster, Valentin (2020): The Global Burden of Cardiovascular Diseases and Risks: A Compass for Global Action. In: *Journal of the American College of Cardiology* 76 (25), S. 2980–2981. DOI: 10.1016/j.jacc.2020.11.021.
- Saito, Yuichi; Tateishi, Kazuya; Kanda, Masato; Shiko, Yuki; Kawasaki, Yohei; Kobayashi, Yoshio; Inoue, Takahiro (2022): Volume-Outcome Relationships for Percutaneous Coronary Intervention in Acute Myocardial Infarction. In: *Journal of the American Heart Association* 11 (6), e023805. DOI: 10.1161/JAHA.121.023805.
- Sandoval, Yader; Jaffe, Allan S. (2019): Type 2 Myocardial Infarction: JACC Review Topic of the Week. In: *Journal of the American College of Cardiology* 73 (14), S. 1846–1860. DOI: 10.1016/j.jacc.2019.02.018.
- Sara, Jaskanwal D.; Prasad, Megha; Eleid, Mackram F.; Zhang, Ming; Widmer, R. Jay; Lerman, Amir (2018): Association Between Work-Related Stress and Coronary Heart Disease: A Review of Prospective Studies Through the Job Strain, Effort-Reward Balance, and Organizational Justice Models. In: *Journal of the American Heart Association* 7 (9). DOI: 10.1161/JAHA.117.008073.
- Sarkar, Sagartirtha; Vellaichamy, Elangovan; Young, David; Sen, Subha (2004): Influence of cytokines and growth factors in ANG II-mediated collagen upregulation by fibroblasts in rats: role of myocytes. In: *American journal of physiology. Heart and circulatory physiology* 287 (1), H107-17. DOI: 10.1152/ajpheart.00763.2003.
- Schirone, Leonardo; Forte, Maurizio; D'Ambrosio, Luca; Valenti, Valentina; Vecchio, Daniele; Schiavon, Sonia et al. (2022): An Overview of the Molecular Mechanisms Associated with Myocardial Ischemic Injury: State of the Art and Translational Perspectives. In: *Cells* 11 (7). DOI: 10.3390/cells11071165.
- Schumacher, Sarah M.; Naga Prasad, Sathyamangla V. (2018): Tumor Necrosis Factor- α in Heart Failure: an Updated Review. In: *Current cardiology reports* 20 (11), S. 117. DOI: 10.1007/s11886-018-1067-7.
- Shapouri-Moghaddam, Abbas; Mohammadian, Saeed; Vazini, Hossein; Taghadosi, Mahdi; Esmaeili, Seyed-Alireza; Mardani, Fatemeh et al. (2018): Macrophage plasticity, polarization, and function in health and disease. In: *Journal of cellular physiology* 233 (9), S. 6425–6440. DOI: 10.1002/jcp.26429.
- Shelef, Miriam A.; Bennin, David A.; Mosher, Deane F.; Huttenlocher, Anna (2012): Citrullination of fibronectin modulates synovial fibroblast behavior. In: *Arthritis research & therapy* 14 (6), R240. DOI: 10.1186/ar4083.

- Shen, Shi-Chun; Xu, Jie; Cheng, Cheng; Xiang, Xin-Jian; Hong, Bao-Yu; Zhang, Meng et al. (2024): Macrophages promote the transition from myocardial ischemia reperfusion injury to cardiac fibrosis in mice through GM-CSF/CCL2/CCR2 and phenotype switching. In: *Acta pharmacologica Sinica* 45 (5), S. 959–974. DOI: 10.1038/s41401-023-01222-3.
- Silvestre-Roig, Carlos; Braster, Quinte; Ortega-Gomez, Almudena; Soehnlein, Oliver (2020): Neutrophils as regulators of cardiovascular inflammation. In: *Nature reviews. Cardiology* 17 (6), S. 327–340. DOI: 10.1038/s41569-019-0326-7.
- Sipilä, Kalle H.; Ranga, Vipin; Rappu, Pekka; Torittu, Annamari; Pirilä, Laura; Käpylä, Jarmo et al. (2016): Extracellular citrullination inhibits the function of matrix associated TGF- β . In: *Matrix biology : journal of the International Society for Matrix Biology* 55, S. 77–89. DOI: 10.1016/j.matbio.2016.02.008.
- Slade, Daniel J.; Subramanian, Venkataraman; Fuhrmann, Jakob; Thompson, Paul R. (2014): Chemical and biological methods to detect post-translational modifications of arginine. In: *Biopolymers* 101 (2), S. 133–143. DOI: 10.1002/bip.22256.
- Song, Fang-Qiang; Zhou, Hui-Min; Ma, Wei-Xuan; Li, Yu-Lin; Hu, Bo-Ang; Shang, Yuan-Yuan et al. (2022): CIDEA: A Potential Factor in Diabetic Vascular Inflammation. In: *Journal of vascular research* 59 (2), S. 114–123. DOI: 10.1159/000520685.
- Stadler, Sonja C.; Vincent, C. Theresa; Fedorov, Victor D.; Patsialou, Antonia; Cherrington, Brian D.; Wakshlag, Joseph J. et al. (2013): Dysregulation of PAD4-mediated citrullination of nuclear GSK3 β activates TGF- β signaling and induces epithelial-to-mesenchymal transition in breast cancer cells. In: *Proceedings of the National Academy of Sciences of the United States of America* 110 (29), S. 11851–11856. DOI: 10.1073/pnas.1308362110.
- Sun, Bo; Dwivedi, Nishant; Bechtel, Tyler J.; Paulsen, Janet L.; Muth, Aaron; Bawadekar, Mandar et al. (2017): Citrullination of NF- κ B p65 promotes its nuclear localization and TLR-induced expression of IL-1 β and TNF α . In: *Science immunology* 2 (12). DOI: 10.1126/sciimmunol.aal3062.
- Sutanto, Henry; Lyon, Aurore; Lumens, Joost; Schotten, Ulrich; Dobrev, Dobromir; Heijman, Jordi (2020): Cardiomyocyte calcium handling in health and disease: Insights from *in vitro* and *in silico* studies. In: *Progress in biophysics and molecular biology* 157, S. 54–75. DOI: 10.1016/j.pbiomolbio.2020.02.008.
- Sutton, M. G.; Sharpe, N. (2000): Left ventricular remodeling after myocardial infarction: pathophysiology and therapy. In: *Circulation* 101 (25), S. 2981–2988. DOI: 10.1161/01.CIR.101.25.2981.
- Talman, Virpi; Ruskoaho, Heikki (2016): Cardiac fibrosis in myocardial infarction—from repair and remodeling to regeneration. In: *Cell and tissue research* 365 (3), S. 563–581. DOI: 10.1007/s00441-016-2431-9.
- Tanai, Edit; Frantz, Stefan (2015): Pathophysiology of Heart Failure. In: *Comprehensive Physiology* 6 (1), S. 187–214. DOI: 10.1002/cphy.c140055.
- Tenreiro, Miguel F.; Louro, Ana F.; Alves, Paula M.; Serra, Margarida (2021): Next generation of heart regenerative therapies: progress and promise of cardiac tissue engineering. In: *NPJ Regenerative medicine* 6 (1), S. 30. DOI: 10.1038/s41536-021-00140-4.
- Thomas, Toby P.; Grisanti, Laurel A. (2020): The Dynamic Interplay Between Cardiac Inflammation and Fibrosis. In: *Frontiers in physiology* 11, S. 529075. DOI: 10.3389/fphys.2020.529075.
- Tian, Ming; Yuan, Yun-Chuan; Li, Jia-Yi; Gionfriddo, Michael R.; Huang, Rong-Chong (2015): Tumor necrosis factor- α and its role as a mediator in myocardial infarction: A brief review. In: *Chronic diseases and translational medicine* 1 (1), S. 18–26. DOI: 10.1016/j.cdtm.2015.02.002.
- Townsend, Nick; Kazakiewicz, Denis; Lucy Wright, F.; Timmis, Adam; Huculeci, Radu; Torbica, Aleksandra et al. (2022): Epidemiology of cardiovascular disease in Europe. In: *Nature reviews. Cardiology* 19 (2), S. 133–143. DOI: 10.1038/s41569-021-00607-3.

- Travers, Joshua G.; Kamal, Fadia A.; Robbins, Jeffrey; Yutzey, Katherine E.; Blaxall, Burns C. (2016): Cardiac Fibrosis: The Fibroblast Awakens. In: *Circulation research* 118 (6), S. 1021–1040. DOI: 10.1161/CIRCRESAHA.115.306565.
- Travers, Joshua G.; Tharp, Charles A.; Rubino, Marcello; McKinsey, Timothy A. (2022): Therapeutic targets for cardiac fibrosis: from old school to next-gen. In: *The Journal of clinical investigation* 132 (5). DOI: 10.1172/JCI148554.
- Turner, Neil A. (2016): Inflammatory and fibrotic responses of cardiac fibroblasts to myocardial damage associated molecular patterns (DAMPs). In: *Journal of molecular and cellular cardiology* 94, S. 189–200. DOI: 10.1016/j.yjmcc.2015.11.002.
- van der Laan, Anja M.; Horst, Ellis N. ter; Delewi, Ronak; Begieneman, Mark P. V.; Krijnen, Paul A. J.; Hirsch, Alexander et al. (2014): Monocyte subset accumulation in the human heart following acute myocardial infarction and the role of the spleen as monocyte reservoir. In: *European heart journal* 35 (6), S. 376–385. DOI: 10.1093/eurheartj/eh331.
- van der Laan, Anja M.; Nahrendorf, Matthias; Piek, Jan J. (2012): Healing and adverse remodelling after acute myocardial infarction: role of the cellular immune response. In: *Heart (British Cardiac Society)* 98 (18), S. 1384–1390. DOI: 10.1136/heartjnl-2012-301623.
- Vandendriessche, Sofie; Cambier, Seppe; Proost, Paul; Marques, Pedro E. (2021): Complement Receptors and Their Role in Leukocyte Recruitment and Phagocytosis. In: *Frontiers in cell and developmental biology* 9, S. 624025. DOI: 10.3389/fcell.2021.624025.
- Virani, Salim S.; Alonso, Alvaro; Benjamin, Emelia J.; Bittencourt, Marcio S.; Callaway, Clifton W.; Carson, April P. et al. (2020): Heart Disease and Stroke Statistics-2020 Update: A Report From the American Heart Association. In: *Circulation* 141 (9), e139-e596. DOI: 10.1161/CIR.0000000000000757.
- Vossenaar, E. R.; Radstake, T. R. D.; van der Heijden, A.; van Mansum, M. A. M.; Dieteren, C.; Rooij, D-J de et al. (2004): Expression and activity of citrullinating peptidylarginine deiminase enzymes in monocytes and macrophages. In: *Annals of the rheumatic diseases* 63 (4), S. 373–381. DOI: 10.1136/ard.2003.012211.
- Vossenaar, Erik R.; Zendman, Albert J. W.; van Venrooij, Walther J.; Pruijn, Ger J. M. (2003): PAD, a growing family of citrullinating enzymes: genes, features and involvement in disease. In: *BioEssays : news and reviews in molecular, cellular and developmental biology* 25 (11), S. 1106–1118. DOI: 10.1002/bies.10357.
- Wang, Binhan; Wang, Manni; Ao, Danyi; Wei, Xiawei (2022): CXCL13-CXCR5 axis: Regulation in inflammatory diseases and cancer. In: *Biochimica et biophysica acta. Reviews on cancer* 1877 (5), S. 188799. DOI: 10.1016/j.bbcan.2022.188799.
- Wang, Yahui; Chu, Ying; Cao, Fenghua; Chen, Zhihong; Xu, Huaxi; Wang, Shengjun; Ma, Jie (2023): The emerging role of triggering receptor expressed on myeloid cell-2 in malignant tumor. In: *Central-European Journal of Immunology* 47 (4), S. 373–381. DOI: 10.5114/ceji.2022.124387.
- Willenborg, Sebastian; Lucas, Tina; van Loo, Geert; Knipper, Johanna A.; Krieg, Thomas; Haase, Ingo et al. (2012): CCR2 recruits an inflammatory macrophage subpopulation critical for angiogenesis in tissue repair. In: *Blood* 120 (3), S. 613–625. DOI: 10.1182/blood-2012-01-403386.
- Willis, V. C.; Banda, N. K.; Cordova, K. N.; Chandra, P. E.; Robinson, W. H.; Cooper, D. C. et al. (2017): Protein arginine deiminase 4 inhibition is sufficient for the amelioration of collagen-induced arthritis. In: *Clinical and experimental immunology* 188 (2), S. 263–274. DOI: 10.1111/cei.12932.
- Wu, Meifang; Guo, Yanguang; Wu, Ying; Xu, Kaizu; Lin, Liming (2021a): Protective Effects of Sacubitril/Valsartan on Cardiac Fibrosis and Function in Rats With Experimental Myocardial Infarction Involves Inhibition of Collagen Synthesis by Myocardial Fibroblasts Through Downregulating TGF- β 1/Smads Pathway. In: *Frontiers in pharmacology* 12, S. 696472. DOI: 10.3389/fphar.2021.696472.

- Wu, Yujing; Zheng, Zhenzhong; Cao, Xiantong; Yang, Qing; Norton, Vikram; Adini, Avner et al. (2021b): RIP1/RIP3/MLKL Mediates Myocardial Function Through Necroptosis in Experimental Autoimmune Myocarditis. In: *Frontiers in cardiovascular medicine* 8, S. 696362. DOI: 10.3389/fcvm.2021.696362.
- Wu, Zhuo-Rao; Zhou, Tian-Qi; Ai, Shuang-Chun (2023): Neutrophil extracellular traps correlate with severity and prognosis in patients with ischemic stroke: a systematic review and meta-analysis. In: *Acta neurologica Belgica*. DOI: 10.1007/s13760-023-02409-5.
- Wynn, Thomas A.; Chawla, Ajay; Pollard, Jeffrey W. (2013): Macrophage biology in development, homeostasis and disease. In: *Nature* 496 (7446), S. 445–455. DOI: 10.1038/nature12034.
- Xie, Yangli; Su, Nan; Yang, Jing; Tan, Qiaoyan; Huang, Shuo; Jin, Min et al. (2020): FGF/FGFR signaling in health and disease. In: *Signal transduction and targeted therapy* 5 (1), S. 181. DOI: 10.1038/s41392-020-00222-7.
- Yang, Chao; Dong, Zhen-Zhen; Zhang, Jing; Teng, Dehong; Luo, Xinzhi; Li, Dan; Zhou, Yingtang (2021): Peptidylarginine deiminases 4 as a promising target in drug discovery. In: *European journal of medicinal chemistry* 226, S. 113840. DOI: 10.1016/j.ejmech.2021.113840.
- Yang, Yanzhong; Bedford, Mark T. (2013): Protein arginine methyltransferases and cancer. In: *Nature reviews. Cancer* 13 (1), S. 37–50. DOI: 10.1038/nrc3409.
- Yano, Toshiyuki; Miura, Tetsuji; Whittaker, Peter; Miki, Takayuki; Sakamoto, Jun; Nakamura, Yuichi et al. (2006): Macrophage colony-stimulating factor treatment after myocardial infarction attenuates left ventricular dysfunction by accelerating infarct repair. In: *Journal of the American College of Cardiology* 47 (3), S. 626–634. DOI: 10.1016/j.jacc.2005.09.037.
- Yerra, Veera Ganesh; Advani, Andrew (2022): Role of CCR2-Positive Macrophages in Pathological Ventricular Remodelling. In: *Biomedicines* 10 (3). DOI: 10.3390/biomedicines10030661.
- Yu, Ji Eun; Yeo, In Jun; Han, Sang-Bae; Yun, Jaesuk; Kim, Bongcheol; Yong, Yoon Ji et al. (2024): Significance of chitinase-3-like protein 1 in the pathogenesis of inflammatory diseases and cancer. In: *Experimental & molecular medicine* 56 (1), S. 1–18. DOI: 10.1038/s12276-023-01131-9.
- Yue, Yuan; Huang, Suiqing; Li, Huayang; Li, Wei; Hou, Jian; Luo, Li et al. (2020): M2b macrophages protect against myocardial remodeling after ischemia/reperfusion injury by regulating kinase activation of platelet-derived growth factor receptor of cardiac fibroblast. In: *Annals of translational medicine* 8 (21), S. 1409. DOI: 10.21037/atm-20-2788.
- Yue, Yuan; Huang, Suiqing; Wang, Lexun; Wu, Zixuan; Liang, Mengya; Li, Huayang et al. (2020): M2b Macrophages Regulate Cardiac Fibroblast Activation and Alleviate Cardiac Fibrosis After Reperfusion Injury. In: *Circulation journal : official journal of the Japanese Circulation Society* 84 (4), S. 626–635. DOI: 10.1253/circj.CJ-19-0959.
- Yusuf, Salim; Hawken, Steven; Ounpuu, Stephanie; Dans, Tony; Avezum, Alvaro; Lanas, Fernando et al. (2004): Effect of potentially modifiable risk factors associated with myocardial infarction in 52 countries (the INTERHEART study): case-control study. In: *Lancet (London, England)* 364 (9438), S. 937–952. DOI: 10.1016/S0140-6736(04)17018-9.
- Zhang, Qing; Wang, Lu; Wang, Shiqi; Cheng, Hongxin; Xu, Lin; Pei, Gaiqin et al. (2022): Signaling pathways and targeted therapy for myocardial infarction. In: *Signal transduction and targeted therapy* 7 (1), S. 78. DOI: 10.1038/s41392-022-00925-z.
- Zhang, Wei; Liu, Hui Tu (2002): MAPK signal pathways in the regulation of cell proliferation in mammalian cells. In: *Cell research* 12 (1), S. 9–18. DOI: 10.1038/sj.cr.7290105.
- Zhao, Tieqiang; Zhao, Wenyan; Chen, Yuanjian; Ahokas, Robert A.; Sun, Yao (2010): Vascular endothelial growth factor (VEGF)-A: role on cardiac angiogenesis following myocardial infarction. In: *Microvascular research* 80 (2), S. 188–194. DOI: 10.1016/j.mvr.2010.03.014.

Zhao, Z. Q.; Nakamura, M.; Wang, N. P.; Wilcox, J. N.; Shearer, S.; Ronson, R. S. et al. (2000): Reperfusion induces myocardial apoptotic cell death. In: *Cardiovascular research* 45 (3), S. 651–660. DOI: 10.1016/s0008-6363(99)00354-5.

Zhu, Luojiang; Wang, Wen; Ren, Changzhen; Wang, Yangkai; Zhang, Guanghao; Liu, Jianmin; Wang, Weizhong (2022): Cellular Phenotypic Transformation in Heart Failure Caused by Coronary Heart Disease and Dilated Cardiomyopathy: Delineating at Single-Cell Level. In: *Biomedicines* 10 (2). DOI: 10.3390/biomedicines10020402.

Zhuang, Lingfang; Wang, Yaqiong; Chen, Zhaoyang; Li, Zhigang; Wang, Ziyang; Jia, Kangni et al. (2022): Global Characteristics and Dynamics of Single Immune Cells After Myocardial Infarction. In: *Journal of the American Heart Association* 11 (24), e027228. DOI: 10.1161/JAHA.122.027228.

Erklärung

Ich versichere, dass ich die von mir vorgelegte Dissertation selbstständig angefertigt, die benutzten Quellen und Hilfsmittel vollständig angegeben und die Stellen der Arbeit - einschließlich Tabellen, Karten und Abbildungen -, die anderen Werken im Wortlaut oder dem Sinn nach entnommen sind, in jedem Einzelfall als Entlehnung kenntlich gemacht habe; dass diese Dissertation noch keiner anderen Fakultät oder Universität zur Prüfung vorgelegen hat; dass sie - abgesehen von unten angegebenen Teilpublikationen - noch nicht veröffentlicht worden ist sowie, dass ich eine solche Veröffentlichung vor Abschluss des Promotionsverfahrens nicht vornehmen werde. Die Bestimmungen dieser Promotionsordnung sind mir bekannt. Die von mir vorgelegte Dissertation ist von Prof. Dr. Adhana Paunel-Görgülü betreut worden.

Übersicht der Publikationen:

Submitted paper: Peptidylarginine deiminase 4 deficiency prevents maladaptive cardiac remodeling and improves long-term survival after myocardial infarction

Michelle Holthaus, Xiaolin Xiong, Kaveh Eghbalzadeh, Clara Großmann, Simon Geißen, Fabian Piontek, Martin Mollenhauer, Ali T. Abdallah, Thomas Kamphausen, Markus Rothschild, Thorsten Wahlers, Adhana Paunel-Görgülü

Ich versichere, dass ich alle Angaben wahrheitsgemäß nach bestem Wissen und Gewissen gemacht habe und verpflichte mich, jedmögliche, die obigen Angaben betreffenden Veränderungen, dem Promotionsausschuss unverzüglich mitzuteilen.

10.12.2024, Köln

.....
Datum

.....
Unterschrift

